ภาคผนวก

European Journal of Medicinal Chemistry 45 (2010) 5585–5593

Contents lists available at ScienceDirect

European Journal of Medicinal Chemistry

journal homepage: http://www.elsevier.com/locate/ejmech

Original article

Investigating the structural basis of arylamides to improve potency against *M. tuberculosis* strain through molecular dynamics simulations

Auradee Punkvang [a], Patchreenart Saparpakorn [b], Supa Hannongbua [b], Peter Wolschann [c], Anton Beyer [c], Pornpan Pungpo [a,*]

[a] Department of Chemistry, Ubon Ratchathani University, 85 Sthollmark Road, Warinchamrap, Ubonratchathani 34190, Thailand
[b] Department of Chemistry, Kasetsart University, Chatuchak, Bangkok 10900, Thailand
[c] Institute for Theoretical Chemistry, University of Vienna, A-1090 Vienna, Austria

ARTICLE INFO

Article history:
Received 11 May 2010
Received in revised form
13 August 2010
Accepted 4 September 2010
Available online 17 September 2010

Keywords:
Molecular dynamics simulations
Arylamide
InhA
M. tuberculosis

ABSTRACT

Arylamides have been identified as direct InhA inhibitors which overcome the drug-resistance problem of isoniazid, the first-line drug for tuberculosis treatment. However, arylamide properties are not yet optimal against *Mycobacterium tuberculosis*. Arylamides show high potency in InhA enzyme assay, but they fail in antimycobacterial assay. To achieve the structural basis to improve antimycobacterial activity, the dynamic behavior of arylamide inhibitors and a substrate, *trans*-2-hexadecenoyl-(*N*-acetylcysteamine)-thioester, were carried out by molecular dynamics (MD) simulations. Arylamide inhibitors and a substrate are positioned at the same site which indicates the competitive inhibitor function of arylamides. Based on our findings, the amide carbonyl oxygen causes the selectivity of arylamide inhibitors for InhA inhibition. Moreover, this moiety is crucial for the affinity of the arylamide–InhA interactions with Tyr158 and NADH to form hydrogen bonds. It is possible to enhance the selectivity of arylamide inhibitors to reach the InhA target by introducing a hydrophilic substituent into the aryl ring A. In order to increase the membrane permeability of arylamide inhibitors, more lipophilic properties should be incorporated into the substituent B. Therefore, based on the obtained results, the correct balance between the selectivity and the membrane permeability of arylamide inhibitors should improve their inhibitory activity against *M. tuberculosis* strain.

1. Introduction

Multidrug resistant-tuberculosis (MDR-TB) and extensively drug-resistant tuberculosis (XDR-TB) do not respond to the standard treatment with first-line anti-TB drugs, which makes tuberculosis treatment complicated and expensive [1]. Accordingly, to address these problems the research on novel and more potent drug candidates is very important. The enoyl-acyl-ACP reductase (InhA) catalyzing the NADH-specific reduction of 2-trans-enoyl-ACP [2] is an attractive target for designing novel antibacterial agents [3–8]. InhA has been identified as the primary target of isoniazid (INH), one of the most effective first-line anti-TB drugs [9–14]. As a prodrug, INH must first be activated by catalase-peroxidase (KatG) to generate the reactive acyl radical [15–21]. Thereupon, the reactive species binds covalently to nicotinamide adenine dinucleotide (NAD+) to form the active adduct (INH-NAD) that functions as a highly potent inhibitor of InhA [22,23]. However, the high potency of INH for tuberculosis treatment is diminished by drug resistance. The INH resistance is related to the mutation in several genes of *Mycobacterium tuberculosis* involving *inhA*, *ahpC*, *kasA*, *katG* and ndh [24–30]. Commonly found in *M. tuberculosis* clinical isolates, high levels of INH resistance arise from mutations in *katG* [31,32]. Thus, to overcome the INH resistance associated with mutations in the KatG enzyme, compounds which directly inhibit the InhA enzyme without requiring activation by KatG are to be seen as very promising new agents against tuberculosis. Many compounds functioning as direct InhA inhibitors have been discovered and identified [33–37]. A series of arylamides is one of the novel classes of potent InhA inhibitors that circumvent the resistance mechanism to INH prodrug [38]. Arylamides show high potency for inhibiting the InhA enzyme. The highest InhA inhibitory activity with IC_{50} of 0.09 μM could be observed. On the other hand it has to be taken into account that the majority of arylamides exhibits a lower *M. tuberculosis* growth inhibition with the minimum inhibitory concentrations (MIC) against *M. tuberculosis* strain above 125 μM. However, it can be reasonably assumed that these compounds are extruded from the bacterial cell by efflux pumps. The above given data, especially the direct InhA inhibitor

* Corresponding author. Tel.: +66453534014124; fax: +6645288379.
E-mail address: pornpan_ubu@yahoo.com (P. Pungpo).

0223-5234/$ – see front matter © 2010 Elsevier Masson SAS. All rights reserved.
doi:10.1016/j.ejmech.2010.09.008

property of arylamides justify a more detailed examination of the structural basis to improve antimycobacterial activity.

MD simulations have been widely used for inhibitor–enzyme complexes in order to investigate the structural features and the dynamic behavior providing detailed information about flexibility, conformation and inhibitor–enzyme interactions [39–47]. In the present study, MD simulations have been performed for arylamide–InhA complexes to gain an insight into their structural and dynamic features. Moreover, to compare the dynamic behavior of the interaction between arylamide inhibitors and substrate, MD simulations of a substrate, *trans*-2-hexadecenoyl-(*N*-acetylcysteamine)-thioester, were also carried out. The binding free energies of arylamide–InhA complexes were calculated to gain quantitative insights into the binding affinity of arylamide inhibitors in the InhA binding site. In addition, the binding free energy of the substrate was also calculated to be compared with that of arylamide inhibitors. The interaction energies between arylamide inhibitors and particular amino acids were also evaluated to explore the key residues that are crucial for the binding affinity of arylamide–InhA complexes.

2. Materials and methods

2.1. Starting structures for MD simulations

Two X-ray crystal structures of arylamide B3-NADH-InhA and the substrate-NADH-InhA were taken from the Protein Data Bank with pdb codes of 2NSD [38] and 1BVR [48], respectively. Because of the homotetramer characteristic of InhA [48], only chain A of both X-ray crystal structures served as the initial coordinates for MD simulations. In the case of arylamide A10 and P2 bound complexes, their starting structures were taken from molecular docking calculations using Autodock 3.05 [49]. In this work, the chemical structures and InhA inhibitory activities (the half maximal inhibitory concentration, IC_{50}) of arylamides taken from literature [38] are shown in Table 1.

2.2. Molecular docking calculations

The X-ray crystal structure of arylamide B3 complexed with InhA (pdb code 2NSD) was employed for molecular docking calculations. Docking calculations of arylamide inhibitors were carried out by the Autodock 3.05 program using Lamarckian Genetic Algorithm (LGA) [49]. All hydrogen atoms and Kollman charges were added to the protein using AutoDockTools. Solvation parameters were generated for the protein using the Addsol utility of Autodock. The grid maps representing the protein in the actual docking process were calculated with Autogrid. The dimensions of the grids were 60 × 60 × 60 points with a spacing of 0.375 Å and the center close to the ligand. Docking parameters were used as default values, except for the number of docking runs which was set to 50. Arylamide B3 was docked back into the InhA binding pocket to validate the docking method, and subsequently the other

Table 1
The chemical structures and InhA inhibitory activities of arylamides and the chemical structure of substrate.

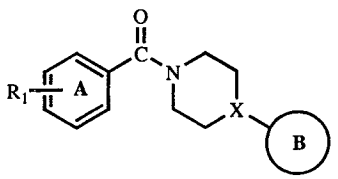

Compound	X	R_1	B	IC_{50} (μM)[a]
A10	N	4-t-Bu	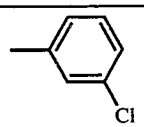	>100
B3	C	4-CH_3	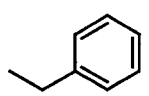	5.16
P2	N	H	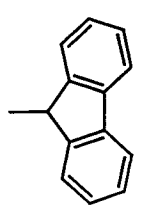	0.09
Substrate			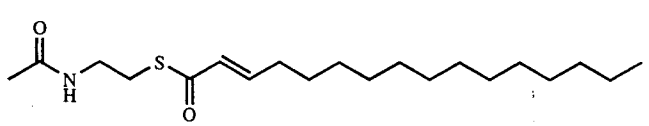	

[a] IC_{50} of all inhibitors were taken from literature [36]. The nomenclature of the inhibitors was taken from the original literature and is also given in Table 1.

compounds were docked. The ligand pose with the lowest final docked energy and the greatest number of members in the cluster was selected as the best binding mode of arylamide inhibitors in the InhA binding pocket.

2.3. Molecular dynamics simulations

Four MD simulations for the substrate-bound complex (substrate-NADH-InhA) and the arylamide inhibitor-bound complexes (A10-NADH-InhA, B3-NADH-InhA and P2-NADH-InhA) were carried out using GROMACS 4.0.4 [50–52] with GROMOS96 43a2 force field [53]. AnteChamber PYthon Parser interfacE (ACPYPE) tool [54] was employed to generate parameters for the MD force field of NADH, the substrate and arylamide inhibitors. Each of the starting complexes was inserted and centered into the cubic periodic box of SPC216 water molecules [55]. A cubic box extended at 3 nm from the starting complexes was set for all simulations. Each simulation system was neutralized by four Na^+ counterions. To remove bad contacts before MD simulations, an energy minimization with all bonds constrained using the steepest descent algorithm (2000 steps) was performed for each simulation system. Afterwards, a 500 ps simulation of each system was performed in the NVT ensemble at 300 K with a time step of 0.002 ps under the conditions of position restraints and LINCS constraints [56]. Finally, 6 ns MD simulations without the position restraints were performed under the same conditions. Long-range electrostatic interactions were evaluated by the particle-mesh Ewald method [57]. Coulomb and van der Waals interactions were cut off at 1.0 nm. The last 1 ns simulation of each system was selected for detailed analysis. The crude average structure was refined using the steepest decent and conjugate gradient minimization.

2.4. Calculations of binding free energies

The linear interaction energy (LIE) method [58] was chosen to calculate the binding free energies for the substrate and arylamide inhibitors in the InhA enzyme. To calculate the binding free energy with LIE method, MD simulations of the substrate and arylamide inhibitors in water were also performed under the same conditions as described above. The binding free energy based on LIE method can be expressed by the following equation;

$$\Delta G_{\text{bind}} = \alpha\left[(V_{\text{LJ}})_{\text{bound}} - (V_{\text{LJ}})_{\text{free}}\right] + \beta\left[(V_{\text{CL}})_{\text{bound}} - (V_{\text{CL}})_{\text{free}}\right] \quad (1)$$

Where $(V_{\text{LJ}})_{\text{bound}}$ = average Lennard–Jones energy for ligand/solvent interaction; $(V_{\text{LJ}})_{\text{free}}$ = average Lennard–Jones energy for ligand/water interaction; $(V_{\text{CL}})_{\text{bound}}$ = average electrostatic energy for ligand/solvent interaction; $(V_{\text{CL}})_{\text{free}}$ = average electrostatic energy for ligand/water interaction; α, β = scaling factors with $\alpha = 0.18$ and $\beta = 0.50$.

It is noted that ligand/solvent interaction denotes interaction of inhibitor with receptor, cofactor and waters.

3. Results and discussion

3.1. Structural stability and flexibility during MD simulations

A molecular dynamics simulation of arylamide B3 in InhA was performed. In order to compare the binding behavior of arylamides that show the highest and lowest InhA inhibitory activities, arylamides P2 and A10 in a InhA binding pocket were selected for MD simulations. Moreover, to compare the binding affinities of the substrate, *trans*-2-hexadecenoyl-(*N*-acetylcysteamine)-thioester, and of the arylamide inhibitors which are competitive inhibitors, a MD simulation of the substrate was carried out. The root mean square deviations (RMSD) as a function of the simulation time of each complex with respect to the starting structure were analyzed as shown in Fig. 1. RMSDs of all atoms of InhA in four complexes, InhA/NADH/substrate, InhA/NADH/B3, InhA/NADH/P2 and InhA/NADH/A10, reach the plateau characteristic at 0.5 ns, 1.5 ns, 1.0 ns and 2.0 ns, respectively. These results indicate that 6 ns unrestrained simulation is enough for stabilizing the fully relaxed systems.

The root mean square fluctuation (RMSF) of residues around the ligand-binding site of InhA (residues 96–104, 149–165, 192–223) was calculated to reveal the mobile flexibility of these residues.

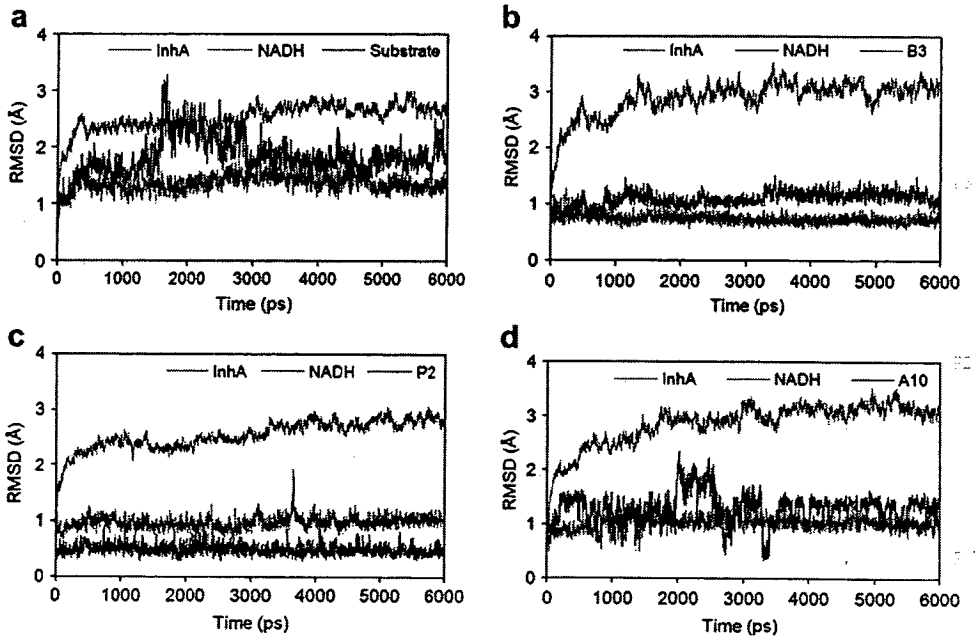

Fig. 1. RMSD of all atoms of each molecule in complexes of (a) InhA/NADH/substrate, (b) InhA/NADH/B3, (c) InhA/NADH/P2, and (d) InhA/NADH/A10.

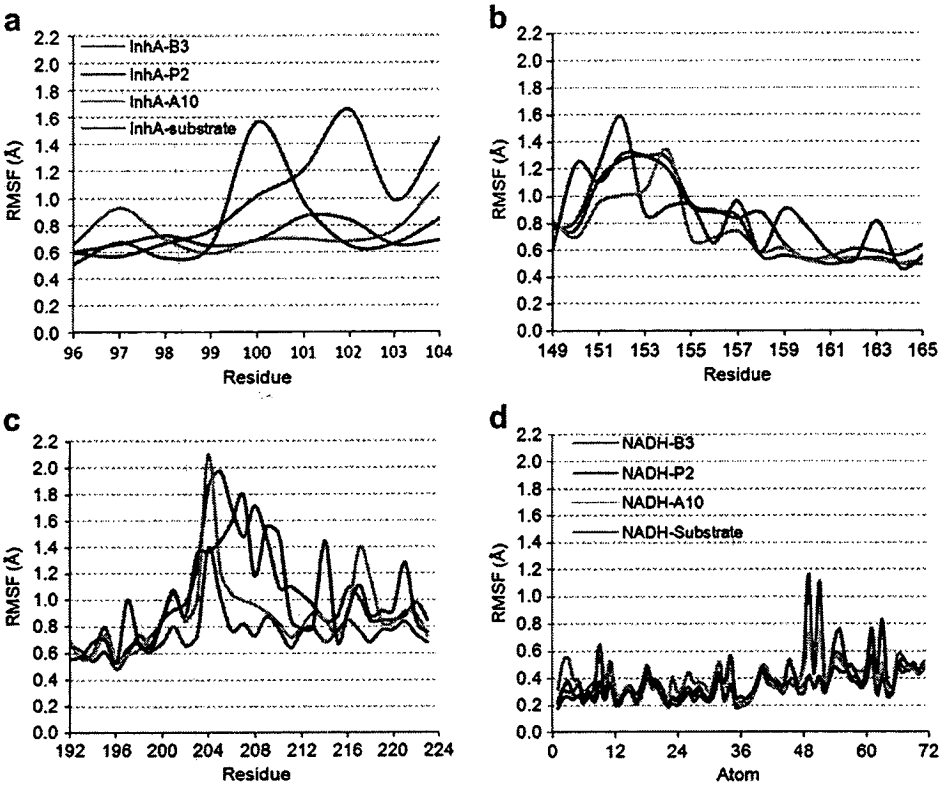

Fig. 2. RMSDF of residues (a) 96–104, (b) 149–165, (c) 192–223 and (d) NADH in four complexes.

RMSF of these residues are shown in Fig. 2(a)–(c). RMSF of all atoms of NADH that directly interacts with inhibitors and the substrate were also calculated as shown in Fig. 2(d). Fig. 2(a)–(c) clearly depict different flexibilities in the binding site of InhA when the substrate and arylamides B3, P2, A10 are bound to their binding sites. All residues of the InhA binding site that bind with the substrate and arylamide inhibitors show a small degree of flexibility with the RMSF less than 2.2 Å. Particularly, residues 96–99, 155–165 and 192–200 fluctuate less than 1 Å indicating that these residues seem to be rigid. These results indicate that the residues are not flexible enough to bind the substrate or arylamide inhibitors. Most of these rigid residues are located around the binding pocket of the aryl ring A of the arylamide inhibitors as shown in Fig. 3. In addition, NADH cofactor is also located adjacent to the aryl ring A of arylamide inhibitors as shown in Fig. 3. The dynamics flexibility of NADH co-binding with a substrate and arylamides B3, P2, A10 is shown in Fig. 2(d). All atoms of NADH seem to be rigid with a RMSF value less than 0.8 Å, except atoms 49 and 51 of NADH-B3 (hydrogen atoms at hydroxyl group of adenine ribose). Thus, the pocket size for the binding of the aryl ring A is limited by NADH cofactor and rigid residues surrounding this pocket. With regard to the substituent size on the aryl ring A of arylamides B3, P2, A10, arylamide P2, bearing the small substituent on the aryl ring A, shows an inhibitory activity better than arylamides B3 and A10 bearing the bulky substituents on the aryl ring A. These results suggest that the aryl ring A of arylamides should not contain too large substituents.

As illustrated in Fig. 2(a)–(c), RMSF of residues 100–104, 149–154 and 201–223 fluctuate in each complex in a wide range from 0.6 Å to 2.1 Å. These results indicate that the residues could be flexible enough for the binding of the substrate and arylamides B3, P2, A10. Most of these flexible residues colored by orange are located around the binding pocket of the substituent B of arylamide inhibitors as shown in Fig. 3. Focusing on the substituent B of arylamides, arylamide P2 bearing the large substituent of the fluorene ring shows the inhibitory activity better than arylamides B3 and A10 bearing the smaller substituent of the phenyl ring. These results imply that the bulky substituent could be incorporated into the substituent B of the arylamide inhibitors and seems to be favorable for inhibitory activity. However, the substituent B should not be too large because some rigid residues (residues 155–158) are also located near this substituent as shown in Fig. 3.

3.2. Structural change of InhA bound to the inhibitor and substrate

To study the structural change of InhA when the inhibitor and the substrate are bound, the superimposition of two X-ray crystal structures of arylamide B3 bound InhA (pdb code 2NSD) [38] and the substrate bound InhA (pdb code 1BVR) [48] was performed. The conformational differences of residues 198–223 including two α-helixes and one loop are shown in Fig. 4. The differences maybe affected by new positional rearrangements of these residues to accommodate the binding of the substrate and arylamide inhibitors. Therefore, the results derived from the superimposition of the experimental data [38,48] and the MD simulations as described above are consistent. The results obtained from both approaches indicate the flexibility of these residues for the binding of each ligand. NADH in two complexes is held at the same position implying that ligand binding has no effect on the binding of NADH cofactor. Arylamide B3 is bound in the same binding site with the substrate above the binding site of NADH. The obtained results clearly indicate that arylamides function as competitive inhibitors of InhA. This is supported by the kinetic study of arylamide proving that arylamide is competitive with the enoyl-CoA substrate [59].

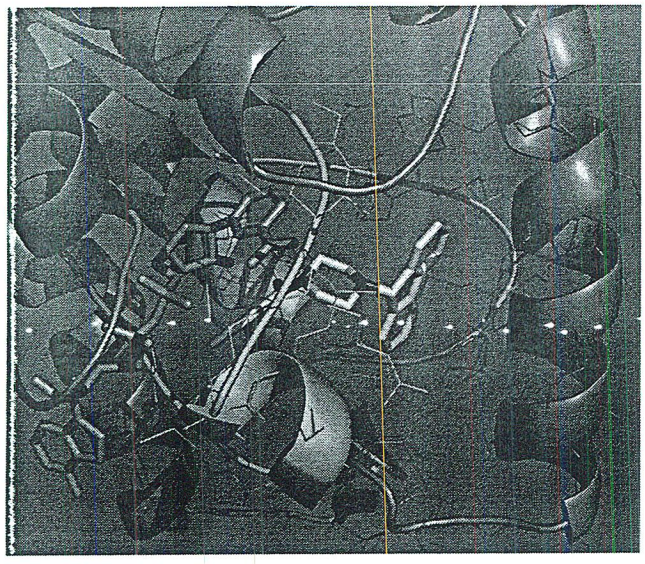

Fig. 3. The residues around the ligand-binding site of InhA (residues 96–104, 149–165, 192–223). The rigid residues colored by green, the flexible residues colored by orange, NADH colored by purple and compound P2 colored by yellow.

3.3. Ligand–InhA interactions

The competitive inhibitor function of arylamides should mimic the behavior of the substrate. When comparing structures of arylamide inhibitors and the substrate, the carbonyl moiety was found to be the only similar part. To compare the binding modes of the arylamide inhibitors and the substrate in an InhA binding pocket, the X-ray crystal structure of arylamide B3 was superimposed on the X-ray crystal structure of the substrate as shown in Fig. 5. The amide carbonyl oxygen of arylamide B3 and the thioester carbonyl oxygen of the substrate are positioned at the same place between two hydroxyl groups of Tyr158 and nicotinamide ribose of NADH. Therefore, the amide carbonyl oxygen is the selective part of arylamide inhibitors to reach the InhA binding pocket and to act as the competitive inhibitor. MD results are consistent with the experimental data which show the same binding site of the arylamide inhibitor and the substrate. The obtained results from MD simulations reveal that the amide carbonyl oxygen of arylamide B3 could form two hydrogen bonds with Tyr158 and NADH with distances of 1.68 Å and 1.76 Å, respectively. In the case of the substrate, the thioester carbonyl oxygen could not form hydrogen bonds with Tyr158 and NADH. However, this moiety is held in the same position with that of arylamide B3 by the hydrogen bond with a NH_3 sidechain of Lys165.

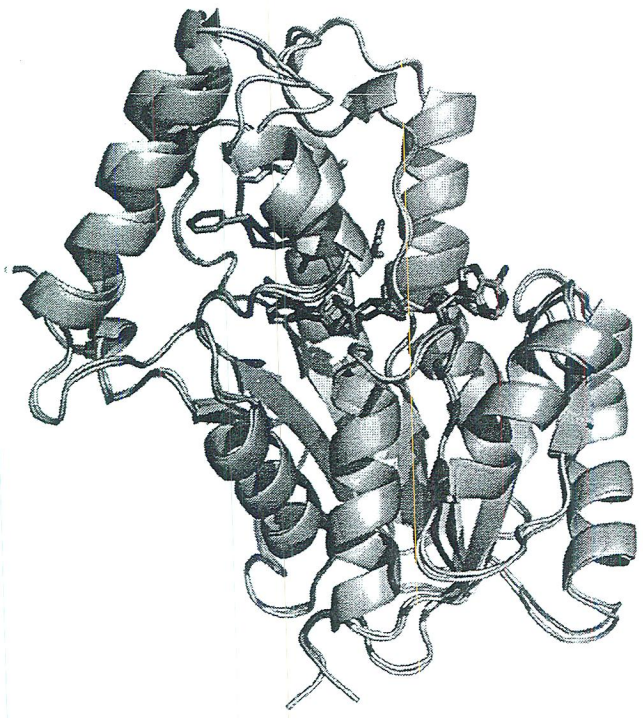

Fig. 4. Superimposition of InhA/B3/NADH of pdb code 2NSD (cyan and yellow), B3 and NADH labeled by orange. InhA/substrate/NADH of pdb code 1BVR (grey), substrate and NADH labeled by green.

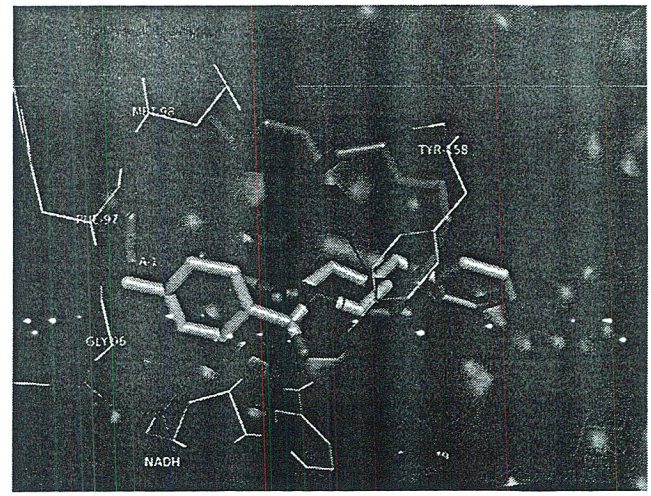

Fig. 5. Superimposition of X-ray crystal structures of arylamide B3 (grey) and substrate (purple) in the InhA binding pocket.

The aryl ring A of arylamide B3 lies in the same site as the acetylcysteamine moiety of the substrate. This binding site is surrounded by hydrophilic groups of pyrophosphate, nicotinamide ribose and amino acid backbones of Gly96, Phe97, Met98 and Ala198 as shown in Fig. 5. Thus, this binding site seems to be favored for the hydrophilic substituent. From MD simulations, NH and the acetyl oxygen of the acetylcysteamine moiety of the substrate form hydrogen bonds with the pyrophosphate oxygen of NADH and the NH backbone of Ala198 with the distance of 2.26 Å and 1.96 Å, respectively. On the other hand, the hydrogen bond interaction could not be found in the aryl ring A of arylamide B3. Besides the carbonyl moiety, it is possible to increase the selectivity of competitive arylamide inhibitors by introducing NH moiety and acetyl oxygen into the aryl ring A of arylamide inhibitors.

To support the influence of the NH moiety at the aryl ring A on the selectivity of competitive arylamide inhibitors, arylamides P4 and P6 were taken into account [38]. InhA inhibition activities of arylamides P4 and P6 are comparable with IC_{50} of 1.04 μM and 2.04 μM, respectively. Interestingly, arylamide P4 having aryl ring A substituted by indolyl group represents the best activity against the *M. tuberculosis* strain with the minimum inhibitory concentrations (MIC) of 62.5 μM. On the other hand, arylamide P6 having aryl ring A substituted by a phenyl group shows higher MIC of 125 μM. The results indicate that a NH moiety at the aryl ring A could increase the selectivity of competitive arylamide inhibitors to reach the InhA target leading to increase the MIC value. To clarify this fact in detail, arylamide P3 where an indolyl group is located at the aryl ring A [38] was also taken into account. Because of the availability of the X-ray structure of arylamide P3 [59], a superimposition of the X-ray crystal structure of P3 bound InhA (pdb code 1P44) and the X-ray

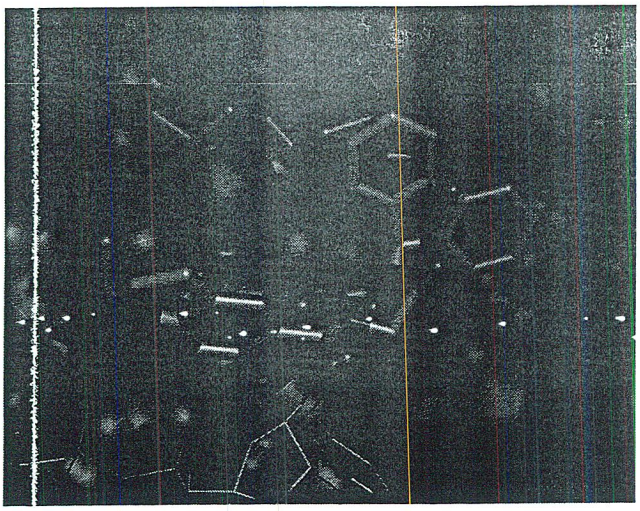

Fig. 6. Superimposition of X-ray crystal structures of arylamide P3 (pink) and substrate (purple) in the InhA binding pocket.

crystal structure of substrate-bound InhA (pdb code 1BVR) was performed (Fig. 6). It was found that NH moiety of arylamide P3 is located at the same position as the NH moiety of the substrate confirming the role of the NH moiety in the aryl ring A of arylamide inhibitors. However, arylamide P3 possessing the lower MIC maybe affected by its poor membrane permeability [38].

The substituent B of arylamide B3 lies in the same site as the fatty acyl chain of the substrate surrounded by the hydrophobic residues 100–104, 149–154 and 201–223 as shown in Fig. 5. This result reveals that the lipophilic substituent is favored for this binding site. Therefore, a greater lipophilicity of the substituent B as well as of the fatty acyl chain of the substrate should enhance the binding of arylamide inhibitors. Moreover, it should increase the membrane permeability of arylamide inhibitors.

For a better understanding of the binding behaviors of arylamide inhibitors in InhA binding pocket, MD simulations of arylamides P2 and A10 were performed. The binding mode of arylamide P2, with the highest InhA inhibitory activity, is shown in Fig. 7. This arylamide is bound to the InhA binding pocket in the same fashion as in the X-ray crystal structure of arylamide B3. The amide carbonyl oxygen of arylamide P2 is held by two hydrogen bonds of Tyr158 and NADH with distances of 1.97 and 1.69 Å, respectively.

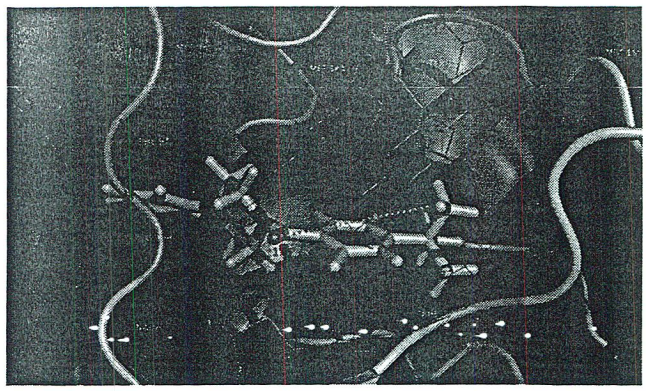

Fig. 8. The binding mode of arylamide A10 in the InhA binding pocket obtained from MD simulation.

The aryl ring A is placed in the hydrophilic pocket, whereas the substituent B, the fluorene ring, is located in the hydrophobic pocket. In the case of the compound with the lowest InhA inhibitory activity, arylamide A10, its binding mode is very different from those of arylamides B3 and P2 as presented in Fig. 8. The aryl ring A of arylamide A10 is switched to bind to the hydrophobic pocket of substituent B. This result clearly shows that the aryl ring A with the bulky substituent as well as the t-butyl group cannot be occupied in the hydrophilic pocket because of the rigidity of this binding site as previously explained. Resulting from the conformational change, the amide carbonyl oxygen of arylamide A10 loses a crucial hydrogen bond contact with Tyr158. Only the hydrogen bond with the hydroxyl group of nicotinamide ribose (1.67 Å) could be observed during the MD simulation as shown in Fig. 8. To confirm the influence of the bulky substituent of the aryl ring A on the InhA inhibitory activity, arylamide A9 [38], one of the lowest active compounds was selected for further studies. Based on the obtained MD simulation results, arylamide A9 is bound to the InhA binding pocket in the same way as arylamides B3 and P2 (Fig. 9). In contrast to the MD simulation structure of arylamide A10 (Fig. 8), the aryl ring A of arylamide A9 could be located in the hydrophilic pocket. However, the iso-propyl substituent of the aryl ring A causes the loss of a crucial hydrogen bond with the hydroxyl group of nicotinamide ribose as shown in Fig. 9. It is obvious, that the bulky substituent of the aryl ring A is not favorable for InhA binding of arylamide inhibitors. These obtained results could successfully

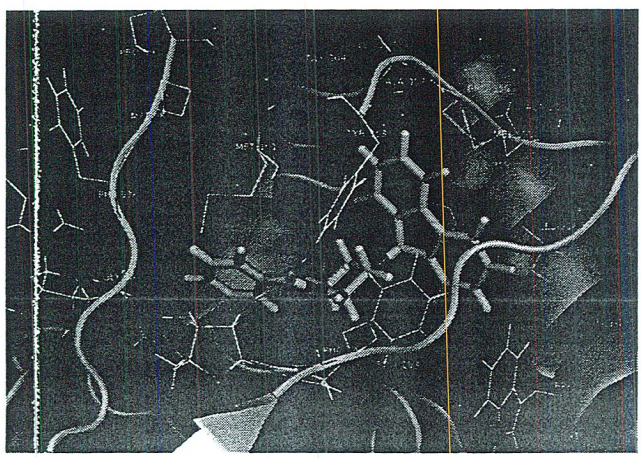

Fig. 7 The binding mode of arylamide P2 in the InhA binding pocket obtained from MD simulation.

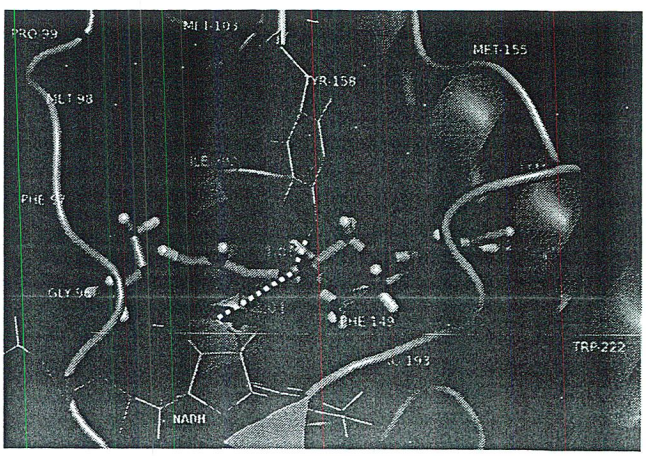

Figure 9. The binding mode of arylamide A9 in the InhA binding pocket obtained from MD simulation.

confirm the structural requirements of the substituent of the aryl ring A of arylamide inhibitors.

3.4. Interaction energy

The interaction energies between arylamide inhibitors and particular amino acids within 6 Å of each arylamide inhibitor were calculated to explore the contribution of each residue. Arylamides P2 and B3 show the highest attractive interaction energies with NADH and Tyr158 as shown in Table 2. These high attractive energies are consistent with the two strong hydrogen bonds observed between the arylamide inhibitors and NADH and Tyr158. In the case of arylamide A10, the interaction energies with Tyr158 and NADH are related to results obtained from MD simulations. A lower attractive interaction energy with Tyr158 can be found because of the loss of the hydrogen bond, whereas the interaction energy with NADH is still high. These results reveal that two hydrogen bonds are essential for the affinity of the arylamide inhibitors in the InhA binding pocket. The substituent B of arylamide P2 interacts with hydrophobic residues more than those of arylamides B3 and A10 as shown in Table 2. Therefore, more interactions with hydrophobic residues of the substituent B could enhance the binding of arylamides in InhA which is clearly shown by the InhA inhibition activity of arylamides P2, B3 and A10.

3.5. The binding free energy

To gain quantitative insights into the affinity for binding of arylamide inhibitors in the InhA binding site, the binding free energies of arylamide–InhA complexes were calculated by the LIE method. In addition, the binding free energy of the substrate is also calculated to compare the binding affinities of the substrate and the competitive arylamide inhibitors. Only the binding free energy of arylamide P2 (−24.99 kJ/mol) shows a higher value than that of substrate (−11.67 kJ/mol) (Table 3). Consequently, the InhA inhibition activity of arylamide P2 is better than those of arylamides B3 and A10 (binding free energies −9.18 kJ/mol and −6.59 kJ/mol, respectively). It is notable that the calculated free binding energies of inhibitors are in the correct order as compared with the IC_{50} values. The obtained results could be successfully used to validate the MD procedure in this study.

Table 2
Average interaction energies between arylamide inhibitors and the particular residue in InhA binding pocket.

The inhibitor portion	Residue	Interaction energy (kJ/mol)		
		A10	B3	P2
The aryl ring A	Gly96	−12.56	−6.49	−7.43
	Phe97	−3.72	−5.17	−1.67
	Met98	−1.75	−2.64	−0.62
	Met103	−12.69	−15.15	−14.18
	Met161	−14.54	−10.20	−6.02
	Lys165	−5.64	–	−3.69
	Leu197	–	–	−5.76
	Ala198	−17.40	−8.07	−21.05
	Ala201	−2.82	–	−1.00
	Ile202	−10.30	−13.69	−1.86
The amide carbonyl	NADH	−149.46	−98.69	−104.95
	Tyr158	−27.21	−68.36	−57.51
The substituent B	Phe149	−9.89	−20.94	−32.79
	Ser152	–	−0.04	−6.31
	Arg153	–	−2.23	−0.32
	Ala154	–	−8.14	−2.94
	Met155	−7.09	−11.80	−7.27
	Pro156	–	−11.75	−21.27
	Ala157	–	−2.76	−11.32
	Gly192	−3.52	–	−0.66
	Pro193	−10.37	−8.92	−10.67
	Ile194	−10.88	–	−2.09
	Thr196	−3.62	−2.53	−2.87
	Met199	−21.86	−20.46	−0.48
	Val203	–	−7.97	–
	Ile215	−11.16	−5.35	−17.05
	Leu218	–	−4.08	−2.28
	Trp222	–	–	−9.06
	Met232	–	–	−4.92

Table 3
The estimate binding free energies (kJ/mol) of arylamide inhibitors and substrate calculated by LIE method.

Compound	IC_{50} (μM)[a]	$(V_{LJ})_{bound}$	$(V_{LJ})_{free}$	$(V_{CL})_{bound}$	$(V_{CL})_{free}$	ΔG_{bind}
A10	>100	−294.39	−184.34	−63.84	−90.50	−6.59
B3	5.16	−288.96	−184.93	−81.18	−100.48	−9.18
P2	0.09	−327.50	−160.36	−77.13	−87.65	−24.99
Substrate	–	−343.36	−188.50	−97.06	−129.78	−11.67

[a] IC_{50} of all inhibitors were taken from literature [36]. The nomenclature of the inhibitors was taken from the original literature and is also given in Table 1.

3.6. The structural basis for inhibitor design

Many arylamides show high potency for inhibiting the InhA enzyme [38]. The highest InhA inhibitory activity with IC_{50} of 0.09 μM, could be observed for the arylamide P2. However, most of the arylamides with the best InhA inhibitory activities show lower *M. tuberculosis* growth inhibition with MIC against *M. tuberculosis* strain above 125 μM. These results suggest that arylamide inhibitors have poor membrane permeability and maybe lower selectivity to reach the enzyme target. Based on our finding, the amide carbonyl oxygen is selective for arylamide inhibitors for InhA inhibition. When simulating the behavior of the acetylcysteamine moiety of the substrate, it is possible to increase the selectivity of arylamide inhibitors by introducing NH or an acetyl oxygen into the aryl ring A. However, the hydrophilic pocket related to the aryl ring A seems to be rigid and unfavorable for a bulky substituent. Thus, the substituent of the aryl ring A should not be too large. Substituent B is located close to hydrophobic residues. Therefore, substituents B, with a higher lipophilicity as well as the fatty acyl chain of the substrate, should enhance the binding affinity of arylamide inhibitors. Moreover, it could help to increase the membrane permeability of arylamide inhibitors leading to improve *M. tuberculosis* growth inhibition. As seen from MD simulations, a bulky lipophilic substituent could be incorporated into the substituent B, because its hydrophobic pocket seems to be flexible enough for ligand binding.

4. Conclusion

The dynamic behavior in terms of flexibility, conformation and the inhibitor–enzyme interaction of arylamide inhibitors and the substrate in the InhA binding pocket was successfully explained by MD simulations using the program package Gromacs. Based on MD simulations, only the hydrophobic binding pocket of InhA is flexible enough to bind arylamide inhibitors and the substrate. These results allow us to gain insight into some structural requirements of arylamide inhibitors to bind to InhA. When comparing the dynamic behavior of competitive arylamide inhibitors and the substrate in the InhA binding pocket, some substituents of arylamide inhibitors should be imitated from the substrate structure. The amide carbonyl oxygen is highly essential for the affinity of the arylamide inhibitor InhA interactions. The presence of small hydrophilic substituents at the aryl ring A of the arylamide inhibitors, as well as NH and the acetyl oxygen in the acetylcysteamine moiety of the

substrate should improve arylamide selectivity. A bulky substituent with higher lipophilicity as well as the fatty acyl chain of the substrate, should enhance the binding affinity of the arylamide inhibitors. Moreover, it could increase their membrane permeability. Based on our findings, the correct balance between the hydrophilic property of the aryl ring A and the lipophilic property of the substituent B should improve suitable therapeutic activity against *M. tuberculosis* strain. Therefore, this study should facilitate the design of new and more potentially effective antitubercular agents.

Acknowledgements

This research was supported by the Thailand Research Fund (DBG5380006, RTA5080005 and MRG5080267). A. Punkvang is grateful to the grant from under the program Strategic Scholarships for Frontier Research Network for the Ph.D. ASEA-UNINET and Vienna Scientific Cluster are gratefully acknowledged for research support.

References

[1] World Health Organization, Multidrug and Extensively Drug-resistant TB (M/XDR-TB) Global report on surveillance and response. WHO, 2010.
[2] A. Quémard, J.C. Sacchettini, A. Dessen, C. Vilcheze, R. Bittman, W.R. Jacobs Jr., J.S. Blanchard, Enzymatic characterization of the target for isoniazid in *Mycobacterium tuberculosis*, Biochemistry 34 (1995) 8235–8241.
[3] J.W. Campbell, J.E. Cronan Jr., Bacterial fatty acid biosynthesis: targets for antibacterial drug discovery, Annu. Rev. Microbiol. 55 (2001) 305–332.
[4] R.J. Heath, C.O. Rock, Fatty acid biosynthesis as a target for novel antibacterials, Curr. Opin. Invest. Drugs 5 (2004) 146–153.
[5] S.W. White, J. Zheng, Y.M. Zhang, C.O. Rock, The structural biology of type II fatty acid biosynthesis, Annu. Rev. Biochem. 74 (2005) 791–831.
[6] Y.M. Zhang, Y.J. Lu, C.O. Rock, The reductase steps of the type II fatty acid synthase as antimicrobial targets, Lipids 39 (2004) 1055–1060.
[7] L. Wen, J.N. Chmielowski, K.C. Bohn, J.K. Huang, Y.N. Timsina, P. Kodali, A.K. Pathak, Functional expression of *Francisella tularensis* FabH and FabI, potential antibacterial targets, Protein Exp. Purif. 65 (2009) 83–91.
[8] H.T. Wright, K.A. Reynolds, Antibacterial targets in fatty acid biosynthesis, Curr. Opin. Microbiol. 10 (2007) 447–453.
[9] D.A. Rozwarski, G.A. Grant, D.H. Barton, W.R. Jacobs Jr., J.C. Sacchettini, Modification of the NADH of the isoniazid target (InhA) from *Mycobacterium tuberculosis*, Science 279 (1998) 98–102.
[10] C. Vilchèze, F. Wang, M. Arai, M.H. Hazbón, R. Colangeli, L. Kremer, T.R. Weisbrod, D. Alland, J.C. Sacchettini, W.R. Jacobs Jr., Transfer of a point mutation in *Mycobacterium tuberculosis* inhA resolves the target of isoniazid, Nat. Med. 12 (2006) 1027–1029.
[11] A. Dessen, A. Quémard, J.S. Blanchard, W.R. Jacobs Jr., J.C. Sacchettini, Crystal structure and function of the isoniazid target of *Mycobacterium tuberculosis*, Science 267 (1995) 1638–1641.
[12] B. Lei, C.J. Wei, S.C. Tu, Action mechanism of antitubercular isoniazid. Activation by *Mycobacterium tuberculosis* KatG, isolation, and characterization of inha inhibitor, J. Biol. Chem. 275 (2000) 2520–2526.
[13] K. Johnsson, D.S. King, P.G. Schultz, Studies on the mechanism of action of isoniazid and ethionamide in the chemotherapy of tuberculosis, J. Am. Chem. Soc. 117 (1995) 5009–5010.
[14] A. Quémard, A. Dessen, M. Sugantino, W.R. Jacobs Jr., J.C. Sacchetini, J.S. Blanchard, Binding of catalase-peroxidase-activated isoniazid to wild-type and mutant *Mycobacterium tuberculosis* enoyl-ACP reductases, J. Am. Chem. Soc. 118 (1996) 1561–1562.
[15] B. Saint-Joanis, H. Souchon, M. Wilming, K. Johnsson, P.M. Alzari, S.T. Cole, Use of site-directed mutagenesis to probe the structure, function and isoniazid activation of the catalase/peroxidase, KatG, from Mycobacterium tuberculosis, Biochem. J. 338 (1999) 753–760.
[16] X. Zhao, H. Yu, S. Yu, F. Wang, J.C. Sacchettini, R.S. Magliozzo, Hydrogen peroxide-mediated isoniazid activation catalyzed by *Mycobacterium tuberculosis* catalase-peroxidase (KatG) and its S315T mutant, Biochemistry 45 (2006) 4131–4140.
[17] C. Metcalfe, I.K. Macdonald, E.J. Murphy, K.A. Brown, E.L. Raven, P.C. Moody, The tuberculosis prodrug isoniazid bound to activating peroxidases, J. Biol. Chem. 283 (2008) 6193–6200.
[18] B.K. Sinha, enzymatic activation of hydrazine derivatives, J. Biol. Chem. 258 (1983) 796–801.
[19] M. Nguyen, C. Claparols, J. Bernadou, B. Meunier, A fast and efficient metal-mediated oxidation of isoniazid and identification of isoniazid-NAD(H) adducts, Chem. Bio. Chem. 2 (2001) 877–883.
[20] B. Heym, Y. Zhang, S. Poulet, D. Young, S.T. Cole, Characterization of the katG gene encoding a catalase-peroxidase required for the isoniazid susceptibility of *Mycobacterium tuberculosis*, J. Bacteriol. 175 (1993) 4255–4259.
[21] K. Johnsson, P.G. Schultz, Mechanistic studies of the oxidation of isoniazid by the catalase peroxidase from *Mycobacterium tuberculosis*, J. Am. Chem. Soc. 116 (1994) 7425–7426.
[22] G.S. Timmins, V. Deretic, Mechanisms of action of isoniazid, Mol. Microbiol. 62 (2006) 1220–1227.
[23] K. Johnsson, W.A. Froland, P.G. Schultz, Overexpression, purification, and characterization of the catalase-peroxidase KatG from *Mycobacterium tuberculosis*, J. Biol. Chem. 272 (1997) 2834–2840.
[24] C. Vilcheze, H.R. Morbidoni, T.R. Weisbrod, H. Iwamoto, M. Kuo, J.C. Sacchettini, W.R. Jacobs Jr., Inactivation of the inhA-encoded fatty acid synthase II (FASII) enoyl-acyl carrier protein reductase induces accumulation of the FASI end products and cell lysis of *Mycobacterium smegmatis*, J. Bacteriol. 182 (2000) 4059–4067.
[25] A.S. Piatek, A. Telenti, M.R. Murray, H. El-Hajj, W.R. Jacobs Jr., F.R. Kramer, D. Alland, Genotypic analysis of *Mycobacterium tuberculosis* in two distinct populations using molecular beacons: implications for rapid susceptibility testing, Antimicrob. Agents Chemother. 44 (2000) 103–110.
[26] R.A. Slayden, C.E. Barry 3rd, The genetics and biochemistry of isoniazid resistance in *Mycobacterium tuberculosis*, Microbes Infect. 2 (2000) 659–669.
[27] M.J. Torres, A. Criado, J.C. Palomares, J. Aznar, Use of real-time PCR and fluorimetry for rapid detection of rifampin and isoniazid resistance-associated mutations in *Mycobacterium tuberculosis*, J. Clin.Microbiol. 38 (2000) 3194–3199.
[28] Y. Zhang, B. Heym, B. Allen, D. Young, S. Cole, The catalaseperoxidase gene and isoniazid resistance of *Mycobacterium tuberculosis*, Nature 358 (1992) 591–593.
[29] J.S. Oliveira, J.H. Pereira, F. Canduri, N.C. Rodrigues, O.N. de Souza, W.F. de Azevedo Jr., L.A. Basso, D.S. Santos, Crystallographic and pre-steady-state kinetics studies on binding of NADH to wild-type and isoniazid-resistant enoyl-ACP(CoA) reductase enzymes from *Mycobacterium tuberculosis*, J. Mol. Biol. 359 (2006) 646–666.
[30] M.R. Marques, J.H. Pereira, J.S. Oliveira, L.A. Basso, D.S. Santos, W.F. de Azevedo Jr., M.S. Palma, The inhibition of 5-enolpyruvylshikimate-3-phosphate synthase as a model for development of novel antimicrobials, Curr. Drug Targets 8 (2007) 445–457.
[31] A.I. De La Iglesia, H.R. Morbidoni, Mechanisms of action of and resistance to rifampicin and isoniazid in *Mycobacterium tuberculosis*: new information on old friends, Rev. Argent Microbiol. 38 (2006) 97–109.
[32] A. Banerjee, E. Dubnau, A. Quemard, V. Balasubramanian, K.S. Um, T. Wilson, D. Collins, G. de Lisle, W.R. Jacobs Jr., Inha, a gene encoding a target for isoniazid and ethionamide in *Mycobacterium tuberculosis*, Science 263 (1994) 227–230.
[33] J.S. Freundlich, F. Wang, C. Vilchèze, G. Gulten, R. Langley, G.A. Schiehser, D.P. Jacobus, W.R. Jacobs Jr., J.C. Sacchettini, Triclosan derivatives: towards potent inhibitors of drug-sensitive and drug-resistant *Mycobacterium tuberculosis*, Chem. Med. Chem. 4 (2009) 241–248.
[34] C.W. Am Ende, S.E. Knudson, N. Liu, J. Childs, T.J. Sullivan, M. Boyne, H. Xu, Y. Gegina, D.L. Knudson, F. Johnson, C.A. Peloquin, R.A. Slayden, P.J. Tonge, Synthesis and in vitro antimycobacterial activity of B-ring modified diaryl ether InhA inhibitors, Bioorg. Med. Chem. Lett. 18 (2008) 3029–3033.
[35] M.E. Boyne, T.J. Sullivan, C.W. Am Ende, H. Lu, V. Gruppo, D. Heaslip, A.G. Amin, D. Chatterjee, A. Lenaerts, P.J. Tonge, R.A. Slayden, Targeting fatty acid biosynthesis for the development of novel chemotherapeutics against *Mycobacterium tuberculosis*: evaluation of A-ring-modified diphenyl ethers as high-affinity InhA inhibitors, Antimicrob. Agents Chemother. 51 (2007) 3562–3567.
[36] P.J. Tonge, C. Kisker, R.A. Slayden, Development of modern InhA inhibitors to combat drug resistant strains of *Mycobacterium tuberculosis*, Curr. Top. Med. Chem. 7 (2007) 489–498.
[37] X. He, A. Alian, R. Stroud, P.R. Ortiz de Montellano, Pyrrolidine carboxamides as a novel class of inhibitors of enoyl acyl carrier protein reductase from Mycobacterium tuberculosis, J. Med. Chem. 49 (2006) 6308–6323.
[38] X. He, A. Alian, P.R. Ortiz de Montellano, Inhibition of the *Mycobacterium tuberculosis* enoyl acyl carrier protein reductase InhA by arylamides, Bioorg. Med. Chem. 15 (2007) 6649–6658.
[39] S. Alcaro, A. Artese, F. Ceccherini-Silberstein, F. Ortuso, C.F. Perno, T. Sing, V. Svicher, Molecular dynamics and free energy studies on the wild-type and mutated HIV-1 protease complexed with four approved drugs: mechanism of binding and drug resistance, J. Chem. Inf. Model 49 (2009) 1751–1761.
[40] H.A. Wahab, Y.S. Choong, P. Ibrahim, A. Sadikun, T. Scior, Elucidating isoniazid resistance using molecular modeling, J. Chem. Inf. Model 49 (2009) 97–107.
[41] A. Ivetac, J.A. McCammon, Elucidating the inhibition mechanism of HIV-1 non-nucleoside reverse transcriptase inhibitors through multicopy molecular dynamics simulations, J. Mol. Biol. 388 (2009) 644–658.
[42] J.J. Tan, R. Kong, C.X. Wang, W.Z. Chen, Molecular dynamics simulation on the complexes of N-terminal region of HIV-1 gp41 and its C-peptide inhibitors, Theochem 682 (2004) 9–15.
[43] S. Weerasinghe, R. Samantha Dassanayake, Simulation of structural and functional properties of mevalonate diphosphate decarboxylase (MVD), J. Mol. Model. 16 (2010) 489–498.
[44] V. Nukoolkarn, V.S. Lee, M. Malaisree, O. Aruksakulwong, S. Hannongbua, Molecular dynamic simulations analysis of ritonavir and lopinavir as SARS-CoV 3CL(pro) inhibitors, J. Theor. Biol. 254 (2008) 861–886.

group, hydrophobic and hydrogen donor properties. The substituent attached to the 2 and 3 position of phenyl ring C suggested that bulky substituent, electron withdrawing, hydrophobic and properties. The substituent attached to the 4 position of phenyl ring C for WT and K103N/Y181C HIV-1 RT binding pockets suggested that bulky substituent, electron withdrawing group and hydrogen acceptor hydrophobic. The substituent attached to the 6 position of phenyl ring C for WT and K103N/Y181C HIV-1 RT binding pockets suggested that small substituent, electron withdrawing group, hydrophobic and hydrogen donor properties on these positions to enhance the inhibitory activity against the WT and K103N/Y181C HIV-1 RT.

The obtained results from ONIOM (ONIOM2) method demonstrate that residues around the binding pocket (Lys101, Lys103Asn, Tyr181Cys, Phe227, Trp229 and Glu138 of the p51 palm domain) are the main contribution for WT and the K103N/Y181C HIV-1 RT binding pockets.

Based on the binding energy, the mutations of amino acid residues are decreasing the stability of DAPY in HIV-1 RT binding pocket. The structural basis derived from molecular docking, QSAR and ONIOM2 approaches provide a gainful guideline to design highly potent DAPYs for WT and K103N/Y181C HIV-1 RT inhibitions. Based on the integrated results, 19 and 7 newly designed compounds for WT and K103N/Y181C HIV-1 RT inhibitions, respectively showing the higher inhibitory activities as compared with the parent compounds have been proposed in this study.

INH for tuberculosis treatment can be diminished if mutations arise in KatG, as found in previous clinical studies [18, 28]. Therefore, new inhibitors targeting the InhA without the activation process from KatG are required. The first inhibitor, triclosan, inhibiting the InhA directly has been reported [29]. Based on the mechanism action of triclosan, triclosan and diphenyl ether derivatives have been developed by using structure-based drug design [30–35]. A diphenyl ether derivative, 5-octyl-2-phenoxy phenol, shows the highest potent InhA inhibitor with IC_{50} of 5 nM [33]. Recently, molecular modeling and computer-aided molecular design approaches have been performed to develop the InhA inhibitors [36–48]. To gain insight into the structural requirement of highly potent diphenyl ether derivatives as the InhA inhibitors, three-dimensional quantitative structure–activity relationships (3D-QSAR) based on comparative molecular similarity indices analysis (CoMSIA) was performed. Moreover, molecular dynamics (MD) simulations were also performed to gain deeper insight into a fundamental basis of structural behavior, inhibitor–InhA interactions and thermodynamic properties. The molecular information obtained from both CoMSIA and MD simulations should be valuable for the design of new and better InhA inhibitors as anti-tubercular agents.

Materials and methods

Data sets for QSAR study

The 52 diphenyl ether derivatives [30, 31, 33, 35] listed in Table 1 were used to build the CoMSIA model. The experimentally obtained IC_{50} values of each compound for InhA inhibition were converted to the corresponding log ($1/IC_{50}$) values and used as dependent variables for the QSAR model. The chemical structures of these compounds were constructed using standard tools available in the GaussView 3.07 program [49] and were then fully optimized using the ab initio quantum chemical method (HF/3-21G) implemented in the Gaussian 09 program [50]. The compounds were divided into a training set of 43 compounds, and a test set of nine compounds for model development and validation, respectively. The test set was randomly selected based on a structural diversity and wide range of activity in the data sets.

Molecular docking calculations

The X-ray crystal structure of diphenyl ether complexed with InhA (PDB code 2X23) [34] was used as a template for molecular docking calculations. Docking calculations for all 52 diphenyl ether derivatives were carried out by the Autodock 4.02 program using the Lamarckian genetic algorithm (LGA) [51]. Docking parameters were used as default values, except for the number of docking runs, which was set to 50. The parameters of the docking calculations were validated by successfully reproducing the X-ray conformation of the ligand in the PDB structure 2X23, as well as its orientation in the binding pocket. The RMSD value between original and docked coordinates was lower than 1 Å and therefore acceptable. For all 52 candidate compounds, the ligand pose with the lowest final docked energy was selected as the best binding mode of these potential InhA inhibitors.

CoMSIA study

The binding mode of compound **21**, representing the best active compound for the InhA inhibition, was taken from the X-ray structure (PDB code 2B37) [33] and used as a template for molecular alignment. The pharmacophore alignment module with the GALAHAD fit implemented in SYBYL 8.0 program [52] was employed to align all compounds to the molecular template. SYBYL 8.0 molecular modeling software was then used to construct CoMSIA models. Five CoMSIA descriptors including steric, electrostatic, hydrophobic, hydrogen bond donor, and hydrogen bond acceptor fields were calculated using an sp^3 carbon probe atom, with a formal charge of +1, which was placed at the intersections in a grid spacing of 2 Å. CoMSIA descriptors were set as independent variables and log ($1/IC_{50}$) values were used as dependent variables in the partial least square (PLS) analysis to derive a linear relationship between molecular descriptors and activities. The cross-validation was performed using the leave-one-out method with a 2.0-kcal/mol^{-1} column filter to minimize the influence of noisy columns. A final non-cross-validated analysis with the optimal number of components was sequentially performed and was then employed to analyze the results. The non-cross-validated correlation coefficient (r^2) and the leave-one-out (LOO) cross-validated correlation coefficient (q^2) were used to evaluate the predictive ability of the CoMSIA model. To estimate the predictive abilities of the best CoMSIA model, external validation using several statistical data was employed. According to Golbraikh and Tropsha [53], the best CoMSIA model is considerably acceptable if they satisfy all of the following criteria: $q^2>0.50$, $r^2>0.60$, and $0.85 \leq k \leq 1.15$.

MD simulations

In a subsequent step, MD simulations were performed on compounds **17**, **18**, **19**, and **29**, which are representative compounds that cover a wide range from highly active (**17** and **29**) to less active compounds (**18**) among the candidate series in this study. Compound **19** was also included in the simulations to represent a moderate inhibitory activity.

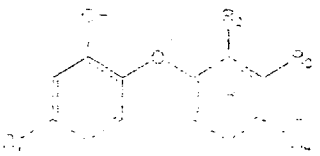

CHAPTER 5

CONCLUSIONS

Computer aided molecular design based on molecular docking calculation, QSAR and quantum chemical calculations (ONIOM) methods were successfully applied to discriminate structural requirements between WT and K103N/Y181C inhibitory activities of the DAPY inhibitors.

The obtained results from molecular docking calculations demonstrate that the important interaction of diarylpyrimidine compounds against the WT and K103N/Y181C HIV-1 RT binding pockets are hydrogen bonding interaction between carbonyl oxygen atom of Lys101 with hydrogen atom of amine group for phenyl ring A. Nitrogen atom of pyrimidine ring B could form hydrogen bonding interaction with hydrogen atom of Lys101. The pyrimidine ring B of inhibitor TMC278 could form hydrogen-pi interaction with Leu100. The phenyl ring C could form hydrogen-pi interaction with Trp229. For R_1 and R_2 substituents the results suggest that should be hydrogen atom to enhance the inhibitory activity. For X substituent the results suggest that should be amine group to enhance the inhibitory activity. For R_3 substituent attached to the 2-position should be bulky group to enhance the inhibitory activity. The R_3 substituent attached to the 4-position should be cyanovinyl group to form hydrogen bonding interaction with Phe227 and Trp229. The R_3 substituent attached to the 6-position should be methoxy group to form hydrogen -pi interaction with Tyr181 for WT HIV-1 RT binding pocket.

The obtained results from 3D-QSAR analyses demonstrate that structural requirement at R_1, R_2, X and R_3 substituent of diarylpyrimidine derivatives on the WT and K103N/Y181C HIV-1 RT binding pockets flowering; R_1 substituent for WT HIV-1 RT binding pocket suggested that favorable hydrophilic and electron donating group. R_1 substituent for K103N/Y181C HIV-1 RT binding pocket suggested that small substituent and hydrophobic properties. R_2 substituent for WT and K103N/Y181C HIV-1 RT binding pockets suggested that small substituent, electron donating group, hydrophobic and hydrogen donor properties. X substituent for WT and K103N/Y181C HIV-1 RT binding pockets suggested that small substituent, electron donating

J Mol Model (2014) 20:2319
DOI 10.1007/s00894-014-2319-0

ORIGINAL PAPER

Elucidating the structural basis of diphenyl ether derivatives as highly potent enoyl-ACP reductase inhibitors through molecular dynamics simulations and 3D-QSAR study

Pharit Kamsri · Auradee Punkvang · Patchareenart Saparpakorn · Supa Hannongbua · Stephan Irle · Pornpan Pungpo

Received: 30 December 2013 / Accepted: 26 May 2014

Abstract Diphenyl ether derivatives are good candidates for anti-tuberculosis agents that display a promising potency for inhibition of InhA, an essential enoyl-acyl carrier protein (ACP) reductase involved in fatty acid biosynthesis pathways in *Mycobacterium tuberculosis*. In this work, key structural features for the inhibition were identified by 3D-QSAR CoMSIA models, constructed based on available experimental binding properties of diphenyl ether inhibitors, and a set of four representative compounds was subjected to MD simulations of inhibitor-InhA complexes for the calculation of binding free energies. The results show that bulky groups are required for the R_1 substituent on the phenyl A ring of the inhibitors to favor a hydrophobic pocket formed by residues Phe149, Met155, Pro156, Ala157, Tyr158, Pro193, Met199, Val203, Leu207, Ile215, and Leu218. Small substituents with a hydrophilic property are required at the R_3 and R_4 positions of the inhibitor phenyl B rings to form hydrogen bonds with the backbones of Gly96 and Met98, respectively. For the R_2 substituent, small substituents with simultaneous hydrophilic or hydrophobic properties are required to favor the interaction with the pyrophosphate moiety of NAD^+ and the methyl side chain of Ala198, respectively. The reported data provide structural guidance for the design of new and potent diphenyl ether-based inhibitors with high inhibitory activities against *M. tuberculosis* InhA.

Keywords *M. tuberculosis* · InhA · 3D-QSAR · MD simulation · Diphenyl ether inhibitors

This paper belongs to Topical Collection 9th European Conference on Computational Chemistry (EuCo-CC9)

Electronic supplementary material The online version of this article (doi:10.1007/s00894-014-2319-0) contains supplementary material, which is available to authorized users.

P. Kamsri · P. Pungpo (✉)
Department of Chemistry, Faculty of Science, Ubon Ratchathani University, 85 Sthollmark Rd., Warinchamrap, Ubonratchathani 34190, Thailand
e-mail: pornpan_ubu@yahoo.com

A. Punkvang
Faculty of Liberal Arts and Sciences, Division of Science, Nakhon Phanom University, Nakhon Phanom 48000, Thailand

P. Saparpakorn · S. Hannongbua
Department of Chemistry, Faculty of Science, Kasetsart University, Chatuchak, Bangkok 10900, Thailand

S. Irle
Institute of Transformative Bio-Molecules (WPI-ITbM) and Department of Chemistry, Graduate School of Science, Nagoya University, Furo-cho, Chikusa-ku, Nagoya 464-8602, Japan

Introduction

Tuberculosis (TB), caused by pathogenic bacterial species *Mycobacterium tuberculosis*, remains a major global health problem and ranks as the second-leading cause of death from an infectious disease worldwide, after the human immunodeficiency virus (HIV). The latest estimates included in World Health Organization (WHO) report were 8.6 million new TB cases and 1.3 million TB deaths in 2012 [1]. The enoyl-acyl carrier protein (ACP) reductase (InhA) catalyzes the NADH-specific reduction of α,β-unsaturated fatty acids bound to the enoyl-ACP, the last step of fatty acids biosynthesis in *M. tuberculosis* [2, 3], and is an attractive target to design novel antitubercular drugs [4–10]. Moreover, InhA has been identified as the primary target of the most effective first-line anti-TB drug, isoniazid (INH) [11–19]. INH is a prodrug that is activated by catalase-peroxidase (KatG) enzymes to form an acyl radical that binds covalently to nicotinamide adenine dinucleotide (NAD^+) at the position 4, producing an active INH-NAD adduct [20–25] that functions as a highly potent inhibitor of InhA [26, 27]. However, such high potency of

Published online: 17 June 2014

[45] M. Liu, X.J. Cong, P. Li, J.J. Tan, W.Z. Chen, C.X. Wang, Study on the inhibitory mechanism and binding mode of the hydroxycoumarin compound NSC158393 to HIV-1 integrase by molecular modeling, Biopolymers 91 (2009) 700–709.
[46] Y. Zhao, W. Li, J. Zeng, G. Liu, Y. Tang, Insights into the interactions between HIV-1 integrase and human LEDGF/p75 by molecular dynamics simulation and free energy calculation, Proteins 72 (2008) 635–645.
[47] S. Han, Molecular dynamics simulations of thioredoxin with S-glutathiolated cysteine-73, Biochem. Biophys. Res. Commun. 362 (2007) 532–537.
[48] D.A. Rozwarski, C. Vilchèze, M. Sugantino, R. Bittman, J.C. Sacchettini, Crystal structure of the *Mycobacterium tuberculosis* enoyl-ACP reductase, InhA, in complex with NAD+ and a C16 fatty acyl substrate, J. Biol. Chem. 274 (1999) 15582–15589.
[49] G.M. Morris, D.S. Goodshell, R.S. Halliday, R. Huey, W.E. Hart, R.K. Belew, A.J. Olson, Automated docking using a lamarckian genetic algorithm and empirical binding free energy function, J. Comput. Chem. 19 (1998) 1639–1662.
[50] D. van der Spoel, E. Lindahl, B. Hess, G. Groenhof, A.E. Mark, H.J.C. Berendsen, GROMACS: fast, flexible and free, J. Comput. Chem. 26 (2005) 1701–1719.
[51] H.J.C. Berendsen, D. van der Spoel, R. van Drunen, GROMACS: a message-passing parallel molecular dynamics implementation, Comput. Phys. Commun. 91 (1995) 43–56.
[52] E. Lindahl, B. Hess, D. van der Spoel, Package for molecular simulation and trajectory analysis, J. Mol. Model. 7 (2001) 306–317.
[53] W.R.P. Scott, P.H. Hunenberger, I.G. Tironi, A.E. Mark, S.R. Billeter, J. Fennen, A.E. Torda, T. Huber, P. Kruger, W.F. van Gunsteren, The GROMOS biomolecular simulation program package, J. Phys. Chem. A 103 (1999) 3596–3607.
[54] J. Wang, R.M. Wolf, J.W. Caldwell, P.A. Kollman, D.A. Case, Development and testing of a general AMBER force field, J. Comput. Chem. 25 (2004) 1157–1174.
[55] H.J.C. Berendsen, J.R. Grigera, T.P. Straatsma, The missing term in effective pair potentials, J. Phys. Chem. 91 (1987) 6269–6271.
[56] B. Hess, H. Bekker, H.J.C. Berendsen, J. Fraaije, LINCS: a linear constraint solver for molecular simulations, J. Comput. Chem. 18 (1997) 1463–1472.
[57] T. Darden, D. York, L. Pedersen, Particle mesh Ewald – an N·Log(N) method for Ewald sums in large systems, J. Chem. Phys. 98 (1993) 10089–10092.
[58] J. Aqvist, C. Medina, J.E. Samuelsson, A new method for predicting binding affinity in computer-aided drug design, Protein Eng. 7 (1994) 385–391.
[59] M.R. Kuo, H.R. Morbidoni, D. Alland, S.F. Sneddon, B.B. Gourlie, M.M. Staveski, M. Leonard, J.S. Gregory, A.D. Janjigian, C. Yee, J.M. Musser, B. Kreiswirth, H. Iwamoto, R. Perozzo, W.R. Jacobs Jr., J.C. Sacchettini, D.A. Fidock, Targeting tuberculosis and malaria through inhibition of enoyl reductase: compound activity and structural data, J. Biol. Chem. 278 (2003) 20851–20859.

List of abbreviation

ACPYPE: AnteChamber PYthon Parser interfacE
IC_{50}: the half maximal inhibitory concentration
INH: isoniazid
LGA: Lamarckian genetic algorithm
LIE: linear interaction energy
MD: molecular dynamics
MDR-TB: multidrug resistant-tuberculosis
MIC: minimum inhibitory concentrations
NADH: nicotinamide adenine dinucleotide
RMSD: root mean square deviations
RMSF: root mean square fluctuation
TB: tuberculosis
XDR-TB: extensively drug-resistant tuberculosis

Table 1 The chemical structures and activities for InhA inhibition of 52 diphenyl ether derivatives

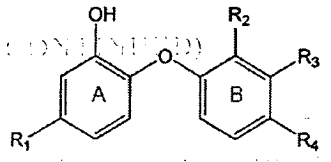

Cpd.	R_1	R_2	R_3	R_4	IC_{50}(nM)	Log(1/IC_{50})		
						Exp.	CoMSIA	Res.
1	Cl	Cl	H	Cl	1,100	5.96	6.03	−0.07
2	CH_3	Cl	H	Cl	800	6.10	6.12	−0.02
3	CH_2Cy	Cl	H	Cl	110	6.96	6.91	0.05
4[a]	CH_2CH_3	Cl	H	Cl	120	6.92	6.80	0.12
5	$(CH_2)_2CH_3$	Cl	H	Cl	91	7.04	6.84	0.20
6	$(CH_2)_3CH_3$	Cl	H	Cl	55	7.26	7.24	0.02
7	$(CH_2)_2CH(CH_3)_2$	Cl	H	Cl	63	7.20	7.27	−0.07
8	$CH_2CH(CH_3)CH_2CH_3$	Cl	H	Cl	130	6.89	6.78	0.11
9	CH_2(2-pyridyl)	Cl	H	Cl	29	7.54	7.39	0.15
10[a]	CH_2(3-pyridyl)	Cl	H	Cl	42	7.38	6.87	0.51
11	CH_2(4-pyridyl)	Cl	H	CN	75	7.12	6.98	0.14
12	o-CH_3-Ph	Cl	H	Cl	1,300	5.89	5.96	−0.07
13	m-CH_3-Ph	Cl	H	Cl	870	6.06	5.96	0.10
14	CH_2Ph	Cl	H	Cl	51	7.29	7.29	0.00
15	CH_2CH_2Ph	Cl	H	Cl	21	7.68	7.81	−0.13
16[a]	$(CH_2)_3Ph$	Cl	H	Cl	50	7.30	6.89	0.41
17	$(CH_2)_5CH3$	H	H	H	11	7.96	7.38	0.58
18	CH_2CH_3	H	H	H	2,000	5.70	6.33	−0.63
19	$(CH_2)_3CH_3$	H	H	H	80	7.10	7.47	−0.37
20	$(CH_2)_4CH_3$	H	H	H	17	7.77	7.78	−0.01
21	$(CH_2)_7CH_3$	H	H	H	5	8.30	8.23	0.08
22	$(CH_2)_{13}CH_3$	H	H	H	150	6.82	7.31	−0.49
23[a]	$(CH_2)_5CH_3$	NO_2	H	H	180	6.74	6.73	0.01
24	$(CH_2)_5CH_3$	H	NO_2	H	48	7.32	7.38	−0.05
25	$(CH_2)_5CH_3$	H	H	NO_2	90	7.05	6.99	0.06
26[a]	$(CH_2)_5CH_3$	NH_2	H	H	62	7.21	6.93	0.28
27	$(CH_2)_5CH_3$	H	NH_2	H	1,090	5.96	5.94	0.02
28	$(CH_2)_5CH_3$	H	H	NH_2	55	7.26	7.27	−0.01
29	$(CH_2)_5CH_3$	Br	H	H	10	8.00	7.93	0.07
30[a]	$(CH_2)_5CH_3$	CF_3	H	H	29.7	7.53	7.36	0.17
31	$(CH_2)_5CH_3$	F	H	H	12.1	7.92	7.92	0.00
32	$(CH_2)_5CH_3$	I	H	H	44.6	7.35	7.39	−0.04
33	$(CH_2)_5CH_3$	OH	H	H	48	7.32	7.29	0.03
34	$(CH_2)_5CH_3$	CN	H	H	235.6	6.63	6.72	−0.09
35	$(CH_2)_5CH_3$	Cl	H	H	49.5	7.31	7.51	−0.20
36[a]	$(CH_2)_5CH_3$	CH_3	H	H	50.7	7.29	7.14	0.15
37	$(CH_2)_5CH_3$	$NHCOCH_3$	H	H	1,550	5.81	5.88	−0.07
38	$(CH_2)_5CH_3$	H	H	$NHCONH_3$	1,300	5.89	5.87	0.02
39	$(CH_2)_5CH_3$	$NHCOCO_2H$	H	H	2,360	5.63	5.72	−0.09
40	$(CH_2)_5CH_3$	H	$NHCOCO_2H$	H	580	6.24	6.32	−0.08
41	$(CH_2)_5CH_3$	H	H		1,930	5.71	5.62	0.09
42[a]	$(CH_2)_5CH_3$	H	NHCO- isoxazole	H	1,220	5.91	6.08	−0.17

REFERENCES

Table 1 (continued)

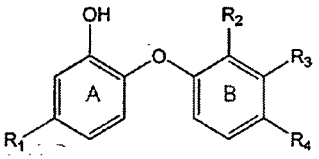

Cpd.	R_1	R_2	R_3	R_4	IC_{50}(nM)	Log(1/IC_{50})		
						Exp.	CoMSIA	Res.
43	$(CH_2)_5CH_3$	CH_2-*N*-CH_3-piperazine	H	H	1,315	5.88	5.76	0.12
44	$(CH_2)_5CH_3$	H	H	CH_2-*N*-CH_3-piperazine	306	6.51	6.53	−0.02
45	CH_2CH_2Ph	H	H	H	144.3	6.84	6.89	−0.05
46	CH_2CH_2Ph	CH_3	H	H	360.1	6.44	6.33	0.12
47	CH_2Ph	Cl	H	H	20.08	7.70	7.44	0.26
48	CH_2Ph	H	H	H	49.6	7.30	7.27	0.03
49	CH_2Ph	CH_3	H	H	56.4	7.25	7.59	−0.34
50	$CH_2CH_2CH_2OH$	CH_3	H	H	4,326	5.36	5.25	0.11
51	$OCH_2CH_2OCH_3$	H	H	H	253.1	6.60	6.55	0.05
52[a]	$O(CH_2)_4CH_3$	H	H	H	94.2	7.03	7.32	−0.29

[a] Test set

Complex InhA structures of these compounds as generated by the previous docking calculations were used as initial coordinates for MD simulations. The AMBER12 [54] software suite was used for all MD simulations to classically describe all relevant interactions within the system: InhA protein was described by the *ff03* force field [55] while NAD^+ and diphenyl ether inhibitors were described by the general AMBER force field (GAFF) [56, 57]. All missing hydrogen atoms of InhA were added using the LEaP module. To obtain the partial atomic charges of diphenyl ether derivatives and NAD^+, the geometry optimization and electrostatic potential calculation of each compound was first calculated at the HF/6-31G* level using the Gaussian 09 program [50]. Then, RESP partial charges [58–62] were assigned using the ANTECHAMBER module implemented in AMBER12. Each complex structure was solvated by TIP3P [63] waters in a truncated octahedral box extending up to 10 Å from each solute species. Five Na^+ cations were added to neutralize the charge in each system. Non-bonded cut-off was set to 10 Å. To relieve bad steric interactions that originated from addition of the water molecules and ions, the systems were first minimized with atomic positions of all solute species restraint (using a force constant of 500 kcal/mol^{-1} $Å^2$). Then, the whole system was fully minimized without restraining conditions. The solvated systems were gradually warmed up from 0 to 300 K in the first 20 ps followed by maintaining the temperature at 300 K during the last 10 ps. An integration time-step of 2 fs was used in a constant volume boundary. After minimization and heating, the position-restrained dynamics simulations were performed for 70 ps at 300 K under an isobaric condition to relax the positions of the solvent molecules. A weak force constant of 10 kcal/mol^{-1} $Å^2$ restraint on solute species was also applied for each simulation. Then, a 5-ns production MD simulation without restraints was performed on each system at a constant temperature of 300 K under isobaric condition. The Particle Mesh Ewald (PME) [64] was applied to treat the long-range electrostatic interactions with a periodic boundary condition during the MD simulations. The cut-off distance for the long-range van der Waals interaction was set to 8 Å. The SHAKE [65] method was applied to constrain the bond lengths of hydrogen atoms attached to heteroatoms. Coordinates and energy outputs during the MD simulation were collected every 2 ps. Finally, the root-mean-square deviations (RMSDs) of the InhA protein, NAD^+, and diphenyl ether ligand, respectively, were analyzed along the MD trajectory relative to the initial structures to determine the stability of the system. The binding free energies were calculated to evaluate the binding affinities of diphenyl ether derivatives in the InhA binding pocket.

Binding free energy calculation

The free energy of binding between InhA and diphenyl ether inhibitors were calculated using the Molecular Mechanics Poisson–Boltzmann Surface Area (MM-PBSA) [66–69] and Normal-mode [70] methods. For MM-PBSA calculation, 125 snapshots were generated

REFERENCES

[1] Stefano, A. and et al. "Molecular and structural aspects of clinically relevant mutantions related to the approved non-nucleoside inhibitors of HIV-1 reverse transcriptase", Drug Resistance Updates. 14(3): 141-149; June, 2011.

[2] Pawan, G. and et al. "Docking-based 3D-QSAR study of HIV-1 integrase inhibitors", European Journal of Medicinal Chemistry. 44(11): 4276-4287; November, 2009.

[3] Andrea, C. M. and et al. "A mechanistic and structurel investigation of modified derivatives of the diaryltriazine class of NNRTIs targeting HIV-1 reverse transcriptase", Biochimica et Biophysica Acta. 1840(7): 2203-2211; July, 2014.

[4] Asim, S M. and Kunal R. "Predictive QSAR modeling of HIV reverse transcriptase inhibitor TIBO derivatives", European Journal of Medicinal Chemistry. 44(4): 1509-1524; April, 2009.

[5] Laura, A. and et al. "Host SAMHD1 Protein Promotes HIV-1 Recombination in Macrophages", The Journal of Biological Chemistry. 289(5): 2489-2496; January, 2014.

[6] Pornpan, P. and et al. "Recent Advances in NNRTI Design: Computer-Aided Molecular Design Approaches", Current Computer-Aided Drug Design. 5(3): 174-199; September, 2009.

[7] Antonello, M. and et al. "5-Alkyl-2-alkylamino-6-(2,6-difluorophenylalkyl)-3,4-dihydropyrimidin-4(*3H*)-ones, a new series of potent, broad-spectrum non-nucleoside reverse transcriptase inhibitors belonging to the DABO family", Bioorganic & Medicinal Chemistry. 13(6): 2065-2077; March, 2005.

[8] Luis, M. A. and et al. "HIV-1 rever transcriptase connection subdomain mutations involved in resistance to approved non-nucleoside inhibitors", Antiviral Research. 92(2): 139-149; August, 2011.

[9] Mariela, B. and et al. "Optimization of diarylazines as anti-HIV agents with dramatically enhanced solubility", Bioorganic & Medicinal Chemistry Leters. 23(18): 5213-5216; September, 2013.

REFERENCES (CONTINUED)

[27] Wolfgang, S. and et al. "3D-QSAR CoMFA/CoMSIA models based on theoretical active conformers of HOE/BAY-793 analogs derived from HIV-1 protease inhibitor complexes", European Journal of Medicinal Chemistry. 44(11): 4344-4352; November, 2009.

[28] Yong, H. L. and Fen, E. C. "QSAR studies for diarylpyrimidines against HIV-1 reverse transcriptase wild-type and mutant strains", European Journal of Medicinal Chemistry. 44(2): 625-631; February, 2009.

[29] Park, Y. H. and et al. "3D-QSAR Studies on DATAs and DAPYs for HIV-1 RT Inhibitors using CoMFA and CoMSIA Approaches", QSAR & Combinatorial Science. 28(2): 218-225; March, 2009.

[30] Bode, L. M. and et al. "Imidazo[1,2-a]pyridin-3-amines as potential HIV-1 non-nucleoside reverse transcriptase inhibitors", Bioorganic & Medicinal Chemistry. 19(14): 4227-4237; July, 2011.

[31] Hao, Z. and et al. "Revealing the Drug-Resistant Mechanism for Diarylpyrimidine Analogue Inhibitors of HIV-1 Reverse Transcriptase", Chemical Biology & Drug Design. 78(3): 427-437; September, 2011.

[32] Barry, C. J. and et al. "A comparison of the ability of rilpivirine (TMC278) and selected analogues to inhibit clinically relevant HIV-1 reverse transcriptase mutants", Retrovirology. 9(99): 1-11; December, 2012.

[33] Xuwang, C. and et al. "Design, synthesis, anti-HIV evaluation and molecular modeling of piperidine-linked amino-triazine derivatives as potent non-nucleoside reverse transcriptase inhibitors", Bioorganic & Medicinal Chemistry. 20(12): 3856-3864; April, 2012.

[34] Sergio, R. R. and et al. "Synthesis, biological evaluation and molecular modeling of 4,6-diarylpyrimidines and diarylbenzenes as novel non-nucleosides HIV-1 reverse transcriptase inhibitors", European Journal of Medicinal Chemistry. 58: 485-492; December, 2012.

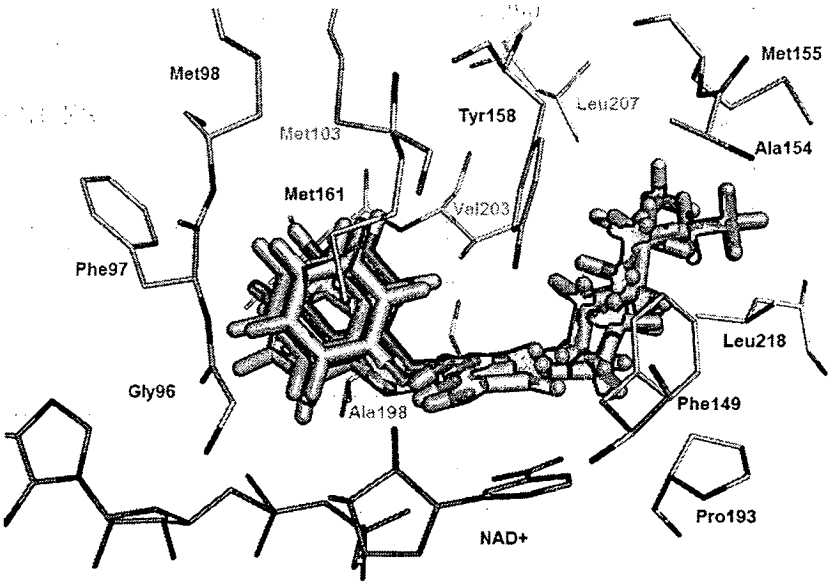

Fig. 3 The superimposition of compounds **17** (stick in *cyan color*), **18** (stick in *yellow color*), **19** (stick in *green color*), and **29** (stick in *pink color*) in the InhA pocket obtained from MD simulation

and Ile215. Therefore, the more hydrophobic interactions at the R_1 position of compounds **17** and **29** should account for better activities against InhA. The phenyl B ring containing the R_2, R_3, and R_4 substituents is surrounded by the pyrophosphate moiety of NAD^+, the hydrophilic backbones of Gly96, Met98, Phe97, and the hydrophobic side chains of Met103, Met161, Ile202, Val203, Ala198. The H and Br substituents at the R_2 position for compounds **17** and **29**, respectively, are closed to the methyl side chain of Ala198 and the pyrophosphate moiety of NAD^+ (Fig. 4). The Br substituent of compound **29** contributes greatly a hydrophobic interaction to the methyl side chain of Ala198 while the H substituent of compound **17** contributes a hydrophilic interaction to the ribose and pyrophosphate moieties of NAD^+. These results might explain why compounds **29** and **17** show the InhA inhibitory activities in the same level with IC_{50} of 10 and 11 nM, respectively. Accordingly, the R_2 substituent would also be hydrophobic or hydrophilic groups. For the R_3 position, the H substituents at this position for compounds **17**, **18**, **19**, and **29** form a hydrogen bond interaction with the carbonyl backbone of Gly96 and, besides the H substituent, other hydrogen bond donor substituents would also be possible. A similar H-bond interaction was also found for the R_4 substituent where all four compounds point to the NH and carbonyl backbone of Met98.

3D-QSAR study

CoMSIA model

The PLS results of CoMSIA models are summarized in Table 3. Ten CoMSIA models were constructed with various combinations of CoMSIA descriptors. Among all models,

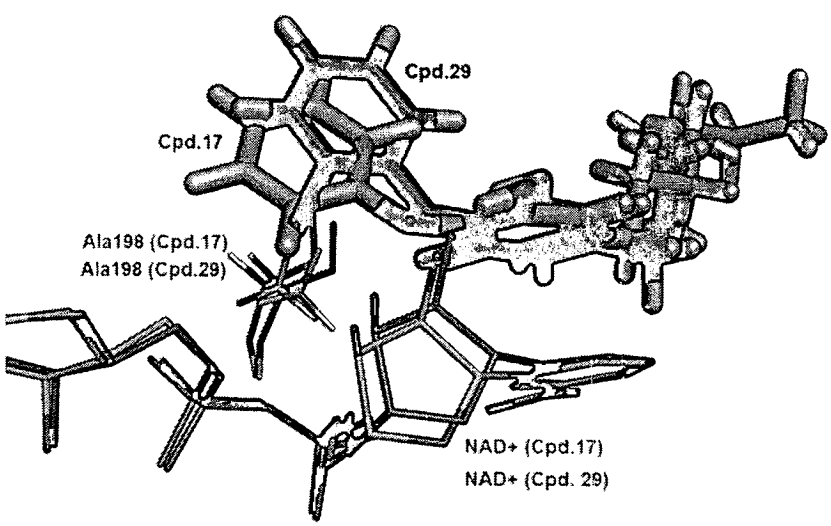

Fig. 4 The interactions of the R_2 substituents of compounds **17** and **29** with Ala198 and the pyrophosphate moiety of NAD^+

REFERENCES (CONTINUED)

[19] Shuang, X. G. and et al. "Synthesis and structure-activity relationship of novel diarylpyrimidines with hydromethyl linker (*CH*(*OH*)-DAPYs) as HIV-1 NNRTIs", Bioorganic & Medicinal Chemistry. 19(17): 5117-5124; September, 2011.

[20] Xiao, D. M. and et al. "Synthesis and Anti-HIV Activity of Aryl-2-[(4-cyanophenyl)amino] -4-pyrimidinone hydrazones as Potent Non-nucleoside Reverse Transcriptase Inhibitors", ChemMedChem. 6: 2225-2232, 2011.

[21] Jingshan, R. and et al. "Structural basis for drug resistance mechanisms for non-nucleoside inhibitors of HIV reverse transcriptase", Virus Research. 134(1-2): 157-170; June, 2008.

[22] Amor, A. and San, J. "3D-QSAR models on clinically relevant K103N mutant HIV-1 reverse transcriptase obtained from two strategic considerations", Bioorganic & Medicinal Chemistry Letters. 18(3): 1181-1194; February, 2008.

[23] Alexandre, G. and et al. "Investigation on the role of the tetrazole in the binding of thiotetrazolylacetanilides with HIV-1 wild type and K103N/Y181C double mutant reverse transcriptases", Bioorganic & Medicinal Chemistry Letters. 19(4): 1199-1205; February, 2009.

[24] Antonio, C. and et al. "Activity and molecular modeling of a new small molecular active against NNRTI-resistant HIV-1 mutants", European Journal of Medicinal Chemistry. 44(12): 5117-5122; December, 2009.

[25] Mingyan, Y. and et al. "Synthesis and biological evaluation of novel 2-(substituted phenylaminocarbonylmethylthio)-6-(2,6-dichlorobenzyl)-pyrimidin-4(3H)-ones as potent HIV-1 NNRTIs", Bioorganic & Medicinal Chemistry. 17(22): 7749-7754; September, 2009.

[26] Dai, S. S. and et al. "Substituted tetrahydroquinolines as potent allosteric inhibitors of reverse transcriptase and its key mutants", Bioorganic & Medicinal Chemistry Letters. 19(17): 5119-5123; September, 2009.

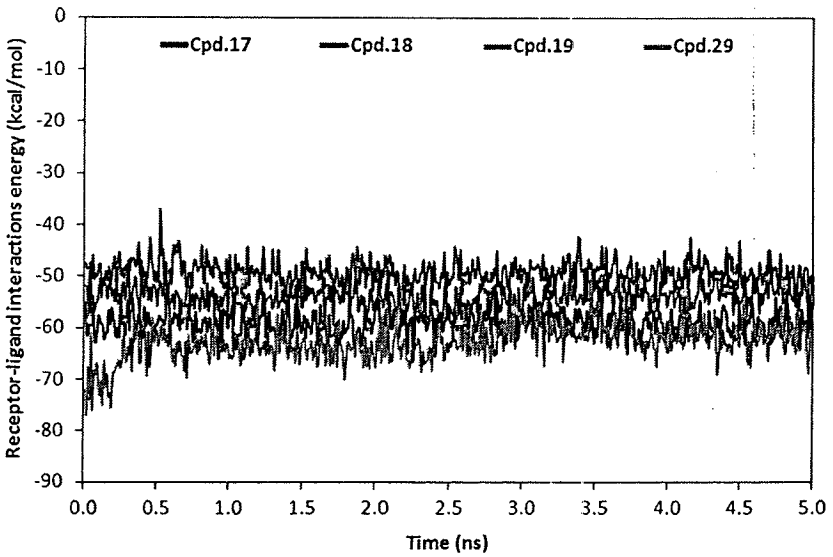

Fig. 2 Receptor–ligand interaction energies for the systems of compounds **17** (**a**), **18** (**b**), **19** (**c**), and **29** (**d**) over the 5 ns simulation

compounds **17**, **18**, **19**, and **29** over the 5-ns simulation time were calculated by MM-PBSA method. The receptor–ligand interaction energies of all compounds reach the equilibrium state at the beginning of the simulation time, except that of compound **29**, which reaches the equilibrium state after the 0.5 ns simulation time (Fig. 2). The average receptor–ligand interaction energies of compounds **17**, **18**, **19**, and **29** are −58.85±2.42, −49.27±2.55, −53.85±2.46, and −62.72±3.55 kcal/mol^{-1}, respectively. Based on the receptor–ligand interaction energy and RMSD plots, Compounds **17**, **18**, **19** and **29** complexed with InhA are sufficiently stable and the production simulations are reliable. Therefore, the subsequent free energy calculation and free energy decomposition analysis based on snapshots extracted from the stable state are reasonable.

Binding free energy calculations

The MM-PBSA method was employed to calculate the binding free energies of compounds **17**, **18**, **19**, and **29** in InhA and the results are shown in Table 2. The binding free energies (ΔG_{bind}) of compounds **17**, **18**, **19**, and **29** bound to the InhA pocket are calculated to be −15.02, −9.03, −13.90, and −15.40 kcal/mol^{-1}, respectively, which are in good agreement with those determined experimentally ($\Delta G_{exp.}$). Pearson correlation and Spearman rank correlation [72] were employed to determine the correlation between $\Delta G_{exp.}$ and ΔG_{bind}. The accepted values of correlation coefficient are in the range of −1 to 1. Based on these methods, the correlation between $\Delta G_{exp.}$ and ΔG_{bind} shows the correlation coefficient of Pearson correlation and Spearman rank correlation to be 0.98 and 1.00, respectively. Therefore, there is the correlation between $\Delta G_{exp.}$ and ΔG_{bind}.

Table 2 The binding free energies (kcal/mol^{-1}) calculated by the MM-PBSA method

Component	Diphenyl ether-InhA complexes			
	17	18	19	29
ΔG_{MM}	−58.77±2.59	−49.49±2.29	−52.90±2.57	−60.82±2.91
$\Delta G_{solv.}$	21.59±2.07	19.33±1.23	20.13±1.60	22.70±2.69
ΔH	−37.18±2.93	−30.16±2.24	−32.77±2.47	−38.06±3.21
-TΔS	22.16±0.85	21.13±1.17	18.87±1.06	22.66±0.57
$\Delta G_{bind.}$	−15.02±1.32	−9.03±.084	−13.90±1.31	−15.40±1.40
$\Delta G_{exp.}$[a]	−10.93	−7.83	−9.75	−10.99

[a] Derived from $\Delta G = RT \ln[IC_{50}]$, R represents the gas constant (1.988 cal/mol^{-1} K), T represents the temperature (300 K)

The binding modes of diphenyl ether derivatives in InhA

The binding modes of compounds **17**, **18**, **19**, and **29** bound with InhA pocket observed from the simulations are superimposed and illustrated in Fig. 3. In general, all compounds showed a similar binding mode and conformation: the OH group of the phenyl A ring lies in between the OH groups of Tyr158 and ribose fragment of NAD^+ to form the hydrogen bond interactions. The phenyl A ring forms the pi–pi interaction with pyridine amide ring of NAD^+. As the phenyl A ring bearing the R_1 substituent as the alkyl chain, it is placed in the hydrophobic pocket that is formed by Phe149, Met155, Pro156, Ala157, Tyr158, Pro193, Met199, Val203, Leu207, Ile215, and Leu218 (Fig. 3). Compounds **17** and **29** that hold the hexyl substituents at the R_1 position could form stronger hydrophobic interactions with Phe149, Met155, Pro156, Ala157, Tyr158, Pro193, Met199, Val203, Leu207, Ile215, and Leu218 when comparing these interactions with compounds **18** and **19** that have shorter alkyl substituents (containing ethyl and butyl, respectively), losing several hydrophobic interactions with Pro156, Ala157, Val203, Leu207,

REFERENCES (CONTINUED)

[10] Dongyue, L. and et al. "Synthesis and biological evaluation of pyridazine derivatives as novel HIV-1 NNRTIs", Bioorganic & Medicinal Chemistry. 21(7): 2128-2134; April, 2013.

[11] David, E. and et al. "Design, synthesis, and biological evaluations of novel quinolones as HIV-1 non-nucleoside reverse transcriptase inhibitors", Bioorganic & Medicinal Chemistry Leters. 16(16): 4246-4251; August, 2006.

[12] Ye, T. and et al. "Fused heterocyclic compounds bearing bridgehead nitrogen as potent HIV-1 NNRITs. Part 1: Design, synthesis and biological evaluation of novel 5,7-disubstituted pyrazolo [1,5-a]pyrimidine derivatives", Bioorganic & Medicinal Chemistry. 22(7): 2052-2059; April, 2014.

[13] Joshua, J. M. and Richard, H. "Etravirine: a second-generation NNRTI for treatment-experienced adults with resistant HIV-1 infection", Future HIV Therapy. 2(6): 525-537; October, 2008.

[14] Mamta, S. and Louis, D. S. "Rilpivirine: a new non-nucleoside reverse transcriptase inhibitor", Journal of Antimicrobial Chemotherapy. 68(2): 250-256; October , 2012.

[15] Céline, M. and et al. "Synthesis of novel diarylpyrimidine analogues of TMC278 and their antiviral activity against HIV-1 wild-type and mutant strains", European Journal of Medicinal Chemistry. 42(5): 567-579; May, 2007.

[16] Yong, H. L. and et al. "Design, Synthesis, and SAR of Naphthyl-Substituted Diarylpyrimidines as Non-Nucleoside Inhibitors of HIV-1 Reverse Transcriptase", ChemMedChem. 4(9): 1537-1545; September, 2009.

[17] Xiao, Q. F. and et al. "Structural Modifications of DAPY Analogues with Potent Anti-HIV-1 Activity", ChemMedChem. 4(2): 219-224; February, 2009.

[18] Xiao, Q. F. and et al. "Synthesis and biological evaluation of 4-(hydroxyimino)arylmethyl diarylpyrimidine analogues as potential non-nucleoside reverse transcriptase inhibitors against HIV", Bioorganic & Medicinal Chemistry. 18(7): 2370-2374; April, 2010.

for each complex from the last 1 ns of MD trajectory with an interval of 8 ps. The binding free energies (ΔG_{bind}) were obtained using Eqs. (1–4).

$$\Delta G_{bind} = G_{com} - (G_{rec} + G_{ligand}) \quad (1)$$

$$\Delta G_{bind} = \Delta H - T\Delta S \quad (2)$$

$$\Delta H = \Delta G_{MM} + \Delta G_{solv} \quad (3)$$

$$\Delta G_{bind} = \Delta G_{MM} + \Delta G_{sol} - T\Delta S \quad (4)$$

where G_{com}, G_{rec}, and G_{ligand} are the free energies of the complex, InhA and the diphenyl ether inhibitors, respectively. In general, the binding free energy is composed of an enthalpic (ΔH) and an entropic contribution ($T\Delta S$). The enthalpic contribution (ΔH) contains the gas-phase molecular mechanics energy (ΔG_{MM}) and the solvation free energy (ΔG_{solv}) as shown in Eq. (3). The entropic contribution ($T\Delta S$) to the binding free energy was estimated using normal-mode analysis with AMBER Nmode module. Due to a highly computational cost in the entropy calculation, the residues around the ligand (less than 12 Å) were only considered as the receptor for normal-mode calculations [69, 71]. For this calculation, 50 snapshots were extracted from the last 1 ns of MD trajectory with an interval of 20 ps.

Results and discussion

MD simulation

System equilibration

Four MD simulations of compounds **17**, **18**, **19**, and **29** bound with InhA were performed for 5 ns to evaluate the structural stability of the complexes and their binding strength. The RMSDs for all atoms of three different solute species (InhA, NAD^+, and inhibitor) relative to the initial structure over the 5 ns of simulation times were analyzed and plotted in Fig. 1. The plateau characteristic of the RMSD plot over the simulation time is the criteria to indicate the equilibrium state of each solute species. Figure 1 shows that NAD^+ and compounds **17**, **18**, **19**, and **29** reach the equilibrium state at the early time. However, RMSDs of all compounds are more fluctuated, particularly compound **17**. InhA complexed with compounds **17**, **18**, **19**, and **29** reach the equilibrium state after 1.0 ns (Fig. 1a), 1.5 ns (Fig. 1b), 2.5 ns (Fig. 1c), and 1.0 ns (Fig. 1d), respectively. Moreover, to reveal the energy stability of each system, the receptor–ligand interaction energies of

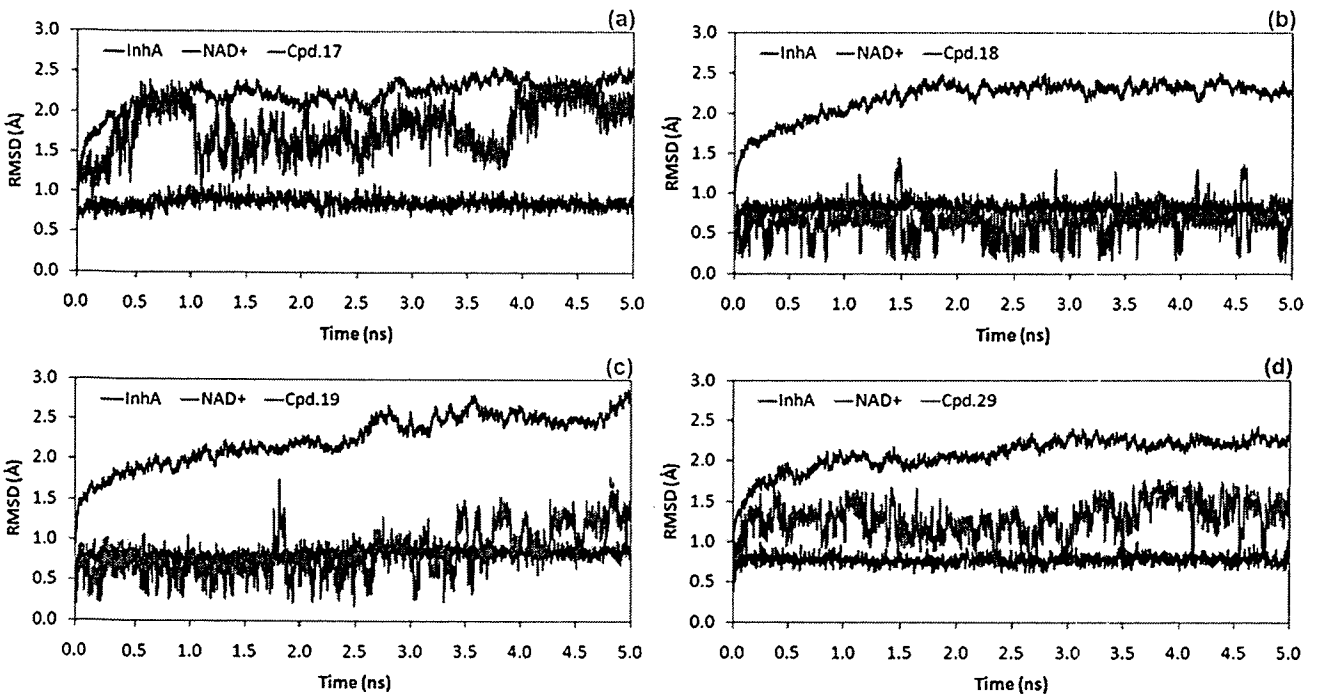

Fig. 1 RMSD plots of compounds **17** (**a**), **18** (**b**), **19** (**c**), and **29** (**d**) complexed with InhA

Table 3 Summary of statistical results of CoMSIA models

Models	Statistical data						Fraction
	q^2	r^2	s	SSE	F	N	
1.S/E	0.29	0.93	0.70	0.21	85.48	6	38.6/61.4
2.S/H	0.08	0.69	0.75	0.44	43.53	2	38.8/61.2
3.S/D	0.54	0.89	0.56	0.27	50.30	6	53.7/46.3
4.S/A	0.13	0.88	0.76	0.28	54.86	5	53.5/46.5
5.S/D/E	0.58	0.93	0.54	0.22	77.34	6	27.9/41.7/30.5
6.S/D/H	0.56	0.93	0.55	0.21	85.19	6	29.9/37.6/32.5
7.S/D/A	0.51	0.93	0.58	0.22	76.55	6	39.9/33.1/27.0
8. S/D/E/H	**0.60**	**0.95**	**0.52**	**0.19**	**104.17**	**6**	**19.0/32.5/23.8/24.8**
9. S/D/E/A	0.50	0.93	0.58	0.22	78.66	6	23.9/34.3/25.9/15.9
10.S/D/E/H/A	0.55	0.95	0.55	0.19	103.76	6	17.2/26.6/21.4/22.1/12.8

Bold values indicate the best CoMSIA model

N optimum number of components; *s* standard error of prediction; *SEE* standard error of estimate; *F* F-test value; *S* steric field; *E* electrostatic field; *H* hydrophobic field; *D* hydrogen donor field; *A* hydrogen acceptor field

model 8 composing the steric, hydrogen bond donor, electrostatic and hydrophobic fields is the best CoMSIA model, giving the best statistical parameters with a q^2 value of 0.60 and an r^2 value of 0.95. The predicted activities of 43 compounds in the training set and nine compounds in test set derived from the best CoMSIA model are summarized in Table 1. There is a good correlation between actual and predicted activities of the training set based on the best CoMSIA model, as depicted in Fig. 4. In order to assess the external predictive ability of this model, the InhA inhibitory activities of the test set were predicted. The predicted values of nine test-set compounds are within one logarithmic unit difference from the experimental values (Fig. 5). Therefore, the best CoMSIA model is reliable with highly predictive ability and could be utilized to predict the InhA activities for newly designed diphenyl ether inhibitors.

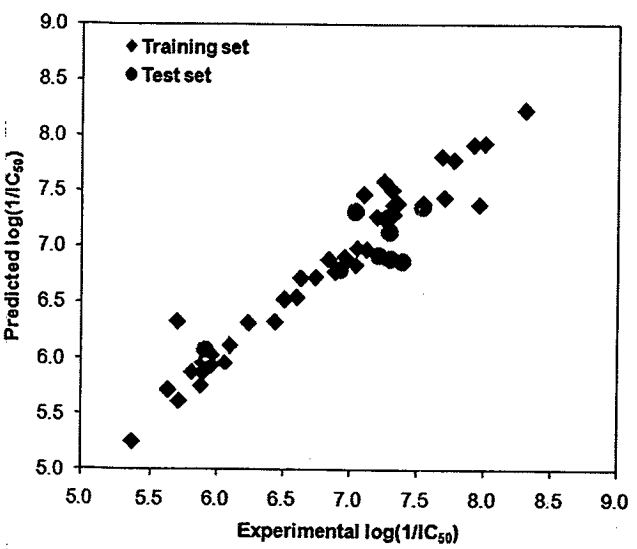

Fig. 5 Plots between the experimental and predicted activities of the training and test sets derived from the CoMSIA model

The predictive abilities of the best CoMSIA model were determined from the test set including nine compounds. For the best CoMSIA model, internal validation of leave-one-out cross-validated q^2 and predicted r^2 ($r^2_{pred.}$ or r^2) were found to be 0.64 and 0.70, respectively. The calculated square correlation coefficient values between the experimental and predicted values of the test-set compounds with intercept set at zero (r^2_0) and without intercept (r^2) were 0.56 and 0.73, respectively. The slope of regression line through the origin (k) of the best CoMSIA model was 1.02, which is close to 1. Based on the statistical results, the best CoMSIA model could be considered reliable.

CoMSIA contour maps

To reveal the importance of molecular descriptor fields on InhA inhibitory activities of diphenyl ether derivatives, CoMSIA contour maps were established. Figures 6 and 7 present the CoMSIA contour maps that reveal the influence of steric, electrostatic, hydrophobic, and hydrogen donor fields to the activity of diphenyl ether derivatives. Green and yellow contours indicate areas where favorable and unfavorable steric bulks are predicted to enhance the activities of diphenyl ether derivatives. Blue and red contours indicate regions where electropositive and electronegative groups lead to an increase of the InhA inhibitory activity, respectively. Magenta and white contours represent areas where the hydrophobic group and the hydrophilic group are predicted to favor the biological activities. The cyan and orange contours indicate regions that favor the hydrogen donor group and unfavor hydrogen donor group, respectively. The interpretation of

REFERENCES (CONTINUED)

[35] Shiqiong, Y. and et al. "Molecular design, synthesis and biological evaluation of BP-O-DAPY andO-DAPY derivatives as non-nucleoside HIV-1 reverse transcriptase inhibitors", European Journal of Medicinal Chemistry. 65: 134-143; May, 2013.

[36] Ravichandran, V. and et al. "Designing hypothesis of diaryl pyrimidine analogs as anti-HIV agent: QSAR approach", Medicinal Chemistry Research. 22(1): 35-44; March, 2013.

[37] Xuwang, C. and et al. "Novel piperidinylamino-diarylpyrimidine derivatives with dual structural conformations as potent HIV-1 non-nucleoside reverse transcriptase inhibitors", Bioorganic & Medicinal Chemistry Letters. 23(24): 6593-6597; December, 2013.

[38] Dongyue, L. and et al. "Synthesis and biological evaluation of pyridazine derivatives as novel HIV-1 NNRTIs", Bioorganic & Medicinal Chemistry. 21(7): 2128-2134; Apiril, 2013.

[39] Wenmin, C. and et al. "Discovery of 2-pyridone derivatives as potent HIV-1 NNRTIs using molecular hybridization based on crystallographic overlays", Bioorganic & Medicinal Chemistry. 22(6): 1863-1872; March, 2014.

[40] Lingzi, Z. and et al. "Design, synthesis and preliminary SAR studies of novelN-arylmethyl substituted piperidine-linked aniline derivatives as potent HIV-1 NNRTIs", Bioorganic & Medicinal Chemistry. 22(1): 633-642; November, 2014.

[41] Mayuso, K. Supa, H and Keiji, M. "Theoretical investigation on nevirapine and HIV-1 reverse transcriptase binding site interaction, based on ONIOM method", Chemical Physics Letters. 380(3-4): 456–463; October, 2003.

[42] Francesco, F. and Gianfraco, L. M. "ONIOM study on the equilibrium geometries of some cyclopeptides", Journal of Molecular Structure (Theochem). 634: 181-186; February, 2003.

[43] Peerapol, N. and et al. "Particular interaction between efavirenz and the HIV-1 reverse transcriptase binding site as explained by the ONIOM2 method", Chemical Physics Letters. 405(1-3): 198-202; March, 2005.

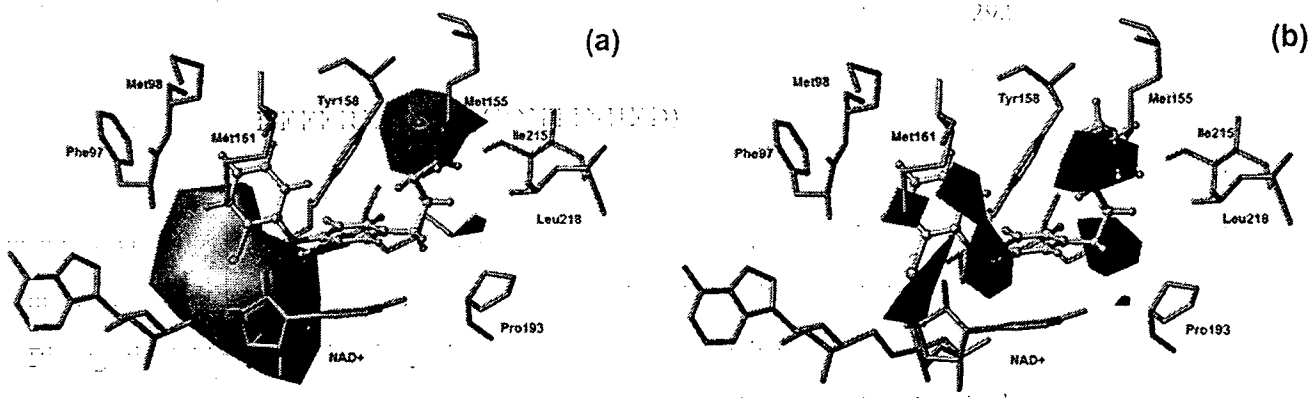

Fig. 6 CoMSIA steric (**a**) and electrostatic (**b**) contours in combination with compound **29** (ball and stick in atom type colors) in InhA binding pocket (stick in *greenblue*)

CoMSIA contour maps reveals the structural requirement of each substituent position in the scaffold of diphenyl ether derivatives helpful for rational design of novel and potent InhA inhibitors.

Structural requirement for the R_1 positions on the phenyl A ring

The appearance of cyan contours near the OH group of the phenyl A ring emphasizes the important role of this moiety to the InhA inhibitory activity of diphenyl ether derivatives (Fig. 7b). The C4 and C6 atoms of hexyl side chain of compound **29** are covered by green and red contours (Fig. 6a and b). Therefore, the R_1 substituent containing the bulky size and high electron density would be favorable for this region. In case of the R_1 substituent as the alkyl chain, the alkyl chain with the carbon atoms higher than two atoms should be preferable for the InhA inhibitory activity. As exemplified, compound **21**, containing an octyl group at the R_1 position, possesses the most active compound in this series, whereas compound **18** containing ethyl substituent exhibits much lower inhibitory activity than those of compounds **19**, **20**, **17**, and **21** bearing butyl, pentyl, hexyl, and octyl substituents at the R_1 position, respectively. Corresponding to the MD results, the longer alkyl chain at R_1 substituent could form hydrophobic interactions more than the shorter alkyl chain.

Structural requirement for the R_2, R_3, and R_4 positions on the phenyl B ring

The unfavorable hydrophobic white contour and the unfavorable steric yellow contour present near the R_2, R_3, and R_4 substituents (Figs. 6a and 7a). These results indicate that the small hydrophilic substituents at the R_2, R_3, and R_4 positions are required for the InhA inhibitory activity of diphenyl ether derivatives. Therefore, compounds **37**–**44** containing the bulky hydrophilic substituents at the R_2, R_3, and R_4 positions show poor activities for InhA inhibition with IC_{50} more than 360 nM. These suggestions are in agreement with the binding modes of compounds **17**, **18**, **19**, and **29** observed from the MD simulations that the R_2, R_3, and R_4 substituents are located near the pyrophosphate moiety of NAD^+, the hydrophilic backbones of Gly96 and Met98, respectively. Accordingly, the small substituent with hydrophilic property

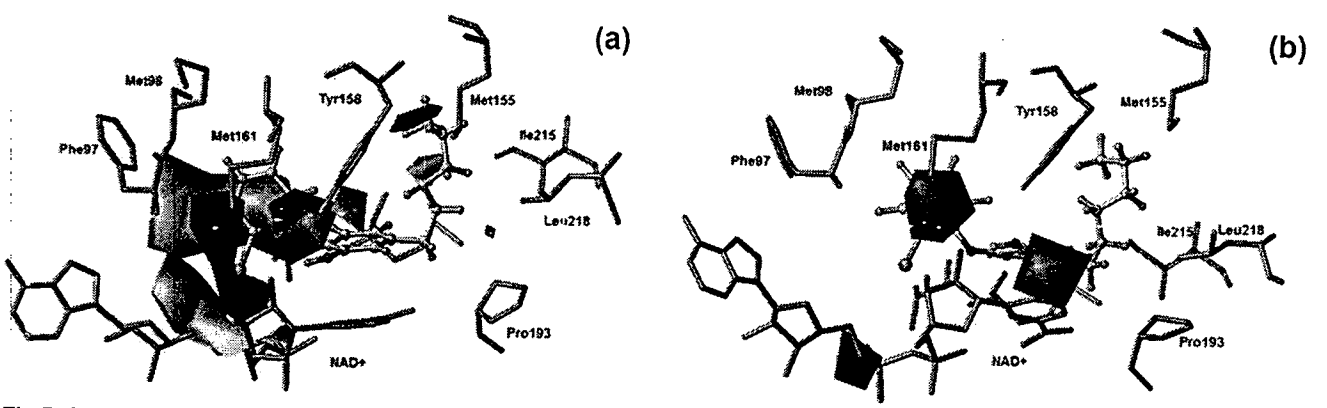

Fig. 7 CoMSIA hydrophobic (**a**) and hydrogen bond donor (**b**) contours in combination with compound **29** (ball and stick in atom type colors) in InhA binding pocket (stick in *greenblue*)

REFERENCES (CONTINUED)

[44] Suwipa, S. and et al. "Binding energy analysis for wild-type and Y181C mutant HIV-1 RT/8-Cl TIBO complex structures: Quantum chemical calculations based on the ONIOM method", Proteins: Structure, Function, and Bioinformatics. 61(4): 859-869; December, 2005.

[45] Mayuso, K. Rattapon, H and Supa, H. "ONIOM-BSSE scheme for H...π system and applications on HIV-1 reverse transcriptase", Chemical Physics Letters. 424(1-3): 172-177; April, 2006.

[46] Yong, H L. and Fen, E C. "ONIOM DFT/PM3 calculations on the interaction between dapivirine and HIV-1 reverse transcriptase, a theoretical study", Drug Discoveries & Therapeutics. 1(1): 57-60; June, 2007.

[47] Pensri, S. and Supa, H. "A Study of the Binding Energies of Efavirenz to Wild-Type and K103N/Y181C HIV-1 Reverse Transcriptase Based on the ONIOM Method", ChemMedChem. 3(5): 803-811; May, 2008.

[48] Rajesh, K R. Neil, A B. and Ian, H H. "Modelling the binding of HIV-reverse transcriptase and nevirapine: an assessment of quantum mechanical and force field approaches and predictions of the effect of mutations on binding†", Physical Chemistry Chemical Physics. 12(26): 7117-71251; May, 2012.

[49] Shao, Y L. and et al. "Insight into analysis of interactions of GW9508 to wild-type and H86F and H137FGPR40: A combined QM/MM study and pharmacophore modeling", Journal of Molecular Graphics and Modelling. 29(6): 818-825; Apiril, 2011.

[50] Pornthip, B. Mayuso, K. and Supa, H. "Key interactions of the mutant HIV-1 reverse transcriptase/efavirenz: an evidence obtained from ONIOM method†", Medicinal Chemistry Communication. 2 (12): 1181-1187; June, 2011.

[51] Nareerat, K. and et al. "Binding of huperzine A and galanthamine to acetylcholinesterase, based on ONIOM method", Nanomedicine: Nanotechnology, Biology, and Medicine. 7 (1): 60-68; February, 2011.

at the R_2, R_3 and R_4 substituents should be optimal for the InhA binding pocket. Moreover, the magenta and blue contours close to the R_2 substituent suggest additional structural requirement at this position, which should contain the hydrophobic property and less electron density. This suggestion is consistent with the MD results, which indicate that the R_2 position can be substituted with hydrophobic or hydrophilic groups so that the phenyl B ring could be favorable in binding with the methyl side chain of Ala198, and the pyrophosphate moiety of NAD^+, respectively. Apart from the hydrophobic properties, the R_2 substituent with the less electron density should be optimal for the pyrophosphate moiety of NAD^+ presenting the negative charge.

Conclusions

MD simulations were successfully applied to reliably predict binding modes, inhibitor–enzyme interactions, and binding free energies of diphenyl ether derivatives in the InhA binding pocket. The graphic interpretation of the obtained CoMSIA model reveals the key structural elements of diphenyl ether derivatives necessary for good InhA inhibitory activities. The structural requirements derived from the CoMSIA model correspond well with the binding interactions of diphenyl ether derivatives in the InhA pocket found in the MD simulations. The presented integrated results should be useful as guiding principles for the design of novel InhA inhibitors based on suitable modifications of the diphenyl ether scaffold.

Acknowledgments This research has been supported by the Thailand Research Fund (DBG5380006, MRG5680169, and RTA5380010), the National Research Council of Thailand and Higher Education Research Promotion. The financial support from Royal Golden Jubilee Ph.D. Program (PHD/004/2554) to P. Kamsri is gratefully acknowledged. Faculty of Science, Ubon Ratchathani University, University of Vienna, ASEA-Uninet (Austrian - South-East Asian University Partnership Network), NECTEC (National Electronics and Computer Technology Center) and BIOTEC (National center for genetic engineering and biotechnology) are gratefully acknowledged for supporting this research.

References

1. World Health Organization (2013) Global tuberculosis report, Available at http://apps.who.int/iris/bitstream/10665/91355/1/9789241564656_eng.pdf
2. Quemard A, Sacchettini JC, Dessen A, Vilcheze C, Bittman R, Jacobs WR Jr, Blanchard JS (1995) Enzymatic characterization of the target for isoniazid in *Mycobacterium tuberculosis*. Biochemistry 34(36):8235–8241
3. Rozwarski DA, Vilchèze C, Sugantino M, Bittman R, Sacchettini JC (1999) Crystal structure of the Mycobacterium tuberculosis enoyl-ACP reductase, InhA, in complex with NAD^+ and a C16 fatty acyl substrate. J Biol Chem 274(22):15582–15589
4. Agüero F, Al-Lazikani B, Aslett M, Berriman M, Buckner FS, Campbell RK, Carmona S, Carruthers IM, Chan AW, Chen F, Crowther GJ, Doyle MA, Hertz-Fowler C, Hopkins AL, McAllister G, Nwaka S, Overington JP, Pain A, Paolini GV, Pieper U, Ralph SA, Riechers A, Roos DS, Sali A, Shanmugam D, Suzuki T, Van Voorhis WC, Verlinde CL (2008) Genomic-scale prioritization of drug targets: the TDR targets database. Nat Rev Drug Discov 7(11):900–907
5. Campbell JW, Cronan JE Jr (2001) Bacterial fatty acid biosynthesis: targets for antibacterial drug discovery. Annu Rev Microbiol 55:305–332
6. Heath RJ, Rock CO (2004) Fatty acid biosynthesis as a target for novel antibacterials. Curr Opin Invest Drugs 5(2):146–153
7. White SW, Zheng J, Zhang YM, Rock CO (2005) The structural biology of type II fatty acid biosynthesis. Annu Rev Biochem 74:791–831
8. Zhang YM, Lu YJ, Rock CO (2004) The reductase steps of the type II fatty acid synthase as antimicrobial targets. Lipids 39(11):1055–1060
9. Wen L, Chmielowski JN, Bohn KC, Huang JK, Timsina YN, Kodali P, Pathak AK (2009) Functional expression of *Francisella tularensis* FabH and FabI, potential antibacterial targets. Protein Exp Purif 65(1):83–91
10. Wright HT, Reynolds KA (2007) Antibacterial targets in fatty acid biosynthesis. Curr Opin Microbiol 10(5):447–453
11. Rozwarski DA, Grant GA, Barton DH, Jacobs WR Jr, Sacchettini JC (1998) Modification of the NADH of the isoniazid target (InhA) from *Mycobacterium tuberculosis*. Science 279(5347):98–102
12. Vilcheze C, Wang F, Arai M, Hazbon MH, Colangeli R, Kremer L, Weisbrod TR, Alland D, Sacchettini JC, Jacobs WR Jr (2006) Transfer of a point mutation in *Mycobacterium tuberculosis* InhA resolves the target of isoniazid. Nat Med 12(9):1027–1029
13. Dessen A, Quemard A, Blanchard JS, Jacobs WR Jr, Sacchettini JC (1995) Crystal structure and function of the isoniazid target of *Mycobacterium tuberculosis*. Science 267(5204):1638–1641
14. Johnsson K, Schultz PG (1994) Mechanistic studies of the oxidation of isoniazid by the catalase peroxidase from *Mycobacterium tuberculosis*. J Am Chem Soc 116(16):7425–7426
15. Lei B, Wei CJ, Tu SC (2000) Action mechanism of antitubercular isoniazid. Activation by *Mycobacterium tuberculosis* KatG, isolation, and characterization of InhA inhibitor. J Biol Chem 275(4):2520–2526
16. Johnsson K, King DS, Schultz PG (1995) Studies on the mechanism of action of isoniazid and ethionamide in the chemotherapy of tuberculosis. J Am Chem Soc 117(17):5009–5010
17. Zhang Y, Heym B, Allen B, Young D, Cole S (1992) The catalase-peroxidase gene and isoniazid resistance of *Mycobacterium tuberculosis*. Nature 358(6387):591–593
18. Banerjee A, Dubnau E, Quemard A, Balasubramanian V, Um KS, Wilson T, Collins D, de Lisle G, Jacobs WR Jr (1994) InhA, a gene encoding a target for isoniazid and ethionamide in *Mycobacterium tuberculosis*. Science 263(5144):227–230
19. Quemard A, Dessen A, Sugantino M, Jacobs WR Jr, Sacchetini JC, Blanchard JS (1996) Binding of catalase-peroxidase-activated isoniazid to wild-type and mutant *Mycobacterium tuberculosis* enoyl-ACP reductases. J Am Chem Soc 118(6):1561–1562
20. Saint-Joanis B, Souchon H, Wilming M, Johnsson K, Alzari PM, Cole ST (1999) Use of site-directed mutagenesis to probe the structure, function and isoniazid activation of the catalase/peroxidase, KatG, from *Mycobacterium tuberculosis*. Biochem J 338(Pt 3):753–760
21. Zhao X, Yu H, Yu S, Wang F, Sacchettini JC, Magliozzo RS (2006) Hydrogen peroxide-mediated isoniazid activation catalyzed by *Mycobacterium tuberculosis* catalase-peroxidase (KatG) and its S315T mutant. Biochemistry 45(13):4131–4140
22. Metcalfe C, Macdonald IK, Murphy EJ, Brown KA, Raven EL, Moody PC (2008) The tuberculosis prodrug isoniazid bound to activating peroxidases. J Biol Chem 283(10):6193–6200
23. Sinha BK (1983) Enzymatic activation of hydrazine derivatives. J Biol Chem 258(2):796–801

REFERENCES (CONTINUED)

[52] Pongthep, P. Darinee, S. T. P. and Supa, H. "Key role of hydrazine to the interaction between oxaloacetic against phosphoenolpyruvic carboxykinase (PEPCK): ONIOM calculations", Nanomedicine: Journal of Molecular Modeling. 19 (8): 3165-3174; August, 2013.

[53] Kalyan, D. and et al. "High-resolution structures of HIV-1 reverse transcriptase/TMC278 complexes: Strategic flexibiloty explains potency against resistance mutations", Proceedings of the National Academy of Sciences. 105(5): 1466-1471; February, 2008.

[54] Rongjing, H. and et al. "Receptor- and ligand-based 3D-QSAR study for a series of non-nucleoside HIV-1 reverse transcriptase inhibitors", Bioorganic & Medicinal Chemistry. 17(6): 2400-2409; March, 2009.

[55] Frisch, M. J. and et al. "Gaussian 09", Gaussian 09 Revision D.01 Release Notes. http://www.gaussian.com. released in June 2009.

[56] Rongjing, H. and et al. "Lead Optimization of Diarylpyrimidines as Non-nucleoside Inhibitors of HIV-1 Reverse Transcriptase", ChemMedChem. 5(6): 837-840; June, 2010.

[57] Lihui, Z. and et al. "Insight into the binding mode and the structural features of the pyrimidine derivatives as human A_{2A} adenosine receptor antagonists", BioSystems. 115: 13-22; January, 2014.

[58] Jun, W. and et al. "Discovery of nitropyridine derivatives as potent HIV-1 non-nucleoside reverse transcriptase inhibitorsviaa structure-based core refining approach", European Journal of Medicinal Chemistry. 76(9): 531-538; April, 2014.

[59] Ge, M. and et al. "Design and synthesis of a new series of modified CH-diarylpyrimidines as drug-resistant HIV non-nucleoside reverse transcriptase inhibitors", European Journal of Medicinal Chemistry. 82(23): 600-611; July, 2014.

[60] Zi, H. Y. and et al. "Structural modifications of *CH(OH)*-DAPYs as new HIV-1 non-nucleoside reverse transcriptase inhibitors", Bioorganic & Medicinal Chemistry. 22(8): 2535-2541; April, 2014.

24. Nguyen M, Claparols C, Bernadou J, Meunier B (2001) A fast and efficient metal-mediated oxidation of isoniazid and identification of isoniazid-NAD(H) adducts. ChemBioChem 2(12):877–883
25. Heym B, Zhang Y, Poulet S, Young D, Cole ST (1993) Characterization of the katG gene encoding a catalase-peroxidase required for the isoniazid susceptibility of *Mycobacterium tuberculosis*. J Bacteriol 175(13):4255–4259
26. Timmins GS, Deretic V (2006) Mechanisms of action of isoniazid. Mol Microbiol 62(5):1220–1227
27. Johnsson K, Froland WA, Schultz PG (1997) Overexpression, purification, and characterization of the catalase-peroxidase KatG from *Mycobacterium tuberculosis*. J Biol Chem 272(5):2834–2840
28. De La Iglesia AI, Morbidoni HR (2006) Mechanisms of action of and resistance to rifampicin and isoniazid in *Mycobacterium tuberculosis*: new information on old friends. Rev Argent Microbiol 38(2):97–109
29. Parikh SL, Xiao G, Tonge PJ (2000) Inhibition of InhA, the enoyl reductase from *Mycobacterium tuberculosis*, by triclosan and isoniazid. Biochemistry 39(26):7645–7650
30. Freundlich JS, Wang F, Vilchèze C, Gulten G, Langley R, Schiehser GA, Jacobus DP, Jacobs WR Jr, Sacchettini JC (2009) Triclosan derivatives: towards potent inhibitors of drug-sensitive and drug-resistant *Mycobacterium tuberculosis*. ChemMedChem 4(2):241–248
31. am Ende CW, Knudson SE, Liu N, Childs J, Sullivan TJ, Boyne M, Xu H, Gegina Y, Knudson DL, Johnson F, Peloquin CA, Slayden RA, Tonge PJ, Ende CW, Knudson SE, Liu N, Childs J, Sullivan TJ, Boyne M, Xu H, Gegina Y, Knudson DL, Johnson F, Peloquin CA, Slayden RA, Tonge PJ (2008) Synthesis and in vitro antimycobacterial activity of B-ring modified diaryl ether InhA inhibitors. Bioorg Med Chem Lett 18(10):3029–3033
32. Boyne ME, Sullivan TJ, am Ende CW, Lu H, Gruppo V, Heaslip D, Amin AG, Chatterjee D, Lenaerts A, Tonge PJ, Slayden RA (2007) Targeting fatty acid biosynthesis for the development of novel chemotherapeutics against *Mycobacterium tuberculosis*: evaluation of A-ring-modified diphenyl ethers as high-affinity InhA inhibitors. Antimicrob Agents Chemother 51(10):3562–3567
33. Sullivan TJ, Truglio JJ, Boyne ME, Novichenok P, Zhang X, Stratton CF, Li HJ, Kaur T, Amin A, Johnson F, Slayden RA, Kisker C, Tonge PJ (2006) High affinity InhA inhibitors with activity against drug-resistant strains of *Mycobacterium tuberculosis*. ACS Chem Biol 1(1):43–53
34. Luckner SR, Liu N, am Ende CW, Tonge PJ, Kisker C (2010) A slow, tight-binding inhibitor of InhA, the enoyl-ACP reductase from *Mycobacterium tuberculosis*. J Biol Chem 285(19):14330–14337
35 Pan P (2012) Lead optimization and slow-onset inhibition of the enoyl-ACP reductase (InhA) from *Mycobacterium tuberculosis*. PhD Diss., Stony Brook University
36. Lu XY, Chen YD, Jiang YJ, You QD (2009) Discovery of potential new InhA direct inhibitors based on pharmacophore and 3D-QSAR analysis followed by in silico screening. Eur J Med Chem 44(9): 3718–3730
37 Kumar A, Siddiqi MI (2008) CoMFA based de novo design of pyrrolidine carboxamides as inhibitors of enoyl acyl carrier protein reductase from *Mycobacterium tuberculosis*. J Mol Model 14(10): 923–935
38 Andrade CH, Salum Lde B, Castilho MS, Pasqualoto KF, Ferreira EI, Andricopulo AD (2008) Fragment-based and classical quantitative structure-activity relationships for a series of hydrazides as antituberculosis agents. Mol Divers 12(1):47–59
39. Lu XU, Chen YD, You QD (2010) 3D-QSAR studies of arylcarboxamides with inhibitory activity on InhA using pharmacophore-based alignment. Chem Bio Drug Des 75(2): 195–203
40. Punkvang A, Saparpakorn P, Hannongbua S, Wolschann P, Beyer A, Pungpo P (2010) Investigating the structural basis of arylamides to improve potency against *M. tuberculosis* strain through molecular dynamics simulations. Eur J Med Chem 45(12):5585–5593
41. Punkvang A, Saparpakorn P, Hannongbua S, Wolschann P, Pungpo P (2010) Elucidating drug-enzyme interactions and their structural basis for improving the affinity and potency of isoniazid and its derivatives based on computer modeling approaches. Molecules 15(4):2791–2813
42. Punkvang A, Saparpakorn P, Hannongbua S, Wolschann P, Berner H, Pungpo P (2010) Insight into crucial inhibitor–enzyme interaction of arylamides as novel direct inhibitors of the enoyl ACP reductase (InhA) from *Mycobacterium tuberculosis*: computer-aided molecular design. Monatsh Chem 141(9):1029–1041
43. Pauli I, dos Santos RN, Rostirolla DC, Martinelli LK, Ducati RG, Timmers LF, Basso LA, Santos DS, Guido RV, Andricopulo AD, Norberto de Souza O (2013) Discovery of new inhibitors of *Mycobacterium tuberculosis* InhA enzyme using virtual screening and a 3D-pharmacophore-based approach. J Chem Inf Model 53(9): 2390–2401
44. Kinjo T, Koseki Y, Kobayashi M, Yamada A, Morita K, Yamaguchi K, Tsurusawa R, Gulten G, Komatsu H, Sakamoto H, Sacchettini JC, Kitamura M, Aoki S (2013) Identification of compounds with potential antibacterial activity against *Mycobacterium* through structure-based drug screening. J Chem Inf Model 53(5):1200–1212
45. Kumar UC, Bvs SK, Mahmood S, Sriram D, Kumar-Sahu P, Pulakanam S, Ballell L, Alvarez-Gomez D, Malik S, Jarp S (2013) Discovery of novel InhA reductase inhibitors: application of pharmacophore- and shape-based screening approach. Future Med Chem 5(3):249–259
46. Stigliani JL, Bernardes-Génisson V, Bernadou J, Pratviel G (2012) Cross-docking study on InhA inhibitors: a combination of Autodock Vina and PM6-DH2 simulations to retrieve bio-active conformations. Org Biomol Chem 10:6341–6349
47. Subba Rao G, Vijayakrishnan R, Kumar M (2008) Structure-based design of a novel class of potent inhibitors of InhA, the enoyl acyl carrier protein reductase from *Mycobacterium tuberculosis*: a computer modelling approach. Chem Biol Drug Des 72(5):444–449
48. Stigliani JL, Arnaud P, Delaine T, Bernardes-Génisson V, Meunier B, Bernadou J (2008) Binding of the tautomeric forms of isoniazid-NAD adducts to the active site of the *Mycobacterium tuberculosis* enoyl-ACP reductase (InhA): a theoretical approach. J Mol Graph Model 27(4):536–545
49. (2006) GaussView 03, Revision 3.07, Gaussian, Inc., Wallingford, CT
50. Frisch MJ, Trucks GW, Schlegel HB, Scuseria GE, Robb MA, Cheeseman JR, Scalmani G, Barone V, Mennucci B, Petersson GA, Nakatsuji H, Caricato M, Li X, Hratchian HP, Izmaylov AF, Bloino J, Zheng G, Sonnenberg JL, Hada M, Ehara M, Toyota K, Fukuda R, Hasegawa J, Ishida M, Nakajima T, Honda Y, Kitao O, Nakai H, Vreven T, Jr. JAM, Peralta JE, Ogliaro F, Bearpark M, Heyd JJ, Brothers E, Kudin KN, Staroverov VN, Kobayashi R, Normand J, Raghavachari K, Rendell A, Burant JC, Iyengar SS, Tomasi J, Cossi M, Rega N, Millam JM, Klene M, Knox JE, Cross JB, Bakken V, Adamo C, Jaramillo J, Gomperts R, Stratmann RE, Yazyev O, Austin AJ, Cammi R, Pomelli C, Ochterski JW, Martin RL, Morokuma K, Zakrzewski VG, Voth GA, Salvador P, Dannenberg JJ, Dapprich S, Daniels AD, Farkas O, Foresman JB, Ortiz JV, Cioslowski J, Fox DJ (2009) Gaussian 09, revision B.01, Gaussian Inc., Wallingford CT
51. Morris GM, Goodsell DS, Huey R, Olson AJ (1996) Distributed automated docking of flexible ligands to proteins: parallel applications of AutoDock 2.4. J Comput Aided Mol Des 10(4):293–304
52. Tripos International (2008) SYBYL v8.0, Tripos International, 1699 South Hanley Rd., St. Louis, MO
53. Golbraikh A, Tropsha A (2002) Beware of q^2! J Mol Graph Model 20:267–276
54. Case DA, Darden TA, Cheatham TE, Simmerling CL, Wang J, Duke RE, Luo R, Crowley M, Walker RC, Zhang W, Merz KM, Wang B, Hayik S, Roitberg A, Seabra G, Kolossvry I, Wong KF, Paesani F, Vanicek J, Wu X, Brozell SR, Steinbrecher T, Gohlke H, Yang L, Tan

REFERENCES (CONTINUED)

[61] Santosh, N. M. and et al. "Synthesis, biological activity and docking study of imidazol-5-one as novel non-nucleoside HIV-1 reverse transcriptase inhibitors", Bioorganic & Medicinal Chemistry. 20(9): 3119-3127; May, 2012.

[62] Somayeh, P. and et al. "Pharmacophore Identification, Molecular Docking, Virtual Screening, and In Silico ADME Studies of Non- Nucleoside Reverse Transcriptase Inhibitors", Molecular Informatics. 31(11-12): 856-866; December, 2012.

[63] Manivannan, E. and Chaturvedi, S. C. "Analogue-based design, synthesis and molecular docking analysis of 2,3-diaryl quinazolinones as non-ulcerogenic anti-inflammatory agents", Bioorganic & Medicinal Chemistry. 19(15): 4520-4528; August, 2011.

[64] Katarzyna, M. M. and et al. "X-ray and molecular modelling in fragment-based design of three small quinoline scaffolds for HIV integrase inhibitors", Bioorganic & Medicinal Chemistry. 19(5): 1606-1612; March, 2011.

[65] Mohammad, G. and et al. "QSAR and docking studies of novel antileishmanial diaryl sulfides and sulfonamides", European Journal of Medicinal Chemistry. 45(11): 4879-4889; November, 2010.

[66] Elena, C. and et al. "Thiocarbamates as non-nucleoside HIV-1 reverse transcriptase inhibitors: Docking-based CoMFA and CoMSIA analyses", European Journal of Medicinal Chemistry. 44(5): 2059-2070; May, 2009.

[67] Dhaval, G. P. and et al. "The search for potent, small molecule NNRTIs: A review", Bioorganic & Medicinal Chemistry. 17(16): 5744-5762; August, 2009.

[68] Elaine, F. F. and et al. "3D-QSAR CoMFA/CoMSIA models based on theoretical active conformers of HOE/BAY-793 analogs derived from HIV-1 protease inhibitor complexes", European Journal of Medicinal Chemistry. 44(11): 4344-4352; November, 2009.

[69] Rongjing, H. and et al. "Receptor- and ligand-based 3D-QSAR study for a series of non-nucleoside HIV-1 reverse transcriptase inhibitors", Bioorganic & Medicinal Chemistry. 17(6): 2400-2409; March, 2009.

C, Mongan J, Hornak V, Cui G, Mathews DH, Seetin MG, Sagui C, Babin V, Kollman PA (2008) AMBER12. University of California, San Francisco

55. Duan Y, Wu C, Chowdhury S, Lee MC, Xiong G, Zhang W, Yang R, Cieplak P, Luo R, Lee T, Caldwell J, Wang J, Kollman P (2003) A point-charge force field for molecular mechanics simulations of proteins based on condensed-phase quantum mechanical calculations. J Comput Chem 24(16):1999–2012
56. Wang J, Wang W, Kollman PA, Case DA (2006) Automatic atom type and bond type perception in molecular mechanical calculations. J Mol Graphics Model 25(2):247–260
57. Wang J, Wolf RM, Caldwell JW, Kollman PA, Case DA (2004) Development and testing of a general AMBER force field. J Comput Chem 25(9):1157–1174
58. Cornell WD, Cieplak P, Bayly CI, Kollman PA (1993) Application of RESP charges to calculation conformational energies, hydrogen bond energies, and free energies of salvation. J Am Chem Soc 115(21): 9620–9631
59. Bayly CI, Cieplak P, Cornell WD, Kollman PA (1993) A well-behaved electrostatic potential based method using charge-restraints for deriving charges: The RESP model. J Phys Chem 97(40):10269–10280
60. Wang J, Cieplak P, Kollman PA (2000) How well does a restrained electrostatic potential (RESP) model perform in calculating conformational energies of organic and biological molecules? J Comput Chem 21(12):1049–1074
61. Gavernet L, Gonzalez Funes JL, Blanch LB, Estiu G, Maresca A, Supuran CT (2010) Affinity of sulfamates and sulfamides to carbonic anhydrase II isoform: experimental and molecular modeling approaches. J Chem Inf Model 50(6):1113–1122
62. Li W, Fu J, Cheng F, Zheng M, Zhang J, Liu G, Tang Y (2012) Unbinding pathways of GW4064 from human farnesoid X receptor as revealed by molecular dynamics simulations. J Chem Inf Model 52(11):3043–3052
63. Mahoney MW, Jorgensen WL (2000) A five-site model for liquid water and the reproduction of the density anomaly by rigid, nonpolarizable potential functions. J Chem Phys 112(20):8910–8922
64. Darden T, York D, Pedersen L (1993) Particle mesh Ewald: an N·log(N) method for Ewald sums in large systems. J Chem Phys 98(12):10089–10092
65. Ryckaert JP, Ciccotti G, Berendsen HJC (1977) Numerical integration of the Cartesian equations of motion of a system with constraints: molecular dynamics of *n*-alkanes. J Comp Phys 23(3):327–341
66. Homeyer N, Gohlke H (2012) Free energy calculations by the molecular mechanics Poisson–Boltzmann surface area method. Mol Inf 31(2):114–122
67. Wang J, Hou T, Xu X (2006) Recent advances in free energy calculations with a combination of molecular mechanics and continuum models. Curr Comput Aided Drug Des 2(3):95–103
68. Wang J, Morin P, Wang W, Kollman PA (2001) Use of MM-PBSA in reproducing the binding free energies to HIV1 RT of TIBO derivatives and predicting the binding mode to HIV1 RT of Efavirenz by docking and MM-PBSA. J Am Chem Soc 123(22):5221–5230
69. Hou T, Wang J, Li Y, Wang W (2011) Assessing the performance of the MM/PBSA and MM/GBSA Methods. 1. The accuracy of binding free energy calculations based on molecular dynamics simulations. J Chem Inf Model 51(1):69–82
70. Kaledin M, Brown A, Kaledin AL, Bowman JM (2004) Normal mode analysis using the driven molecular dynamics method. II. An application to biological macromolecules. J Chem Phys 121(12):5646–5653
71. Xue W, Qi J, Yang Y, Jin X, Liu H, Yao X (2012) Understanding the effect of drug-resistant mutations of HIV-1 intasome on raltegravir action through molecular modeling study. Mol BioSyst 8:2135–2144
72. Zar JH (1998) Biostatistical analysis. Prentice Hall, Upper Saddle River

REFERENCES (CONTINUED)

[70] Eamonn, F. H. and et al. "A docking study of L-chicoric acid with HIV-1 integrase", Journal of Molecular Graphics and Modelling. 27(5): 584-589; January, 2009.

[71] Pawan, G. Nilanjan, R. and Prabha, G. "Docking-based 3D-QSAR study of HIV-1 integrase inhibitors", European Journal of Medicinal Chemistry. 44(11): 4276-4287; November, 2009.

[72] Asim, S. and Kunal, R. "Predictive QSAR modeling of HIV reverse transcriptase inhibitor TIBO derivatives", European Journal of Medicinal Chemistry. 44(4): 1509-1524; April, 2009.

[73] Marco, R. and et al. "Towards novelS-DABOC inhibitors: Synthesis, biological investigation, and molecular modeling studies", Bioorganic & Medicinal Chemistry Letters. 18(21): 5777-5780; November, 2008.

[74] Zeng, L. J. Jin, H. and Hai, F. C. "Revealing Interaction Mode Between HIV-1 Reverse Transcriptase and Diaryltriazine Analog Inhibitor", Chemical Biology & Drug Design. 72(5): 350-359; December, 2008.

[75] David, J. K. and et al. "Identification and optimization of N^3,N^6-diaryl-1H-pyrazolo[3,4-d] pyrimidine-3,6-diamines as a novel class of ACK1 inhibitors", Bioorganic & Medicinal Chemistry Letters. 18(24): 6352-6356; December, 2008.

[76] Serdar, D. Thomas, M. and Manthos, G. P. "3D QSAR CoMFA/CoMSIA, molecular docking and molecular dynamics studies of fullerene-based HIV-1 PR inhibitors", Bioorganic & Medicinal Chemistry. 18(23): 6283-6289, December, 2008.

[77] Maria, L. B. and et al. "Discovery of novel benzimidazolones as potent non-nucleoside reverse transcriptase inhibitors active against wild-type and mutant HIV-1 strains". Bioorganic & Medicinal Chemistry Letters 17(7): 1956-1960; April, 2007.

[78] Ravichandran, V. and Agrawal, K. R. "Predicting anti-HIV activity of PETT derivatives: CoMFA approach". Bioorganic & Medicinal Chemistry Letters 17(8): 2197–2202; April, 2007.

The structural requirement of direct InhA inhibitors for high potency against *M. Tuberculosis* based on computer aided molecular design

A. Punkvang[1], P. Kamsri[1], A. Kumkong[1], K. Kunasa[1], P. Saparpakorn[2], S. Hannongbua[2], P. Wolschann[3], P. Pungpo[1*]

[1] Department of Chemistry, Faculty of Science, Ubon Ratchathani University, Ubonratchathani, Thailand,34190
[2] Department of Chemistry, Faculty of Science, Kasetsart University, Chatuchak, Bangkok, Thailand, 10900
[3] Institute for Theoretical Chemistry, University of Vienna, A-1090 Vienna, Austria

Many series of direct InhA inhibitors, arylamide, pyrrolidine carboxamide, diphenyl ether and triclosan derivatives, have been developed as antituberculosis agents to combat the drug-resistance of isoniazid (INH). However, an effort to design novel antituberculosis drugs in the class of direct InhA inhibitors is confronted with a poor in vitro antibacterial activity of the available compounds. To evaluate the key structural features relating to the antibacterial activity of direct InhA inhibitors against *M. tuberculosis*, 2D and 3D QSAR approaches, HQSAR, CoMFA and CoMSIA are convenient tools to establish correlations between biological activities and various molecular properties. The results obtained from the graphic interpretation designed in different QSAR models indicate the structure requirement to improve the antibacterial activity of direct InhA inhibitors. Moreover, our results are the first findings which provide the quantitative relationship between the structural property and antibacterial activity of direct InhA inhibitors. Consequently, the obtained results suggest a structural guideline for design and synthesis of a new generation of direct InhA inhibitors which will display a better potency against *M. tuberculosis*.

Keywords *M. tuberculosis*; InhA; QSAR; antituberculosis

1. Introduction

Tuberculosis (TB) is a chronic infection disease caused by *Mycobacterium tuberculosis* (*M. tuberculosis*). HIV coinfection with tuberculosis, multidrug resistant tuberculosis (MDR-TB) and extensively drug-resistant tuberculosis (XDR-TB) have brought tuberculosis into the failure of current standard treatment regimens [1]. This fact prompts the research to develop novel and more potent drug candidates to treat *M. tuberculosis* strains resistant to existing drugs. The enoyl-acyl ACP reductase (InhA) of *M. tuberculosis* catalyzing the NADH-specific reduction of 2-trans-enoyl-ACP [2] is an attractive target for designing novel antibacterial agents [3-8]. InhA has been identified as the primary target of isoniazid (INH), one of the most effective first-line anti-TB drugs [9-14]. InhA is inhibited by the active adduct of INH (INH-NAD) [15-16] which is covalently formed between NAD+ and the reactive acyl radical of INH generated by the activation of catalase-peroxidase (KatG) [17-23]. The major mechanism of INH resistance arises from mutations in KatG [24-25]. To overcome the INH resistance associated with mutations in KatG, compounds which directly inhibit the InhA enzyme without requiring activation of KatG called direct InhA inhibitors are new promising agents against tuberculosis. Because of the remarkable properties of direct InhA inhibitors, many research groups have been attempting to develop direct InhA inhibitors, e.g. triclosan [26], diphenyl ether [27-29], pyrrolidine carboxamide [30] and arylamide derivatives [31-32]. However, the development of these compounds is confronted with a poor activity against *M. tuberculosis* in antimycobacterial assay of many of these compounds. Recently, new series of direct InhA inhibitors have been discovered, and their minimum inhibitory concentrations (MIC) against *M. tuberculosis* have been evaluated [33]. Interestingly, these new direct InhA inhibitors show MIC values better than those of the existing direct InhA inhibitors. Therefore, the present article describes the relationship between MIC values and structural properties of these new direct InhA inhibitors by means of computer aided molecular design (CAMD). Approaches based on 2D and 3D QSAR methods, HQSAR (Hologram QSAR), CoMFA (Comparative Moleclar Field Approach) and CoMSIA (Comparative Molecular Similarity Indices Analysis) [34-36] have been used. A better understanding of the key structural features relating to the MIC values of direct InhA inhibitors is the consequence of these investigations.

2. Materials and calculation methods

2.1 Data sets and antitubercular activities

34 direct InhA inhibitors [26, 31, 33], listed in Table 1, were used to build CoMFA, CoMSIA and HQSAR models. The MIC value of each compound against *M. tuberculosis* was converted to the corresponding log (1/MIC) and used as dependent variables for the QSAR models. The structures of these 34 compounds were constructed using standard tools available in GaussView 3.07 program [37] and were then fully optimized using an *ab initio* quantum chemical method

(HF/3-21G) implemented in the Gaussian 03 program [38]. The compounds were divided into a training set of 29 compounds and a test set of 5 compounds for the model development and model validation, respectively. The representatives of the test set were manually selected and are covering the utmost range of activity and structural diversity of direct InhA inhibitors in the data set.

Table 1 The chemical structures and MIC values against *M. tuberculosis* of 34 direct InhA inhibitors.

No.	Structure	MIC(μM)	Log 1/MIC)	No.	Structure	MIC (μM)	Log (1/MIC)
1	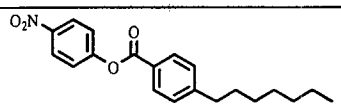	187.40	3.73	18	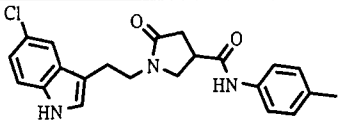	80.83	4.09
2	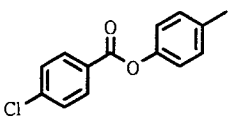	259.42	3.59	19	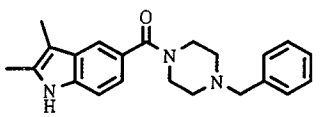	368.38	3.43
3	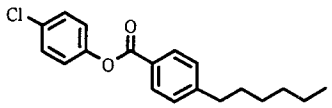	202.00	3.69	20	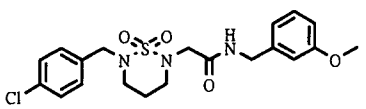	146.13	3.86
4	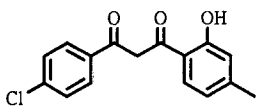	13.85	4.86	21	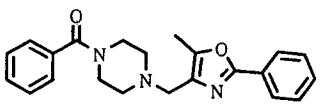	187.48	3.73
5	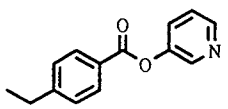	563.20	3.25	22[a]	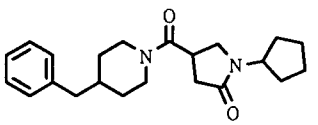	361.07	3.44
6	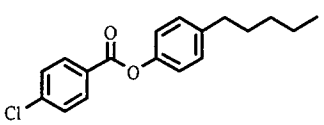	105.68	3.98	23	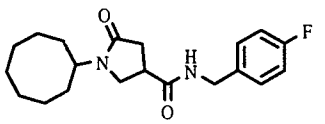	369.46	3.43
7	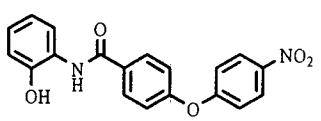	5.70	5.24	24[a]	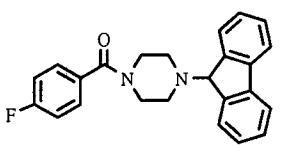	85.91	4.07
8[a]	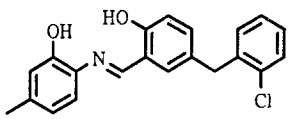	181.90	3.74	25	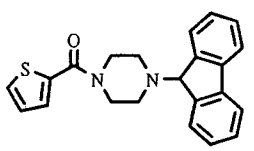	355.08	3.45
9	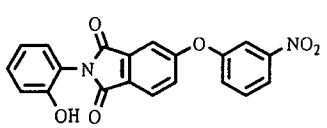	85.03	4.07	26	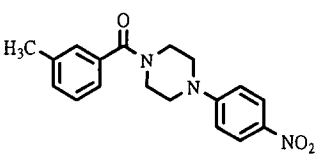	125.00	3.90
10	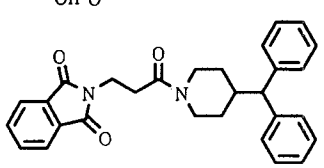	141.10	3.85	27	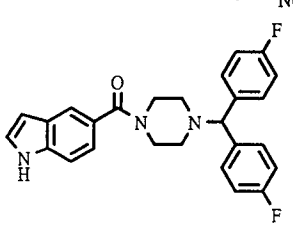	62.50	4.20
11	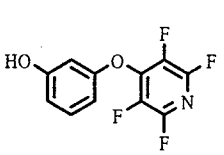	246.95	3.61	28	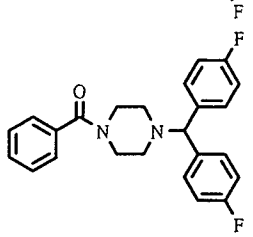	125.00	3.90

12	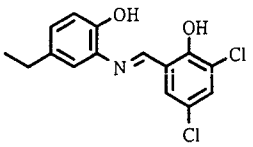	206.33	3.69	29	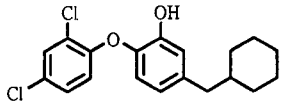	27.00	4.57
13[a]	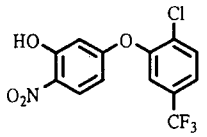	383.63	3.42	30	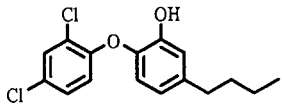	30.00	4.52
14	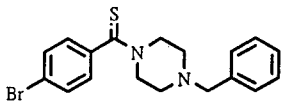	85.25	4.07	31	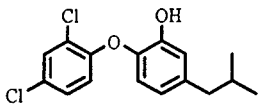	60.00	4.22
15	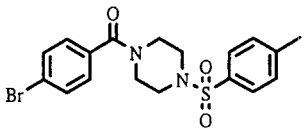	302.36	3.52	32	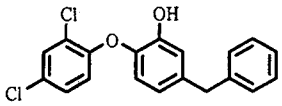	27.00	4.57
16	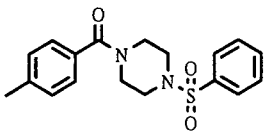	371.61	3.43	33[a]	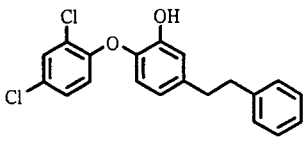	52.00	4.28
17	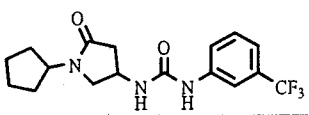	180.09	3.74	34	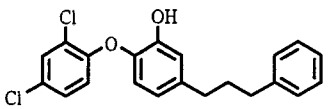	13.00	4.89

[a] Test set compounds

2.2 Molecular docking calculations

The X-ray crystal structure of InhA complexed with a direct InhA inhibitor (pdb code 2NSD) was employed for molecular docking calculations. Docking calculations of the data set were carried out by the Autodock 3.05 program using Lamarckian Genetic Algorithm (LGA) [39]. Docking parameters were used as default values, except for the number of docking runs which was set to 50. The docking calculation was validated by reproducing the X-ray conformation of the ligand as well as the orientation in its pocket. A RMSD value between the original and docked coordinates lower than 1Å is acceptable. The ligand pose with the lowest final docked energy was selected as the best binding mode of direct InhA inhibitors. Then, the conformations according to this binding mode, as shown in Fig. 1, were used for CoMFA and CoMSIA setups.

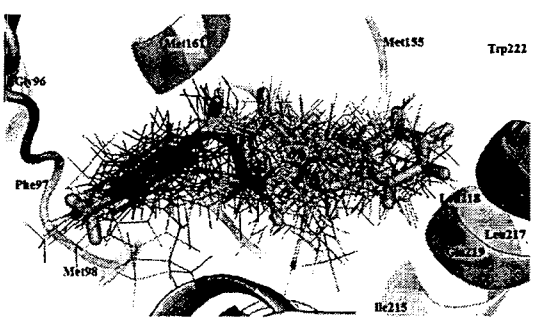

Fig. 1 The best binding modes of direct InhA inhibitors (line) in InhA pocket (ribbon) predicted by docking calculations.

2.3 CoMFA and CoMSIA techniques

The structural alignment of compounds is an important prerequisite for the setup of appropriate CoMFA and CoMSIA models. In the present study, the reasonable binding modes of compounds in the data set obtained from the validated docking calculations were employed for the molecular alignment. SYBYL 8.0 molecular modeling software [40] was used to construct CoMFA and CoMSIA models. CoMFA descriptors, steric and electrostatic fields, were calculated using sp^3 carbon probe atom with a formal charge of +1 which was placed at the intersections in a grid with the spacing

of 2Å. The maximum steric and electrostatic energies were truncated at 30 kcal/mol. Five CoMSIA descriptors, steric, electrostatic, hydrophobic, hydrogen bond donor and hydrogen bond acceptor fields, were derived with the same grid as used for the CoMFA field calculation. There are no energy cutoffs necessary for CoMSIA calculations because a distance-dependent Gaussian type potential was used in contrary to the procedure of CoMFA calculations. CoMFA and CoMSIA descriptors were set as independent variables and log (1/MIC) values were used as dependent variables in the partial least square (PLS) analysis to derive a linear relationship between molecular descriptors and activities. The cross-validation was performed using the leave-one-out method with a 2.0 kcal/mol column filter to minimize the influence of noisy columns. A final non cross-validated analysis with the optimal number of components was sequentially performed and was then employed to analyze the results. The non-cross-validated correlation coefficient (r^2) and the leave-one-out (LOO) cross-validated correlation coefficient (q^2) were used to evaluate the predictive ability of the CoMFA and CoMSIA models.

2.4 HQSAR

Hologram QSAR (HQSAR) does not require information about the three-dimensional geometry of the inhibitors. Hence, contrary to CoMFA and CoMSIA methods, HQSAR needs no molecular alignment. Each compound in the data set was converted into all possible molecular fragments including linear, branched, cyclic, and overlapping fragments in the size of 4-7 atoms. Molecular fragment generation utilizes the fragment distinction parameters including atoms (A), bonds (B), connections (C), hydrogen atoms (H), chirality (Ch), and hydrogen donor and acceptor properties (DA). The generated molecular fragments are counted in bins of a fixed length array to produce a molecular hologram. PLS statistical method was applied to establish a correlation of the molecular hologram descriptors with the biological data. The HQSAR module of SYBYL 8.0 was employed for the HQSAR study. The same training and test sets as for CoMFA and CoMSIA studies were used. The most convenient model was selected based on the best crossvalidated r^2.

3. Results and discussion

3.1 CoMFA, CoMSIA and HQSAR models

The PLS results of CoMFA, CoMSIA and HQSAR models are summarized in Table 2. QSAR models 1, 3 and 5 derived from PLS analyses of all compounds in the training set show a poor q^2. To improve the quality of these QSAR models, compound 4 was considered as an outlier, and compounds 23 and 9 were consecutively outliers of models 1 and 5, respectively. Omission of these compounds results in better q^2 values of models 2, 4 and 6 as shown in Table 2. The final CoMFA model, composing of steric and electrostatic fields, model 2, gives q^2 of 0.53 and r^2 of 0.97. In the case of the best CoMSIA model including steric, electrostatic and hydrophobic fields, model 4, shows a higher q^2 value of 0.68 as compared with that of the final CoMFA model with r^2 of 0.98 for 4 components. This result indicates that the best CoMSIA model performs better in the prediction than the final CoMFA model. Among the considered descriptors of the best CoMSIA model, the hydrophobic field contributing of 46.5% is the most important parameter influencing the MIC values of the direct InhA inhibitors in the training set. With regard to the best HQSAR model, model 6, generated based on the combination of the different fragment types including bonds, atoms and connections (B/A/C), q^2 value of 0.63 with r^2 value of 0.97 of the model is comparable with those of the best CoMSIA model.

Table 2 Summary of statistical results of CoMFA, CoMSIA and HQSAR models.

	Models	Statistical parameters						Fraction
		q^2	r^2	N	s	SEE	F	
	CoMFA							
1	S/E	0.12	0.66	2	0.49	0.30	24.75	41.4/58.6
2	**S/E**	**0.53**	**0.97**	**5**	**0.37**	**0.09**	**146.25**	**44.2/55.8**
	CoMSIA							
3	E/H/S	0.31	0.89	3	0.44	0.17	67.78	40.1/44/15.9
4	**E/H/S**	**0.68**	**0.98**	**4**	**0.29**	**0.08**	**229.15**	**37.2/ 46.5/16.2**
	HQSAR							
5	B/A/C	0.39	0.59	2	0.40	0.33	-	-
6	**B/A/C**	**0.63**	**0.97**	**5**	**0.33**	**0.10**	-	-

Bold fonts indicate the best QSAR model. N, optimum number of components; s, standard error of prediction, SEE, standard error of estimate; F, F-test value; S, steric field; E, electrostatic field; H, hydrophobic field; A, atom; B, bond; C, connection

3.2 Validation of the QSAR models

Satisfyingly good correlations between actual and predicted activities of the training set, based on the final CoMFA, CoMSIA and HQSAR models, are depicted in Fig. 2. The predicted activities of the training set derived from the best QSAR models are close to the experimental activities indicating the high degree of correlation between the actual and predicted activities. In order to assess the external predictive ability of selected QSAR models, antitubercular activities of the test set were predicted. The predicted values of test set compounds are within one logarithmic unit difference from the experimental values as presented in Fig. 2 revealing that all selected QSAR models are reliable with high predictive ability. Therefore, the best CoMFA, CoMSIA, and HQSAR models can be utilized for designing new direct InhA inhibitors with improved activity.

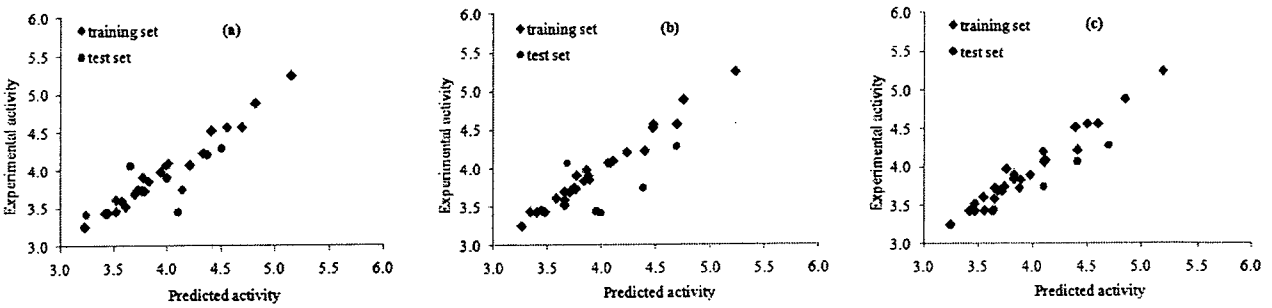

Fig. 2 Plots between the actual and predicted activities of the training and test sets derived from the best CoMFA (a), CoMSIA (b) and HQSAR (c) models, respectively.

3.3 Activities against InhA and *M. tuberculosis* of direct InhA inhibitors

Before a detailed discussion of the CoMFA and CoMSIA contour maps, the activities against the enzyme InhA (given in IC_{50} values) and the complete organism *M. tuberculosis* (expressed in MIC values) of the direct InhA inhibitors has to be mentioned in this section. Direct InhA enzyme inhibitors are very important among other compounds with activities against *M. tuberculosis*. The crucial interactions of these compounds in the InhA binding pocket, the key parameter for InhA inhibition, have been clarified by mean of X-ray crystallography [26, 29, 31, 32]. The conserved interactions of direct InhA inhibitors are two hydrogen bonds between inhibitors and Tyr158 as well as NAD+. Besides, more hydrophobic contacts of direct InhA inhibitors exist such as the interaction of aromatic rings or of long alkyl chains in the hydrophobic pocket constituted from the hydrophobic residues of Phe149, Pro193, Met199, Ile215, Leu217, Leu218 and Trp222. Moreover, these inhibitors could interact with the hydrophilic pocket formed by the backbone of Gly96, Phe97, Met98 and the pyrophosphate group of NAD+. As shown in our previous work [41], the hydrophobic pocket of InhA is flexible for the binding of inhibitors, whereas the hydrophilic pocket seems to be more rigid. Although the InhA inhibitory activity of direct InhA inhibitors is important for the MIC value against *M. tuberculosis*, both activities are not in a linear relationship. Most of the formerly discovered direct InhA inhibitors displaying efficacious activities against InhA have poor MIC values [26-32]. As examples from a series of arylamides [31], some selected compounds with the best enzyme inhibitory activities, compounds p1, p2 and p3, indicate modest antibacterial activities. The majority of the compounds exhibit MIC values above 125 μM. Compound p4, exhibiting IC_{50} value of 1.04 μM, displays a high MIC value of 65.2 μM. Compounds p6 and a6 giving IC_{50} values of 2.04 and 15.47 μM, respectively, have MIC values of 125 μM. This phenomenon may be accounted by the poor druglikeness of these direct InhA inhibitors as well as their low solubility, ClogP value greater than 5, unsuitable membrane permeability and the efflux pump of the bacterial cell [27, 29-31]. Accordingly, to improve the potency of the direct InhA inhibitors, the key structural feature which is beneficial for both activities against InhA and *M. tuberculosis* should be taken into account. Therefore, our present study attempts to link the key structural requirement for better MIC values of direct InhA inhibitors derived from QSAR models toward the InhA inhibition of these compounds. This is the reason why the obtained CoMFA, CoMSIA contour maps revealing the key structural requirement are interpreted in the combination with the InhA pocket complexed with direct InhA inhibitors as shown in Fig. 3. Moreover, the reliable binding modes derived from docking calculations of these inhibitors in InhA pocket were used for our QSAR study.

3.4 CoMFA and CoMSIA contour maps

To reveal the importance of molecular descriptor fields on antitubercular activities of direct InhA inhibitors, CoMFA and CoMSIA contour maps were established. Because of the slightly lower predictive ability of the final CoMFA model as compared with that of the best CoMSIA model, only CoMSIA contour maps including steric, electrostatic and hydrophobic contours merged with the InhA binding pocket are shown in Fig. 3. Green and yellow contours indicate areas where favorable and unfavorable steric bulks are predicted to enhance the antitubercular activities of direct InhA

inhibitors. Blue and red contours indicate regions where electropositive and electronegative groups lead to increasing antitubercular activity, respectively. Purple and white contours represent areas, where the hydrophobic group and the hydrophilic group are predicted to favour the biological activities. Compound 7, the most active compound in the present data set, was selected as the template for graphic interpretation of the CoMSIA model. With regard to 2-hydroxy-phenylamide of compound 7, buried in the rigid hydrophilic InhA pocket, formed by the backbone of Gly96, Phe97, Met98, Met161 and NAD+, there is a red contour at the *para*-position indicating that this position prefers an electron donating substituent such as OH and NH_2. Also, two yellow contours - one is overlapped with a white contour near the OH - suggest that these areas favour a small substituent and a hydrophilic group to increase the activities. According to the obtained results, above structural requirements are favourable not only for MIC values but also for binding of direct InhA inhibitors in the rigid hydrophilic InhA pocket. Therefore, these characteristics are good for both activities against InhA and *M. tuberculosis*. There is a large magenta contour covering the benzamide ring of compound 7 and immediately bumped by a large yellow contour over the benzamide ring. This result indicates that the hydrophobic group as well as the aromatic ring at this position is favourable for better activities against *M. Tuberculosis*. However, there should be an optimal size of the substituent at this position because of the presence of an unfavorable steric area. Regarding the 4-nitro-phenylether of compound 7, occupied in the hydrophobic pocket of InhA constituted by Pro193, Trp222, Leu218, Leu217, Ile215 and Met155, this moiety is buried in a prominent green contour and immediately flanked by a minor purple contour and a large white contour. Therefore, the presence of the bulky group containing the suitable hydrophobic and hydrophilic properties could improve the MIC value of direct InhA inhibitors. Remarkably, although this hydrophilic property is favourable for MIC value, it seems to be unfavourable for the binding affinity of the direct InhA inhibitors in the hydrophobic pocket of InhA leading to decrease the activity against InhA. The obtained result implies that the hydrophilic requirement may be helpful for better solubility, ClogP value and membrane permeability of direct InhA inhibitors resulting in the better activity against *M. tuberculosis*. Accordingly, the correct balance between the hydrophobic and hydrophilic requirements in this area of direct InhA inhibitors should be beneficial for both activities against InhA and *M. tuberculosis* leading to good antitubercular activities. It is important to note that in order to combine all structural requirements presented by the CoMSIA contour maps into a molecule to improve the antitubercular activity, a direct InhA inhibitor should be a more extended compound, like e.g. compound 7. This reason may be one of the factors accounted for the lower activity against *M. tuberculosis* of compounds 2, 5, 11, 12, 13 which are less extended compounds.

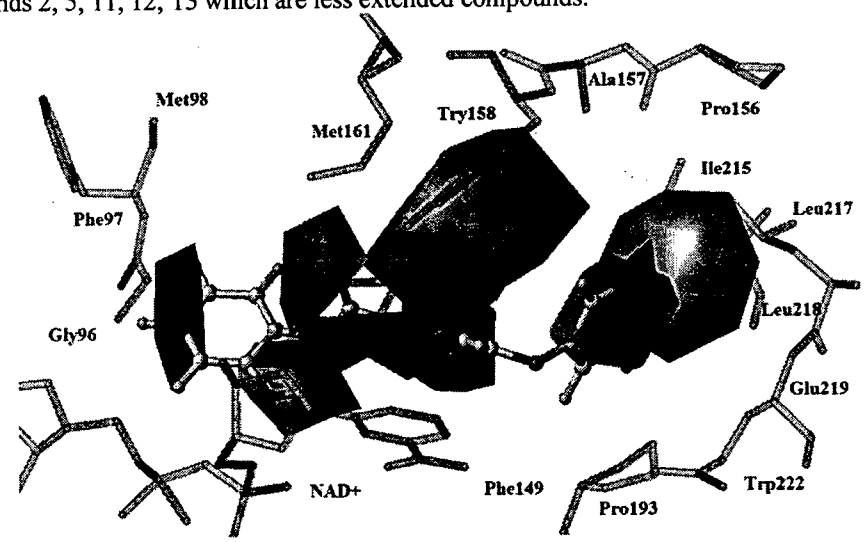

Fig. 3 CoMSIA steric, electrostatic and hydrophobic contours in combination with compound 7 (colored by atom type) in InhA binding pocket (cyan). Green (G) and yellow (Y) contours represent favourable and unfavourable steric regions, respectively. Blue (B) and red (R) contours are favoured for electropositive and electronegative groups, respectively. Purple (P) and white (W) contours show favourable and unfavourable hydrophobic regions, respectively.

3.5 HQSAR contribution maps

The contributions of molecular fragments to the antitubercular activities of direct InhA inhibitors in the present data set can be visualized through HQSAR contribution maps. The color codes indicate the different contributions of all atoms in each compound to the biological activity. An atom with negative contribution is represented at the red end of the spectrum, whereas an atom with positive contributions is presented at the green end of the spectrum. The white colored atoms are giving intermediate contributions. Fig. 4 depicts the individual atomic contributions to the activity against *M. tuberculosis* of the most active compound, compound 7. The hydroxyl group, the two carbons connected to OH and NH fragments of 2-hydroxy-phenylamide are colored by green indicating their positive contributions to the antitubercular activity. In CoMSIA contours, these positive contributing moieties are surrounded by yellow, blue and white contours

implying that these fragments of compound 7 are suitable for steric, electrostatic and hydrophobic requirements. On the other hand, a carbon atom of 2-hydroxy-phenylamide buried in a red contour, as shown in Fig. 3, is colored by white indicating that this atom has no contributions to the antitubercular activity. Besides, an oxygen carbonyl atom is represented by green which emphasizes the important contribution of this atom. Considering the benzamide ring which is covered by a large purple contour and located under a bulky yellow contour in the CoMSIA model, most atoms in this part are given by green. This finding indicates that the benzamide ring is good for steric and hydrophobic requirements and crucial for the activity against *M. tuberculosis*. In contrast, the majority of 4-nitro-phenylether occupied in green, white and purple CoMSIA contours is colored by white suggesting that this part has no contribution and should be modified in order to enhance the antitubercular activity. In case of the lower active compound, compound 16, atoms colored by orange are presented in the piperazine ring indicating the negative contributions of molecular fragments to the antitubercular activity exist. Therefore, the modification of this part following the CoMSIA suggestion may improve the antitubercular activity.

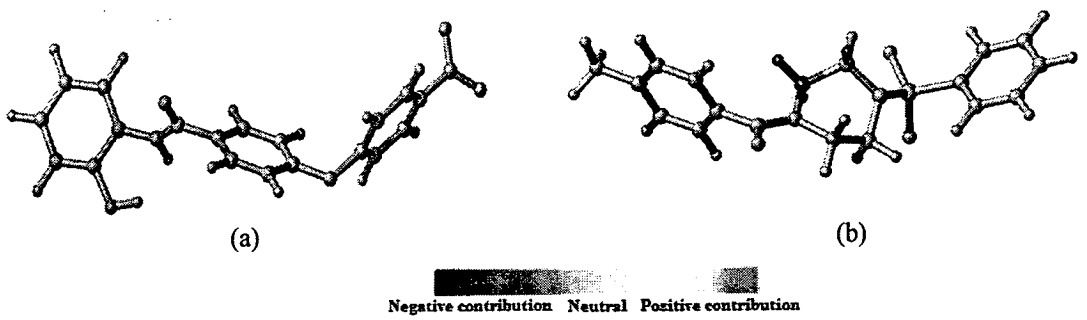

Fig. 4 The final HQSAR contribution maps for compounds 7 (a) and 16 (b).

4. Conclusion

The graphic interpretation of the obtained CoMSIA model based on docking alignment and the HQSAR model clearly elucidates the key structural elements of direct InhA inhibitors required for a good antitubercular activity. Among all standard descriptor fields of CoMSIA, only steric, electrostatic and hydrophobic field descriptors were considered for such models which suggest that these molecular descriptors are the important factors influencing the MIC value of the direct InhA inhibitor against *M. tuberculosis*. The correct balance between the hydrophilic and hydrophobic properties of direct InhA inhibitors suggested by CoMSIA model should compromise the inhibitory activities against InhA and *M. tuberculosis* leading to improve the antitubercular activity. Besides, the characteristics of 3D contour plots derived in this study imply that the feature of good direct InhA inhibitor should belong to the long length molecules. In agreement with CoMSIA results, the HQSAR contribution maps show the individual contribution of the atoms to the MIC values of direct InhA inhibitors. Concluding, the integrated results obtained from the 2D and 3D QSAR studies provide the basis for rational design of high potency drugs in the future and for possible syntheses of novel and more active antitubercular agents in the series of the direct InhA inhibitors.

Acknowledgements This investigation was supported by the Thailand Research Fund (DBG5380006,DBG5380042, RTA53800010). A. Punkvang is grateful to the grant from under the program Strategic Scholarships for Frontier Research Network for the Ph.D. Faculty of science, Ubon Ratchathani University, University of Vienna and ASEA-Uninet are gratefully acknowledged for supporting this research.

References

[1] World Health Organization. Multidrug and extensively drug-resistant TB (M/XDR-TB): 2010 global report on surveillance and response.
[2] Quemard A, Sacchettini JC, Dessen A, Vilcheze C, Bittman R, Jacobs Jr WR, Blanchard JS. Enzymatic characterization of the target for isoniazid in Mycobacterium tuberculosis. *Biochemistry*.1995;34:8235-8241.
[3] Campbell JW, Cronan Jr JE. Bacterial fatty acid biosynthesis: Targets for antibacterial drug discovery. *Annu. Rev. Microbiol.* 2001;55:305-332.
[4] Heath RJ, Rock CO. Fatty acid biosynthesis as a target for novel antibacterials. *Curr. Opin. Invest. Drugs.* 2004;5:146-153.
[5] White SW, Zheng J, Zhang YM, Rock CO. The structural biology of type II fatty acid biosynthesis. *Annu. Rev. Biochem.* 2005;74:791-831.
[6] Zhang YM, Lu YJ, Rock CO. The reductase steps of the type II fatty acid synthase as antimicrobial targets. *Lipids.*2004;39:1055-1060.
[7] Wen L, Chmielowski JN, Bohn KC, Huang JK, Timsina YN, Kodali P, Pathak AK. Functional expression of Francisella tularensis FabH and FabI, potential antibacterial targets. *Protein Expr. Purif.* 2009;65:83-91.

[8] Wright HT, Reynolds KA. Antibacterial targets in fatty acid biosynthesis. *Curr. Opin. Microbiol.* 2007;10:447-453.
[9] Rozwarski DA, Grant GA, Barton DH, Jacobs Jr. WR, Sacchettini JC. Modification of the NADH of the isoniazid target (InhA) from Mycobacterium tuberculosis. *Science* 1998;279:98–102.
[10] Vilcheze C, Wang F, Arai M, Hazbon MH, Colangeli R, Kremer L, Weisbrod TR, Alland D, Sacchettini JC, Jacobs Jr WR. Transfer of a point mutation in Mycobacterium tuberculosis inhA resolves the target of isoniazid. *Nat. Med.* 2006;12:1027–1029.
[11] Dessen A, Quemard A, Blanchard JS, Jacobs Jr WR, Sacchettini JC. Crystal structure and function of the isoniazid target of Mycobacterium tuberculosis. *Science* 1995;267:1638–1641.
[12] Lei B, Wei CJ, Tu SC. Action mechanism of antitubercular isoniazid. Activation by Mycobacterium tuberculosis KatG, isolation, and characterization of inha inhibitor. *J. Biol. Chem.* 2000;275:2520–2526.
[13] Johnsson K, King DS, Schultz PG. Studies on the mechanism of action of isoniazid and ethionamide in the chemotherapy of tuberculosis. *J. Am. Chem. Soc.*1995;117:5009–5010.
[14] Quemard A, Dessen A, Sugantino M, Jacobs Jr WR, Sacchetini JC, Blanchard JS. Binding of catalase-peroxidase-activated isoniazid to wild-type and mutant Mycobacterium tuberculosis enoyl-ACP reductases. *J. Am. Chem. Soc.* 1996;118:1561-1562.
[15] Timmins GS, Deretic V. Mechanisms of action of isoniazid. *Mol. Microbiol.* 2006;62:1220-1227.
[16] Johnsson K, Froland WA, Schultz PG. Overexpression, purification, and characterization of the catalase-peroxidase KatG from Mycobacterium tuberculosis. *J. Biol. Chem.*1997;272:2834-2840.
[17] Saint-Joanis B, Souchon H, Wilming M, Johnsson K, Alzari PM, Cole ST. Use of site-directed mutagenesis to probe the structure, function and isoniazid activation of the catalase/peroxidase, KatG, from Mycobacterium tuberculosis. *Biochem. J.* 1999;338:753-760.
[18] Zhao X, Yu H, Yu S, Wang F, Sacchettini JC, Magliozzo RS. Hydrogen peroxide-mediated isoniazid activation catalyzed by Mycobacterium tuberculosis catalase-peroxidase (KatG) and its S315T mutant. *Biochemistry*. 2006;45:4131-4140.
[19] Metcalfe C, Macdonald IK, Murphy EJ, Brown KA, Raven EL, Moody PC. The tuberculosis prodrug isoniazid bound to activating peroxidises. *J. Biol. Chem.*2008;283:6193-6200.
[20] Sinha BK. Enzymatic activation of hydrazine derivatives. *J. Biol. Chem.*1983;258:796-801.
[21] Nguyen M, Claparols C, Bernadou J, Meunier B. A fast and efficient metal-mediated oxidation of isoniazid and identification of isoniazid-NAD(H) adducts. *ChembioChem.*2001;2:877-883.
[22] Heym B, Zhang Y, Poulet S, Young D, Cole ST. Characterization of the katG gene encoding a catalase-peroxidase required for the isoniazid susceptibility of Mycobacterium tuberculosis. *J. Bacteriol.* 1993;175:4255-4259.
[23] Johnsson K, Schultz PG. Mechanistic studies of the oxidation of isoniazid by the catalase peroxidase from Mycobacterium tuberculosis. *J. Am. Chem. Soc.* 1994;116:7425–7426.
[24] De La Iglesia AI, Morbidoni HR. Mechanisms of action of and resistance to rifampicin and isoniazid in Mycobacterium tuberculosis: new information on old friends. *Rev. Argent Microbiol.* 2006;38:97-109.
[25] Banerjee A, Dubnau E, Quemard A, Balasubramanian V, Um KS, Wilson T, Collins D, de Lisle G, Jacobs Jr WR. inhA, a gene encoding a target for isoniazid and ethionamide in Mycobacterium tuberculosis. *Science*. 1994;263:227–230.
[26] Freundlich JS, Wang F, Vilcheze C, Gulten G, Langley R, Schiehser GA, Jacobus DP, Jacobs Jr WR, Sacchettini JC. Triclosan derivatives: Towards potent inhibitors of drug-sensitive and drug-resistant Mycobacterium tuberculosis. *Chem. Med. Chem.* 2009;4:241-248.
[27] am Ende CW, Knudson SE, Liu N, Childs J, Sullivan TJ, Boyne M, Xu H, Gegina Y, Knudson DL, Johnson F, Peloquin CA, Slayden RA, Tonge PJ. Synthesis and in vitro antimycobacterial activity of B-ring modified diaryl ether InhA inhibitors. *Bioorg. Med. Chem. Lett.* 2008;18:3029-3033.
[28] Boyne ME, Sullivan TJ, am Ende CW, Lu H, Gruppo V, Heaslip D, Amin AG, Chatterjee D, Lenaerts A, Tonge PJ, Slayden RA. Targeting fatty acid biosynthesis for the development of novel chemotherapeutics against Mycobacterium tuberculosis: evaluation of A-ring-modified diphenyl ethers as high-affinity InhA inhibitors. *Antimicrob. Agents Chemother.* 2007;51:3562-3567.
[29] Sullivan TJ, Truglio JJ, Boyne ME, Novichenok P, Zhang X, Stratton CF, Li H J, Kaur T, Amin A, Johnson F, Slayden RA, Kisker C, Tonge PJ. High affinity InhA inhibitors with activity against drug-resistant strains of Mycobacterium tuberculosis. *ACS Chem Biol.* 2006;17:43-53.
[30] He X, Alian A, Stroud R, Ortiz de Montellano PR. Pyrrolidine carboxamides as a novel class of inhibitors of enoyl acyl carrier protein reductase from Mycobacterium tuberculosis. *J. Med. Chem.* 2006;49:6308-6323.
[31] He X, Alian A, Ortiz de Montellano PR, Inhibition of the Mycobacterium tuberculosis enoyl acyl carrier protein reductase InhA by arylamides. *Bioorg. Med. Chem.* 2007;15:6649–6658.
[32] Kuo MR, Morbidoni HR, Alland D, Sneddon SF, Gourlie BB, Staveski MM, Leonard M, Gregory JS, Janjigian AD, Yee C, Musser JM, Kreiswirth B, Iwamoto H, Perozzo R, Jacobs Jr WR, Sacchettini JC, Fidock DA. Targeting tuberculosis and malaria through inhibition of Enoyl reductase: compound activity and structural data. *J. Biol. Chem.* 2003;278:20851-20859.
[33] Muddassar M, Jang JW, Hong SK, Cho YS, Kim EE, Keum KC, Oh T, Cho SN, Pae AN. Identification of novel antitubercular compounds through hybrid virtual screening approach. *Bioorg. Med. Chem.* 2010;18:6914-21.
[34] Cramer R D III, Patterson D E, Bunce J D. Comparative molecular field analysis (CoMFA). 1. Effect of shape on binding of steroids to carrier proteins. *J. Am. Chem. Soc.* 1998;110:5959-5967.
[35] Klebe G, Abraham U, Mietzner T. Molecular similarity indices in a comparative analysis (CoMSIA) of drug molecules to correlate and predict their biological activity. *J. Med. Chem.* 1994;37:4130-4146.
[36] Tong W, Lowis DR, Perkins R, Chen Y, Welsh WJ, Goddette DW, Heritage TW, Sheehan DM. Evaluation of quantitative structure–activity relationship methods for large-scale prediction of chemicals binding to the estrogen receptor. *J Chem. Inf. Comput. Sci.* 1998;38:669-677.
[37] GaussView 03, Revision 3.07 (2006) Gaussian, Inc., Wallingford CT
[38] Gaussian 03 (2004) Gaussian, Inc., Wallingford CT

10

Insight into the Key Structural Features of Potent Enoyl Acyl Carrier Protein Reductase Inhibitors Based on Computer Aided Molecular Design

Auradee Punkvang[1], Pharit Kamsri[1], Kodchakon Kun-asa[1], Patchreenart Saparpakorn[2], Supa Hannongbua[2], Peter Wolschann[3] and Pornpan Pungpo[1]
[1]*Ubon Ratchathani University*
[2]*Kasetsart University*
[3]*University of Vienna*
[1,2]*Thailand*
[3]*Austria*

1. Introduction

Tuberculosis (TB) caused by *Mycobacterium tuberculosis* (*M. tuberculosis*) is one of the leading reason of mortality and is still spread worldwide, indicated by more than 9 million incident cases of TB in 2009 (World Health Organization, 2010). Current standard treatment regimens of TB are severely hampered by multidrug resistant tuberculosis (MDR-TB), extensively drug-resistant tuberculosis (XDR-TB) and HIV co-infection with TB (WHO, 2010). This fact prompts the research to develop novel and more potent drug candidates to treat *M. tuberculosis* strains resistant to existing drugs. The enoyl acyl carrier protein reductase (InhA) of *M. tuberculosis* catalyzing the NADH-specific reduction of 2-trans-enoyl-ACP (Quemard et al., 1995) is an attractive target for designing novel antibacterial agents (Campbell et al., 2001; Heath et al., 2004; White et al., 2005; Zhang et al., 2004; Wen et al., 2009; Wright et al., 2007). InhA has been identified as the primary target of isoniazid (INH), one of the most effective first-line anti-TB drugs (Rozwarski et al., 1998; Vilcheze et al., 2006; Dessen et al., 1995; Lei et al., 2000; Johnsson et al., 1995; Quemard et al., 1996). InhA is inhibited by the active adduct of INH (INH-NAD) (Timmins et al., 2006; Johnsson et al., 1997) which is covalently formed between NAD+ and the reactive acyl radical of INH generated by the activation of catalase-peroxidase (KatG) (Saint-Joanis et al., 1999; Zhao et al., 2006; Metcalfe et al., 2008; Sinha et al., 1983; Nguyen et al., 2001; Heym et al., 1993; Johnsson et al., 1994). The mutations in KatG have been linked to the major mechanism of INH resistance (de la Iglesia et al., 2006; Banerjee et al., 1994). To overcome the INH resistance associated with mutations in KatG, compounds that directly inhibit the InhA enzyme without requiring activation of KatG have been developed as new promising agents against tuberculosis (Freundlich et al., 2009; am Ende et al., 2008; Boyne et al., 2007; Sullivan et al., 2006; He et al., 2006; He et al., 2007; Kuo et al., 2003). Triclosan, 5-chloro-2-(2,4-

dichlorophenoxy)phenol as shown in Fig.1, has been shown to inhibit InhA without the requirement for KatG-mediated activation (Parikh et al., 2000; Kuo et al., 2003). Because of the remarkable properties of triclosan, a series of triclosan derivatives with modifications at the 5-chloro of triclosan, 5-substituted triclosan derivatives shown in Fig.1, was synthesized in order to optimize the potency of triclosan against InhA (Freundlich et al., 2009). Furthermore, using structure-based drug design, three lipophilic chlorine atoms of triclosan were removed, and one chlorine atom of ring A was replaced by an alkyl chain of varying length resulting in the alkyl diphenyl ethers shown in Fig. 1 (Sullivan et al., 2006). The most efficacious triclosan derivatives in the two classes of 5-substituted triclosan and alkyl diphenyl ether derivatives are more potent than the parent compound triclosan. Importantly, a subset of these triclosan analogues displays high efficacy against both INH-sensitive and INH-resistant strains of *M. tuberculosis* more than those of isoniazid. Because of the remarkable property of 5-substituted triclosan derivatives and alkyl diphenyl ethers, their structural requirements for a better therapeutic activity against tuberculosis in both cases of drug-sensitive and drug-resistant strains of *M. tuberculosis* are fascinating and need to be thoroughly examined. Therefore, in the present study, a structure based drug design using molecular docking calculations was applied to investigate the important drug-enzyme interactions of 5-substituted triclosan derivatives and the related alkyl diphenyl ethers in the InhA binding pocket. Moreover, approaches based on 2D and 3D QSAR methods, HQSAR (Hologram QSAR), CoMFA (Comparative Molecular Field Analysis) and CoMSIA (Comparative Molecular Similarity Indices Analysis) (Cramer et al., 1998; Klebe et al., 1994; Tong et al., 1998) have been used to elucidate the relationship between the structures and the activities of these compounds. A powerful guideline for designing novel and highly effective antitubercular agents is the consequence of these investigations.

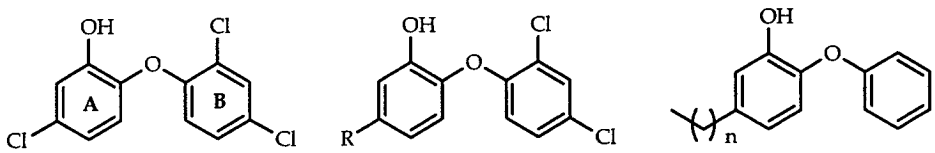

Triclosan 5-substituted triclosan derivatives alkyl diphenyl ethers

Fig. 1. The chemical structures of triclosan and its derivatives

2. Materials and methods of calculations

2.1 Data sets and InhA inhibitory activity

Chemical structures and experimental biological activities expressed as IC_{50} (the half maximal inhibitory concentration) of 17 compounds of 5-substituted triclosan derivatives (Freundlich et al., 2009) and 12 alkyl diphenyl ether derivatives (am Ende et al., 2008; Sullivan et al., 2006) were selected for the present study. All chemical structures of these compounds were constructed using standard tools available in GaussView 3.07 program (Gaussian, Inc., 2006) and were then fully optimized using an *ab initio* quantum chemical method (HF/3-21G) implemented in the Gaussian 03 program (Gaussian, Inc., 2004). The compounds were divided into a training set of 25 compounds and a test set of 4 compounds for the model development and model validation, respectively. The representatives of the test set were manually selected and are covering the utmost range of activity and structural diversity of direct InhA inhibitors in the data set.

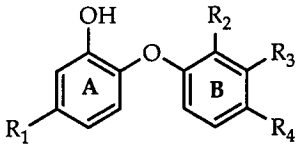

Cpd.	R_1	R_2	R_3	R_4	IC_{50} [nM]	Log(1/ IC_{50})
1	Cl	Cl	H	Cl	1100	2.96
2*	CH_3	Cl	H	Cl	800	3.10
3	$CH_2(C_6H_{11})$	Cl	H	Cl	110	3.96
4	CH_2CH_3	Cl	H	Cl	120	3.92
5	$(CH_2)_2CH_3$	Cl	H	Cl	91	4.04
6*	$(CH_2)_3CH_3$	Cl	H	Cl	55	4.26
7	$CH_2CH(CH_3)_2$	Cl	H	Cl	96	4.02
8	$(CH_2)_2CH(CH_3)_2$	Cl	H	Cl	63	4.20
9	$CH_2CH(CH_3)CH_2CH_3$	Cl	H	Cl	130	3.89
10	CH_2(2-pyridyl)	Cl	H	Cl	29	4.54
11	CH_2(3-pyridyl)	Cl	H	Cl	42	4.38
12	CH_2(4-pyridyl)	Cl	H	CN	75	4.12
13	*o*-CH_3-C_6H_5	Cl	H	Cl	1300	2.89
14	*m*-CH_3-C_6H_5	Cl	H	Cl	870	3.06
15	$CH_2C_6H_5$	Cl	H	Cl	51	4.29
16	$(CH_2)_2C_6H_5$	Cl	H	Cl	21	4.68
17	$(CH_2)_3C_6H_5$	Cl	H	Cl	50	4.30
18	$(CH_2)_5CH_3$	H	H	H	11	4.96
19	CH_2CH_3	H	H	H	2000	2.70
20*	$(CH_2)_3CH_3$	H	H	H	80	4.10
21	$(CH_2)_4CH_3$	H	H	H	17	4.77
22	$(CH_2)_7CH_3$	H	H	H	5	5.30
23	$(CH_2)_{13}CH_3$	H	H	H	150	3.82
24*	$(CH_2)_5CH_3$	NO_2	H	H	180	3.74
25	$(CH_2)_5CH_3$	H	NO_2	H	48	4.32
26	$(CH_2)_5CH_3$	H	H	NO_2	90	4.05
27	$(CH_2)_5CH_3$	NH_2	H	H	62	4.21
28	$(CH_2)_5CH_3$	H	NH_2	H	1090	2.96
29	$(CH_2)_5CH_3$	H	H	NH_2	55	4.26

*The test set compounds

Table 1. The chemical structures and IC_{50} values of 5-substituted triclosan and alkyl diphenyl ether derivatives against InhA

2.2 Molecular docking calculations

The X-ray crystal structures of InhA complexed with 2-(2,4-dichlorophenoxy)-5-(2-phenylethyl)phenol (5-substituted triclosan derivative) and 5-octyl-2-phenoxyphenol (alkyl diphenyl ether derivative) with pdb codes of 3FNH and 2B37, respectively, were employed for molecular docking calculations of compounds 1-17 and compounds 18-29, respectively. Docking calculations of the data set were carried out by the Autodock 3.05 program using Lamarckian Genetic Algorithm (LGA) (Morris et al., 1998). Docking parameters were used as default values, except for the number of docking runs which was set to 50. The docking calculation was validated by reproducing the X-ray conformation of the ligand as well as the orientation in its pocket. The root mean-square deviation (RMSD) value between the original and docked coordinates lower than 1Å is acceptable. The ligand pose with the lowest final docked energy was selected as the best binding mode of 5-substituted triclosan and alkyl diphenyl ether derivatives. Then, the conformations of all compounds were used according to this binding mode for CoMFA and CoMSIA setups.

2.3 CoMFA and CoMSIA techniques

CoMFA and CoMSIA, 3D-QSAR methods, are successfully used to derive a correlation between the biological activities of a set of compounds with a special alignment and their three-dimensional descriptors. In both CoMFA and CoMSIA, a set of compounds is aligned and the structurally aligned molecules are represented in terms of fields around the molecule (three-dimensional descriptors). CoMFA and CoMSIA are based on the assumption that changes in biological activities of compounds are related to changes in molecular properties represented by fields around the molecule. Therefore, the structural alignment of compounds is an important prerequisite for the setup of appropriate CoMFA and CoMSIA models. In the present study, the reasonable binding modes of the compounds in the data set obtained from the validated docking calculations were employed for the molecular alignment. SYBYL 8.0 molecular modeling software (Tripos, Inc, 2007) was used to construct CoMFA and CoMSIA models. CoMFA descriptors, steric and electrostatic fields, were calculated using a sp^3 carbon probe atom with a formal charge of +1 which was placed at the intersections in a grid with the spacing of 2Å. The maximum steric and electrostatic energies were truncated at 30 kcal/mol. Five CoMSIA descriptors, steric, electrostatic, hydrophobic, hydrogen bond donor and hydrogen bond acceptor fields, were derived with the same grid as used for the CoMFA field calculation. There are no energy cutoffs necessary for CoMSIA calculations because a distance-dependent Gaussian type potential was used in contrary to the procedure of CoMFA calculations. CoMFA and CoMSIA descriptors were set as independent variables and log ($1/IC_{50}$) values were used as dependent variables in the partial least square (PLS) analysis to derive a linear relationship between molecular descriptors and activities. The cross-validation was performed using the leave-one-out method with a 2.0 kcal/mol column filter to minimize the influence of noisy columns. A final non cross-validated analysis with the optimal number of components was sequentially performed and was then employed to analyze the results. The non-cross-validated correlation coefficient (r^2) and the leave-one-out (LOO) cross-validated correlation coefficient (q^2) were used to evaluate the predictive ability of the CoMFA and CoMSIA models. Contour maps were created to visualize the molecular areas responsible for the biological effects.

2.4 HQSAR

Hologram QSAR (HQSAR) does not require information about the three-dimensional geometry of the inhibitors. Hence, in contrary to CoMFA and CoMSIA methods, HQSAR needs no molecular alignment. Each compound of the data set was converted into all possible molecular fragments including linear, branched, cyclic, and overlapping fragments in the size of 4-7 atoms. Molecular fragment generation utilizes the fragment distinction parameters including atoms (A), bonds (B), connections (C), hydrogen atoms (H), chirality (Ch) as well as hydrogen donor and acceptor properties (DA). The generated molecular fragments are counted in bins of a fixed length array to produce a molecular hologram. PLS statistical method was employed to establish a correlation of the molecular hologram descriptors with the biological data. The HQSAR module of SYBYL 8.0 was employed for the HQSAR study. The same training and test sets as for CoMFA and CoMSIA studies were used. The most convenient model was selected based on the best cross-validated r^2 to determine these structural subunits which are important for the biological activities.

3. Result and discussion

3.1 The X-ray crystal structures of 5-substituted triclosan and alkyl diphenyl ether derivatives

To probe the interaction of 5-substituted triclosan and alkyl diphenyl ether derivatives with InhA, the X-ray crystal structures of these compounds complexed with InhA have been solved (Freundlich et al., 2009; Sullivan et al., 2006). To compare the conformational change of InhA complexed with the different ligands, the ligand-unbound InhA (pdb code 1ENY) and InhA bound with 2-(2,4-dichlorophenoxy)-5-(2-phenylethyl)phenol (pdb code 3FNH) and 5-octyl-2-phenoxyphenol (pdb code 2B37), compounds 16 and 22, respectively, are superimposed as shown in Fig. 2.

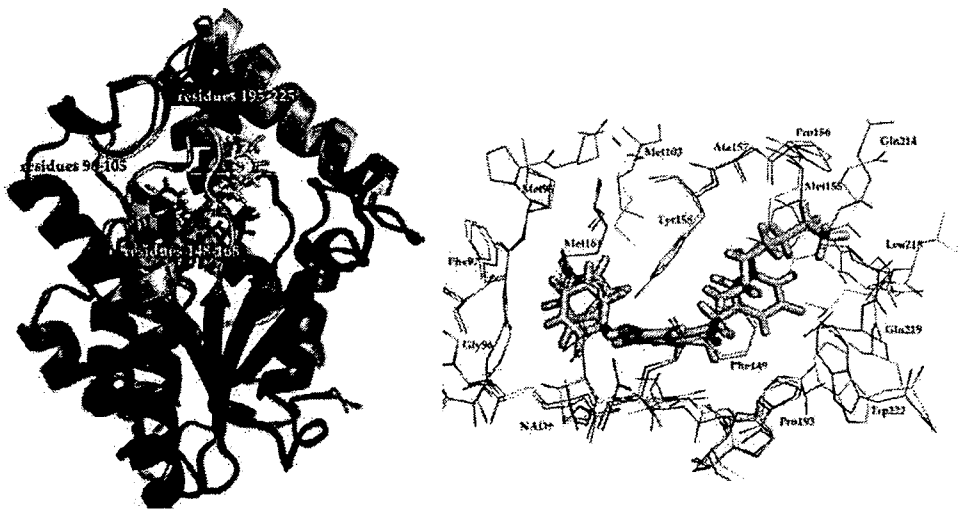

Fig. 2. Superimposition of ligand unbound InhA, InhA bound with compound 16 (cyan) and compound 22 (yellow) with pdb codes of 1ENY, 3FNH and 2B37, respectively. InhAs are colored by purple, whereas residues 96-105, 148-168 and 195-225 complexed with compounds 16 and 22 are colored by cyan and yellow, respectively.

The binding residues within 6Å apart from compounds 16 and 22 consist of residues 96-105, 148-168 and 195-225. As compared with the ligand-unbound InhA, only positions of residues 195-225 including two α-helixes and one loop of the InhA bound with compounds 16 and 22 have been changed to accommodate the binding of two different ligands. On the other hand, the binding residues 96-105 and 148-168 of the InhA bound with these compounds are located in the same position compared to those of the ligand-unbound InhA as shown in Fig. 2. These results imply that residues 195-225 could be sufficiently flexible for the binding of different ligands, whereas residues 96-105 and 148-168 are more rigid, which are consistent with the mobility of these residues investigated by means of molecular dynamics simulations performed in one of our previous investigations (Punkvang et al., 2010). With regard to the binding modes of compounds 16 and 22 in InhA binding site, the B rings of these compounds are bound in a similar orientation and buried with the rigid residues 96-105, 148-168 and the pyrophosphate group of NAD+. The aromatic B ring of compound 22 interacts with the methyl side chain of Met161 to form the methyl-π interaction, whereas that of compound 16 loses this interaction. The hydroxyl group at the A ring of compounds 16 and 22 form two hydrogen bonds with Tyr158 as well as the 2′-hydroxyl group of NAD+. The substituents at the A rings of compounds 16 and 22, the ethyl phenyl and the octyl chain, respectively, are occupied with the flexible residues 195-225. The first four carbons of the octyl chain of compound 22 superimpose well with the ethyl phenyl of compound 16 and interact with the flexible residues of Phe149, Tyr158, Pro193, Met199, Ile215, Leu218, Glu219 and Trp222, respectively. The last four carbons of the octyl chain of compound 22 interact with Met155, Pro156, Ala157, Gln214, whereas these interactions are lost for binding of compound 16. The presence of the methyl-π interaction and more interactions with the flexible residues 195-225 of the substituents at the A rings of compound 22 may be accounted for higher activity of compound 22 as compared with that of compound 16.

3.2 Docking calculations of 5-substituted triclosan and alkyl diphenyl ether derivatives

Molecular docking calculations using the Autodock 3.05 program have been successfully applied to investigate the binding modes of all 5-substituted triclosan and alkyl diphenyl ether derivatives in the InhA binding pocket. The RMSD between the docked and crystallographic conformations is lower than 1Å, indicating that molecular docking calculations are rendering high reliability for reproducing the binding mode of all 5-substituted triclosan and alkyl diphenyl ether derivatives. All predicted binding modes of these inhibitors that are similar to the binding modes as those of the above X-ray crystal structures are shown in Fig. 3.

The B rings are surrounded by the more rigid residues 96-105 and 148-168, whereas the A rings and their substituents are surrounded by the flexible residues 195-225. The hydroxyl groups at the A ring of all 5-substituted triclosan and alkyl diphenyl ether derivatives could create the same hydrogen bonding pattern with NAD+ and Tyr158. The major modification of 5-substituted triclosan and alkyl diphenyl ether derivatives is the variation of substituent R_1 at the A ring. The increasing length of an alkyl chain at the substituent R_1 results in the decreasing IC_{50} values for InhA inhibition of both 5-substituted triclosan and alkyl diphenyl ether derivatives, compounds 2, 4-6, 19-22. Compound 22 bearing the octyl chain at the A ring is the most active compound in the data set. To compare the binding modes of compounds containing alkyl chains of different lengths at the position R_1, the predicted

binding modes of compounds 18-20 containing C6, C2 and C4 alkyl chains, respectively, are superimposed on the X-ray binding mode of compound 22 as shown in Fig. 4.

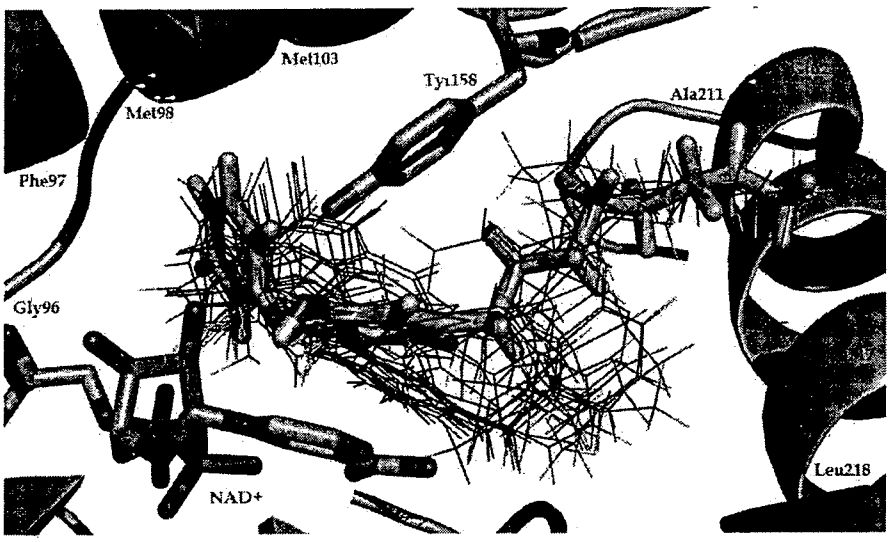

Fig. 3. Superposition of all predicted binding modes of 5-substituted triclosan and alkyl diphenyl ether derivatives (green line) in InhA (pink) derived from molecular docking calculations and the X-ray structure of compound 22 (green stick)

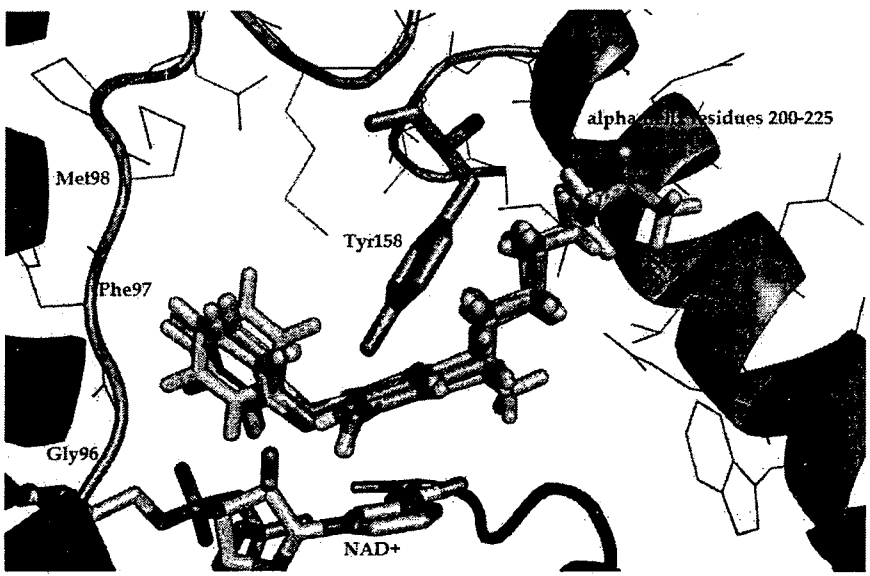

Fig. 4. The predicted binding modes of compounds 18 (yellow), 19 (green) and 20 (orange) containing C6, C2 and C4 chains at the substituent R_1, respectively, and the X-ray binding mode of compound 22 (cyan) in the InhA binding pocket (cyan)

The longer octyl chain of compound 22 could more closely interact with α-helix residues 200-225, whereas C6, C2 and C4 alkyl chains of compounds 18-20 are far from these residues, particularly the C2 alkyl chain of compound 19. This result may explain the higher activity of compound 22 bearing the longer alkyl chain at the position R_1 as compared with those of compounds 18-20. However, when the octyl chain of compound 22 was enlarged to a C14 chain resulting in compound 23, there is a corresponding increase in IC_{50} value for InhA inhibition from 5 nM to 150 nM. In contrast to the C8 chain of compound 22 which lies in a linear conformation in InhA binding pocket, the C14 chain of compound 23 forms a U-like shape within InhA binding pocket and slightly interacts with α-helix residues 200-225 as shown in Fig. 5. Moreover, the B ring of this compound loses the methyl-π interaction with Met161. These results may be accounted for the lower potency of compound 23. In the case of compounds 13 and 14, where phenyl rings are directly attached to the A ring at position R_1, the activity against InhA of these compounds are lower than those of compounds 15-17 which have a linker between the A ring and the phenyl ring at substituent R_1. Based on molecular docking calculations, the phenyl substituents of compounds 13 and 14 overlap with an ethyl linker of compound 16 and are surrounded by the rigid residues 148-168. To avoid the steric clash with these residues, a change of the binding conformation of compounds 13 and 14 has occurred, leading to a loss of the π-π stacking of the A ring with nicotinamide ring of NAD+ as compared with that of compound 16. Moreover, a linker phenyl substituent of compound 16 could create more hydrophobic interactions with the hydrophobic residues in the flexible residues 195-225. These results may explain why compounds 13 and 14 are of lower potency compared to compounds 15-17.

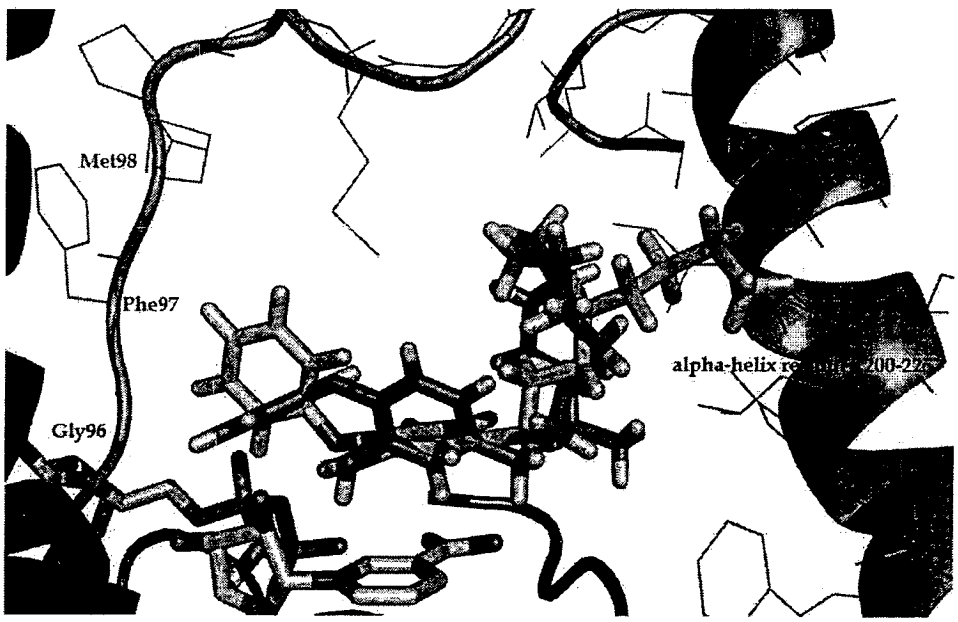

Fig. 5. The predicted binding modes of compound 23 (pink) and the X-ray binding mode of compound 22 (cyan) in InhA binding pocket (cyan)

The presence of NO_2 and NH_2 groups at the B ring of the alkyl diphenyl ether derivatives giving compounds 24-29 results in lower activities (increasing of IC_{50} values) for InhA inhibition of these compounds as compared with that of compound 18. Based on molecular docking calculations, the A rings and hexyl substituents of compounds 24-29 overlap well with that of compound 18 as shown in Fig. 6. However, the NO_2 and NH_2 substituents at the B ring of compounds 24-29 induce the position change of B rings of these compounds to avoid the steric conflict with the rigid residues Gly96, Phe97, Met98, Met161 and the pyrophosphate group of NAD+. Because of this reorientation, the B rings of compounds 24-29 lose the methyl-π interaction with Met161 as compared with compound 27. Therefore, the lower activities against InhA of alkyl diphenyl ether derivatives which contain the NO_2 and NH_2 groups at the B ring may be a consequence of the loss of the methyl-π interaction of the B rings of these compounds.

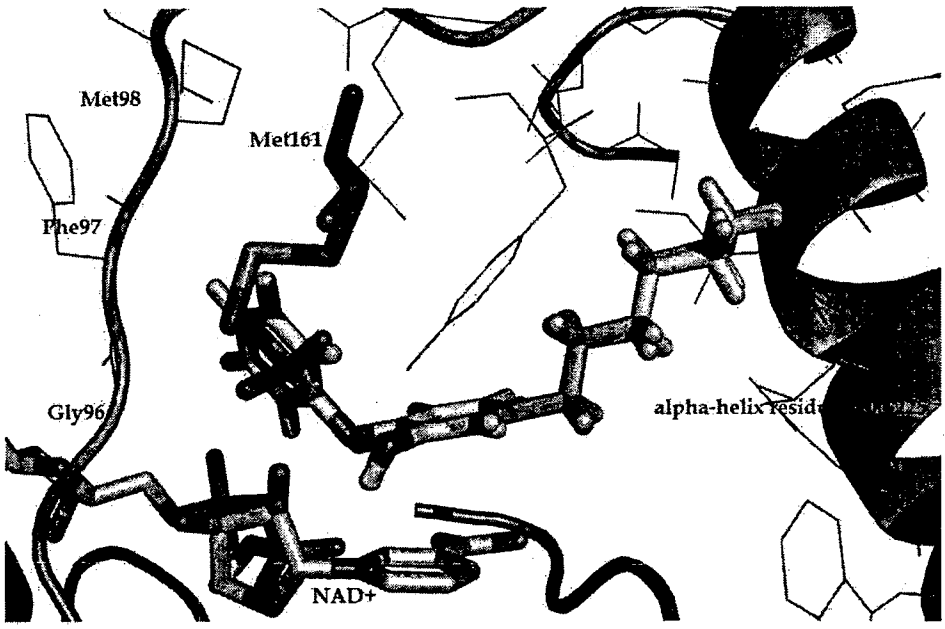

Fig. 6. Superposition of the predicted binding modes of compounds 18 (yellow) and 24 (green)

3.3 CoMFA, CoMSIA and HQSAR models

The results of the PLS analyses of CoMFA, CoMSIA and HQSAR models are summarized in Table 2. QSAR models 1, 3 and 5 derived from the PLS analyses of all compounds in the training set show a poor q^2. To improve the quality of these QSAR models, compound 19 was considered as an outlier resulting in better q^2 values of models 2, 4 and 6. However, HQSAR model 6 still shows a poor q^2 of 0.27. To modify this model, compounds 23 and 28 were omitted from the training set which yields the satisfying HQSAR, model 7. Based on a good q^2, models 2, 4 and 7 were selected as the final CoMFA, CoMSIA and HQSAR models, respectively. The final CoMFA model composing the steric and electrostatic fields gives q^2 of 0.66 and r^2 of 0.99. In the case of the final CoMSIA model including the steric, electrostatic

and hydrophobic fields, a higher q^2 value of 0.73 as compared with that of the final CoMFA model was obtained. This result indicates that the final CoMSIA model performs better in the prediction than the final CoMFA model, which is an indication for the fact that beyond steric and electrostatic effects, hydrogen bonding may be an additional contribution. Among the considered descriptors of the final CoMSIA and CoMFA models, the electrostatic fields of both models are the most important parameter influencing the IC_{50} values of the 5-substituted triclosan and alkyl diphenyl ether derivatives in the training set. With regard to the best HQSAR model generated based on the combination of the different fragment types, atom (A), bond (B) and connection (C), this model shows q^2 value of 0.74 with r^2 value of 0.97 which are in the same level with those of the final CoMSIA model.

	Models	Statistical parameters						Fraction
		q^2	r^2	N	s	SEE	F	
	CoMFA							
1	S/E	0.38	0.91	3	0.56	0.21	73.19	48/52
2	**S/E**	**0.66**	**0.99**	**6**		**0.05**	**698.63**	**39/61**
	CoMSIA							
3	S/E/H	0.45	0.89	4	0.54	0.24	39.27	24/46/30
4	**S/E/H**	**0.73**	**0.99**	**6**		**0.07**	**277.19**	**19/57/24**
	HQSAR							
5	A/B/C	0.14	0.32	1	0.63	0.56	-	-
6	A/B/C	0.27	0.43	1	0.54	0.47	-	-
7	**A/B/C**	**0.74**	**0.97**	**6**		**0.12**	-	-

Table 2. Summary of statistical results of CoMFA, CoMSIA and HQSAR models, N, optimum number of components; s, standard error of prediction, SEE, standard error of estimate; F, F-test value; S, steric field; E, electrostatic field; H, hydrophobic field; A, atom; B, bond; C, connection

3.4 Validation of the QSAR models

Satisfyingly good correlations between actual and predicted activities of the training set based on the final CoMFA, CoMSIA and HQSAR models are depicted in Fig. 7. The predicted activities of the training set derived from the final QSAR models are close to the experimental activities indicating the high degree of correlation between the actual and predicted activities. In order to assess the external predictive ability of selected QSAR models, InhA inhibition activities of the test set were predicted. The IC_{50} values of test set compounds predicted by the final CoMFA, CoMSIA and HQSAR models are within one logarithmic unit difference from the experimental values except those of compound 2 as presented in Fig. 7. This result reveals that all selected QSAR models are reliable to predict the activity of external data set. Therefore, the final CoMFA, CoMSIA, and HQSAR models can be utilized for designing new direct InhA inhibitors with improved activity.

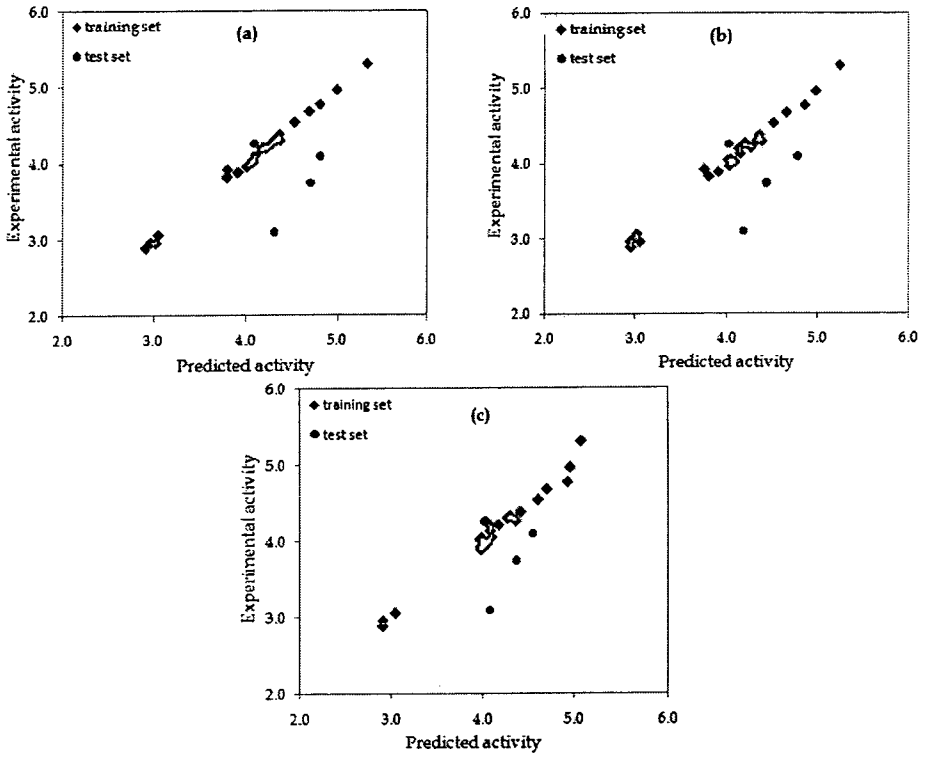

Fig. 7. Plots between the actual and predicted activities of the training and test sets derived from the final CoMFA (a), CoMSIA (b) and HQSAR (c) models, respectively

3.5 CoMFA and CoMSIA contour maps

To reveal the importance of molecular descriptor fields, steric, electrostatic and hydrophobic fields, on the InhA inhibition activities of 5-substituted triclosan and alkyl diphenyl ether derivatives, CoMFA and CoMSIA contour maps were established and depicted in Fig. 8 and 9, respectively. CoMFA and CoMSIA contour maps are merged with the InhA pocket complexed with compounds 16 and 22 in order to link the structural requirement for better activity of 5-substituted triclosan and alkyl diphenyl ether derivatives visualized by CoMFA, CoMSIA contour maps toward the interaction of these compounds in InhA binding pocket. Green and yellow contours indicate areas where favorable and unfavorable steric bulks are predicted to enhance the antitubercular activities of the direct InhA inhibitors. Blue and red contours indicate regions where electropositive and electronegative groups lead to increasing antitubercular activity, respectively. Purple and white contours represent areas where the hydrophobic group and the hydrophilic group, are predicted to favour the biological activities. Compounds 16 and 22 were selected as the template for graphic interpretation of CoMFA and CoMSIA models. CoMFA model shows three yellow contours surrounding the B rings of compounds 16 and 22 buried in the pocket consisting of the rigid residues Gly96, Phe97, Met98, Met161 and NAD+ as shown in Fig. 8(a). These contours indicate that the substituent of the B ring should be small in order to increase the enzyme

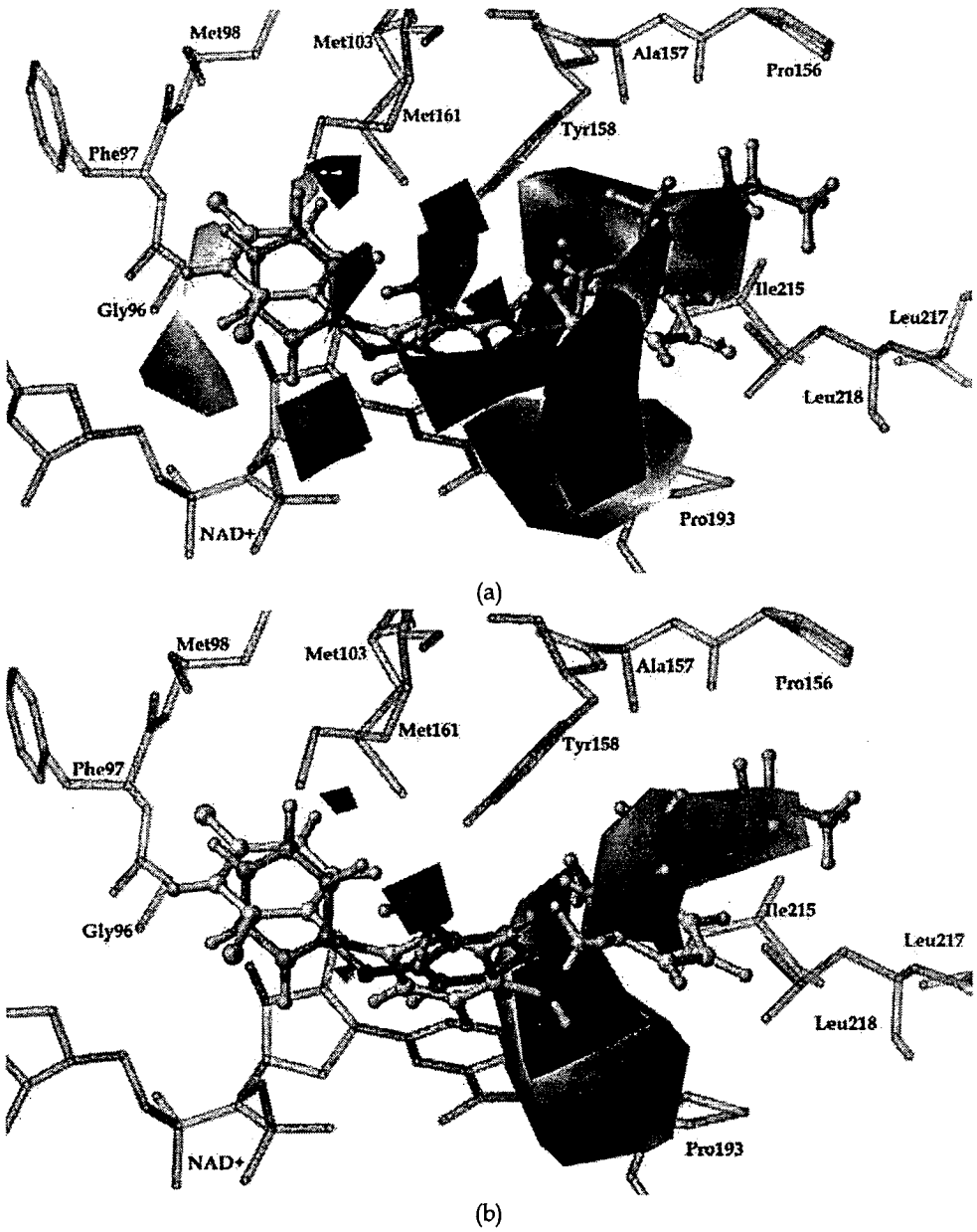

Fig. 8. Steric and electrostatic contours of CoMFA (a) and CoMSIA (b) models in combination with compounds 16 (yellow) and 22 (orange) in InhA binding pocket (cyan). Green and yellow contours represent favourable and unfavourable steric regions, respectively. Blue and red contours are favoured for electropositive and electronegative groups, respectively.

inhibitory activity of 5-substituted triclosan and alkyl diphenyl ether derivatives. Moreover, this structural requirement is preferable for the interaction of the B ring with the rigid moiety consisting of residues Gly96, Phe97, Met98, Met161 and NAD+. In addition, the B rings of compounds 16 and 22 are covered by a large purple contour and immediately flanked by two white contours as shown in Fig. 9. A large purple region conforms to the aromatic B rings of 5-substituted triclosan and alkyl diphenyl ether derivatives which are crucial for the forming of the methyl-π interaction with the methyl side chain of Met161. Furthermore, the presence of hydrophilic substituent with a small size at both sides of the B ring should enhance the activity against InhA of 5-substituted triclosan and alkyl diphenyl ether derivatives.

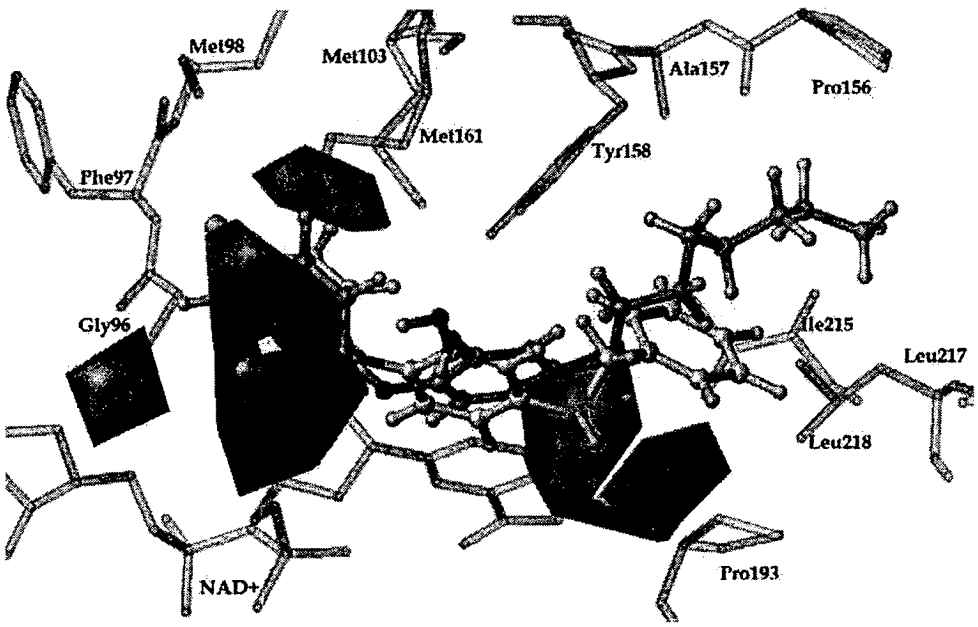

Fig. 9. CoMSIA hydrophobic contours in combination with compounds 16 (yellow) and 22 (orange) in InhA binding pocket (cyan). Purple and white contours show favourable and unfavourable hydrophobic regions, respectively.

With regard to the substituent R_1 of the A ring, CoMFA and CoMSIA models in Fig. 8 and 9 present the large blue, white and yellow contours near the ethyl linker of compound 16 and the first two carbons of the octyl side chain of compound 22 which are surrounded by the rigid residues 148-168. These contours suggest that the blue, white and yellow regions near those of compounds 16 and 22 favor the small moiety with the electropositive and hydrophilic properties. It is important to note that this favored small moiety could be helpful not only for the activities against InhA of 5-substituted triclosan and alkyl diphenyl ether derivatives but also for the binding of these compounds at a position where rigid residues 148-168 are presented. This finding agrees well with the experimental data that compounds with no linker and the methyl linker between the A ring and the analogues of phenyl and pyridyl at substituent R_1, compounds 10-15, show IC_{50} values higher than that of

compound 16 containing the ethyl linker. Based on the obtained molecular docking results, the analogues of bulky phenyl and pyridyl at substituent R_1 of compounds 10-15 overlap with the ethyl linker of compound 16 located near the blue, white and yellow regions. Another interesting contour of CoMFA and CoMSIA models is the large green contour at the phenyl substituent of compound 16 and the last six carbons of the octyl chain of compound 22. The green contour indicates that the presence of the bulky substituent at this region should increase the InhA inhibitory activities of 5-substituted triclosan and alkyl diphenyl ether derivatives. This result is in line with the experimental results that compounds 1-2, 4-9, 19-21 presenting the shorter chain of substituent R_1 display lower activities as compared with that of compound 22 bearing the longer octyl chain. Remarkably, based on the large green area, the combination between substituents R_1 of 5-substituted triclosan derivatives and alkyl diphenyl ether derivatives, the phenyl substituent of compound 16 and the last six carbons of the octyl chain of compound 22, may generate the optimal substituent R_1 such as the phenyl incorporated with alkyl chain. Therefore, the designed compounds should display the better profile against InhA.

3.6 HQSAR contribution maps

HQSAR contribution maps are helpful to visualize the contributions of molecular fragments to the activities against InhA of 5-substituted triclosan and alkyl diphenyl ether derivatives in the present data. The color codes indicate the different contributions of all atoms in each compound to the biological activity. An atom with negative contributions is represented at the red end of the spectrum, whereas an atom with positive contributions is represented at the green end of the spectrum. The white colored atoms stand for intermediate contributions. Fig. 10 depicts the individual atomic contributions to the activity against InhA of compounds 13, 16 and 22. There are green and yellow atoms at the A ring of compounds 16 and 22 indicating the positive contributions of the A ring to the activity against InhA of these compounds. Moreover, the positive contributing fragments are presented at the ethyl linker of compound 16 and the first carbon of the octyl chain of compound 22 emphasizing the importance of these fragments. As previously shown by CoMFA and CoMSIA contours, these positively contributing moieties of compounds 16 and 22 are surrounded by yellow, blue and white contours implying that these fragments are optimal for steric, electrostatic and hydrophobic requirements. Obviously supporting this finding, the omission of the ethyl linker resulting in compound 13 induces the appearance of the negative contributing fragments at the A ring and the phenyl substituent leading to the lower activity of this compound as compared with that of compound 16. Considering the phenyl substituent of compound 16 and the last six carbons of the octyl chain of compound 22 buried in green CoMFA and CoMSIA contours as shown in Fig. 8, these fragments are colored by white indicating that these atoms have no contributions to the activity. Therefore, the modification of these white parts following the CoMFA and CoMSIA suggestions may improve the activity against InhA of 5-substituted triclosan and alkyl diphenyl ether derivatives. In case of the B rings of compounds 16 and 22, most atoms in the B ring and Cl substituents of compound 16 are colored by red and orange, suggesting the negative contributions of these fragments, whereas those of compound 22 are colored by white indicating no contribution of these fragments. This result may be accounted for the higher activity of compound 22 as compared with that of compound 16. Based on the obtained CoMFA and CoMSIA models, the B ring of compounds 16 and 22 are covered by a large purple contour and immediately flanked by two white contours. Therefore, the adjustment of the substituent at the B ring

based on the structural requirement suggested by CoMFA and CoMSIA models may induce the occurrence of the positive contribution on the B ring and its substituents resulting in the better activity against InhA. Noticeably, about the chlorine substituents at the B ring of 5-substituted triclosan derivatives, the precence of a positively contributing fragment at the substituent R_1 of the A ring induces the negative contribution on the chlorine substituents as shown by HQSAR contribution maps of compounds 13 and 16 in Fig. 10. This result implies that more interactions of substituent R_1 of the A ring reduce the role of the B ring chlorines on the activities. Consistent with this finding, alkyl diphenyl ether derivatives without the B ring chlorines, compounds 18, 21 and 22, display activities against InhA higher than those of triclosan and its derivatives bearing the B ring chlorines, compounds 1-17. On the other hand, the B ring chlorines can be more preferable for the activities in case of compounds with less interactions of substituent R_1 to InhA. As exemplified by compounds with shorter lenght of the alkyl chain (C2 and C4 chains at the substituent R_1), compounds 19 and 20 possess lower activites than those of compounds 4 and 6 containing the B ring chlorines. It is important to note that the influence of B ring chlorines on inhibitory activity of triclosan derivatives which is argued in Freundlich's work (Freundlich et al. 2009) and Sullivan's work (Sullivan et al., 2006) could be evaluated by our HQSAR model.

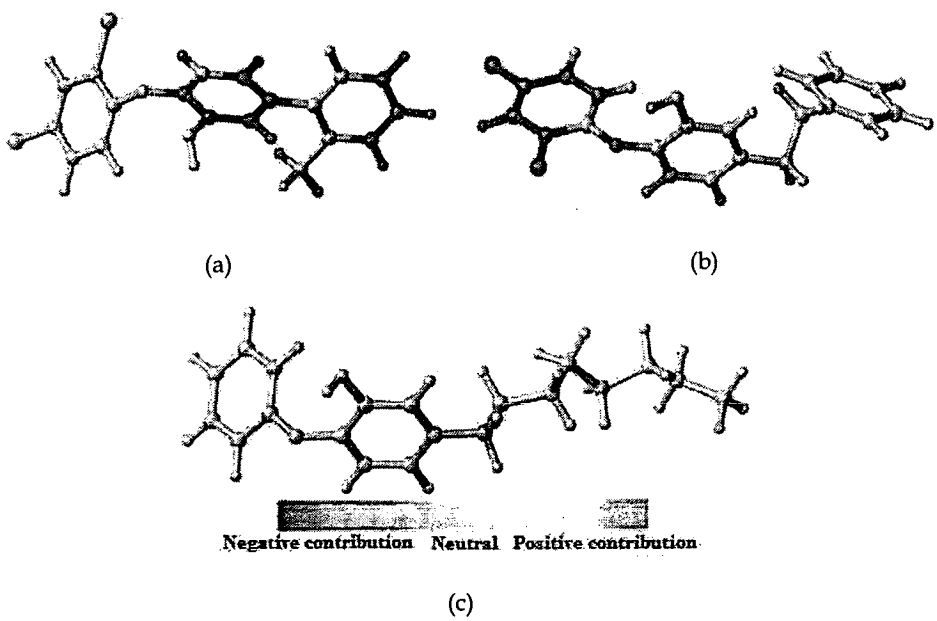

Fig. 10. The final HQSAR contribution maps of compounds 13 (a), 16 (b) and 22 (c)

4. Conclusion

Molecular docking calculations were successfully applied to determine the potential binding modes of 5-substituted triclosan and alkyl diphenyl ether derivatives in the InhA binding pocket. The B rings of these compounds are occupied in the rigid pocket consisting of residues 96-105 and 148-168, whereas the A rings and their substituents are buried in the

flexible residues 195-225. The B ring substituents that could perturb the methyl-π interaction of the B ring with Met161 produce the poor activities of alkyl diphenyl ether derivatives. On the other hand, the substituent R_1 at the A ring that could interact more with the flexible residues 195-225 and avoid the steric conflict with the rigid residues 148-168 might result in the better activities of 5-substituted triclosan and alkyl diphenyl ether derivatives against InhA. Besides, the key structural elements for a good activity against InhA of these compounds based on CoMFA, CoMSIA and HQSAR were clearly elucidated in the present study. Based on CoMFA and CoMSIA guidelines, compounds with the combination of substituents R_1 of 5-substituted triclosan derivatives and alkyl diphenyl ether derivatives should display the better profile against InhA. In agreement with CoMFA and CoMSIA results, the HQSAR contribution maps show the individual contribution of the atoms to IC_{50} values of 5-substituted triclosan and alkyl diphenyl ether derivatives. Moreover, HQSAR contribution maps could reveal the contribution of two chlorine atoms on the B ring of 5-substituted triclosan derivatives to their IC_{50} values. Consequently, the integrated results from the structure-based design using molecular docking calculations and the ligand-based design using various QSAR approaches provide insights into key structural features that can be utilized for designing novel and more active InhA inhibitors in the series of 5-substituted triclosan and alkyl diphenyl ether derivatives. Particularly, the modified compound suggested in the present study might be a member of a next drug generation of InhA inhibitor. These results demonstrate that computer aided molecular design approaches are fruitful for rational design and for possible syntheses of novel and more active InhA inhibitors that might be next generation of antitubercular agents.

5. Acknowledgment

This research was supported by the Thailand Research Fund (DBG5380006, DBG5380042, RTA53800010). A. Punkvang is grateful to the grant from under the program Strategic Scholarships for Frontier Research Network for the Ph.D. K. Kun-asa is grateful to Science Achievement Scholarship of Thailand (SAST). Faculty of Science, Ubon Ratchathani University, University of Vienna and ASEA-Uninet are gratefully acknowledged for supporting this research.

6. References

am Ende, C.W.; Knudson, S.E.; Liu, N.; Childs, J.; Sullivan, T.J.; Boyne, M.; Xu, H.; Gegina, Y.; Knudson, D.L.; Johnson, F.; Peloquin, C.A.; Slayden, R.A. & Tonge, P.J. (2008). Synthesis and in vitro antimycobacterial activity of B-ring modified diaryl ether InhA inhibitors. *Bioorganic & Medicinal Chemistry Letters*, Vol.18, No.10, (May 2008), pp. 3029-3033

Banerjee, A.; Dubnau, E.; Quemard, A.; Balasubramanian, V.; Um, K.S.; Wilson, T.; Collins, D.; de Lisle, G. & Jacobs, W.R., Jr. (1994). inhA, a gene encoding a target for isoniazid and ethionamide in Mycobacterium tuberculosis. *Science*, Vol.263, No.5144, (January 1994), pp. 227–230

Boyne, M.E.; Sullivan, T.J.; am Ende, C.W.; Lu, H.; Gruppo, V.; Heaslip, D.; Amin, A.G.; Chatterjee, D.; Lenaerts, A.; Tonge, P.J. & Slayden, R.A. (2007). Targeting fatty acid

biosynthesis for the development of novel chemotherapeutics against Mycobacterium tuberculosis: evaluation of A-ring-modified diphenyl ethers as high-affinity InhA inhibitors. *Antimicrobial Agents and Chemotherapy*, Vol.51, No.10, (October 2007), pp. 3562-3567

Campbell, J.W. & Cronan, J.E., Jr. (2001). Bacterial fatty acid biosynthesis: Targets for antibacterial drug discovery. *Annual Review of Microbiology*, Vol.55, pp. 305-332

Cramer, R.D. III; Patterson, D.E. & Bunce, J.D. Comparative molecular field analysis (CoMFA). 1. Effect of shape on binding of steroids to carrier proteins. *Journal of the American Chemical Society*, Vol.110, No.18, (August 1998), pp. 5959-5967

De La Iglesia, A.I. & Morbidoni, H.R. (2006). Mechanisms of action of and resistance to rifampicin and isoniazid in Mycobacterium tuberculosis: new information on old friends. *Revista Argentina de microbiología*, Vol.38, No.2, (April-June 2006), pp. 97-109

Dessen, A.; Quemard, A.; Blanchard, J.S.; Jacobs, W.R., Jr. & Sacchettini, J.C. (1995). Crystal structure and function of the isoniazid target of Mycobacterium tuberculosis. *Science*, Vol.267, No.5204, (March 1995), pp. 1638-1641

Freundlich, J.S.; Wang, F.; Vilcheze, C.; Gulten, G.; Langley, R.; Schiehser, G.A.; Jacobus, D.P.; Jacobs, W.R., Jr. & Sacchettini, J.C. (2009). Triclosan derivatives: Towards potent inhibitors of drug-sensitive and drug-resistant Mycobacterium tuberculosis. *ChemMedChem*, Vol.4, No.2, (February 2009), pp. 241-248

GaussView 03, Revision 3.07 (2006) Gaussian, Inc., Wallingford CT

Gaussian 03 (2004) Gaussian, Inc., Wallingford CT

Heath, R.J. & Rock, C.O. (2004). Fatty acid biosynthesis as a target for novel antibacterials. *Current Opinion in Investigational Drugs*, Vol.5, No.2, (February 2004), pp.146-153

He, X.; Alian, A.; Stroud, R. & Ortiz de Montellano, P.R. (2006). Pyrrolidine carboxamides as a novel class of inhibitors of enoyl acyl carrier protein reductase from Mycobacterium tuberculosis. *Journal of Medicinal Chemistry*, Vol.49, No.21, (October 2006), pp. 6308-6323

He, X.; Alian, A. & Ortiz de Montellano, P.R. (2007). Inhibition of the Mycobacterium tuberculosis enoyl acyl carrier protein reductase InhA by arylamides. *Bioorganic & Medicinal Chemistry*, Vol.15, No.21, (2007), pp. 6649–6658

Heym, B.; Zhang, Y.; Poulet, S.; Young, D. & Cole, S.T. (1993). Characterization of the katG gene encoding a catalase-peroxidase required for the isoniazid susceptibility of Mycobacterium tuberculosis. *Journal of Bacteriology*, Vol.175, No.13, (July 1993), pp. 4255-4259

Johnsson, K.; King, D.S. & Schultz, P.G. (1995). Studies on the mechanism of action of isoniazid and ethionamide in the chemotherapy of tuberculosis. *Journal of the American Chemical Society*, Vol.117, No.17, (May 1995), pp. 5009–5010

Johnsson, K. & Schultz, P.G. (1994). Mechanistic studies of the oxidation of isoniazid by the catalase peroxidase from Mycobacterium tuberculosis. *Journal of the American Chemical Society*, Vol.116, No.16, (August 1994), pp. 7425–7426

Johnsson, K.; Froland, W.A. & Schultz, P.G. (1997). Overexpression, purification, and characterization of the catalase-peroxidase KatG from Mycobacterium tuberculosis. *Journal of Biological Chemistry*, Vol.272, No.5, (January 1997), pp. 2834-2840

Klebe, G.; Abraham, U. & Mietzner, T. Molecular similarity indices in a comparative analysis (CoMSIA) of drug molecules to correlate and predict their biological activity. *Journal of Medicinal Chemistry*, Vol.37, No.24, (November 1994), pp. 4130-4146

Kuo, M.R.; Morbidoni, H.R.; Alland, D.; Sneddon, S.F.; Gourlie, B.B.; Staveski, M.M.; Leonard, M.; Gregory, J.S.; Janjigian, A.D.; Yee, C.; Musser, J.M.; Kreiswirth, B.; Iwamoto, H.; Perozzo, R.; Jacobs, W.R., Jr.; Sacchettini, J.C. & Fidock, D.A. (2003). Targeting tuberculosis and malaria through inhibition of Enoyl reductase: compound activity and structural data. *Journal of Biological Chemistry*, Vol.278, No.23, (June 2003), pp. 20851-20859

Lei, B.; Wei, C.J. & Tu, S.C. (2000). Action mechanism of antitubercular isoniazid. Activation by Mycobacterium tuberculosis KatG, isolation, and characterization of inha inhibitor. *Journal of Biological Chemistry*, Vol.275, No.4, (January 2000), pp. 2520-2526

Metcalfe, C.; Macdonald, I.K.; Murphy, E.J.; Brown, K.A.; Raven, E.L. & Moody, P.C. (2008). The tuberculosis prodrug isoniazid bound to activating peroxidises. *Journal of Biological Chemistry*, Vol.283, No.10, (March 2008), pp. 6193-6200

Morris, G.M.; Goodshell, D.S.; Halliday, R.S.; Huey, R.; Hart, W.E.; Belew, R.K. & Olson, A.J. (1998). Automated docking using a lamarckian genetic algorithm and empirical binding free energy function. *Journal of Computational Chemistry*, Vol.19, No.14, (November 1998), pp.1639-1662

Nguyen, M.; Claparols, C.; Bernadou, J. & Meunier, B. A fast and efficient metal-mediated oxidation of isoniazid and identification of isoniazid-NAD(H) adducts. *ChembioChem*, Vol.2, No.12, (December 2001), pp. 877-883

Punkvang, A.; Saparpakorn, P.; Hannongbua, S.; Wolschann, P.; Beyer, A. & Pungpo, P. (2010). Investigating the structural basis of arylamides to improve potency against M. tuberculosis strain through molecular dynamics simulations. *European Journal of Medicinal Chemistry*, Vol.45, No.12, (December 2010), pp.5585-5593

Quemard, A.; Sacchettini, J.C.; Dessen, A.; Vilcheze, C.; Bittman, R.; Jacobs, W.R., Jr & Blanchard, J.S. (1995). Enzymatic characterization of the target for isoniazid in Mycobacterium tuberculosis. *Biochemistry*, Vol.34, No.26, (July 1995), pp. 8235-8241

Quemard, A.; Dessen, A.; Sugantino, M.; Jacobs, W.R., Jr. & Sacchetini, J.C. (1996). Blanchard JS. Binding of catalase-peroxidase-activated isoniazid to wild-type and mutant Mycobacterium tuberculosis enoyl-ACP reductases. *Journal of the American Chemical Society*, Vol.118, No.6, (February 1996), pp. 1561-1562

Rozwarski, D.A.; Grant, G.A.; Barton, D.H.; Jacobs, W.R., Jr & Sacchettini, J.C. (1998). Modification of the NADH of the isoniazid target (InhA) from Mycobacterium tuberculosis. *Science*, Vol.279, No.5347, (January 1998), pp. 98-102

Sullivan, T.J.; Truglio, J.J.; Boyne, M.E.; Novichenok, P.; Zhang, X.; Stratton, C.F.; Li, H.J.; Kaur, T.; Amin, A.; Johnson, F.; Slayden, R.A.; Kisker, C. & Tonge, P.J. (2006). High

affinity InhA inhibitors with activity against drug-resistant strains of Mycobacterium tuberculosis. *ACS Chemical Biology*, Vol.1, No.1, (February 2006), pp.43-53

SYBYL 8.0 (2007) Tripos, Inc.

Saint-Joanis, B.; Souchon, H.; Wilming, M.; Johnsson, K.; Alzari, P.M. & Cole, S.T. (1999). Use of site-directed mutagenesis to probe the structure, function and isoniazid activation of the catalase/peroxidase, KatG, from Mycobacterium tuberculosis. *Biochemical Journal*, Vol.338, No.Pt.3, (March 1999), pp. 753-760

Sinha, B.K. (2001). (1983). Enzymatic activation of hydrazine derivatives. *Journal of Biological Chemistry*, Vol.258, No.2, (January 1983), pp. 796-801

Sullivan, T.J.; Truglio, J.J.; Boyne, M.E.; Novichenok, P.; Zhang, X.; Stratton, C.F.; Li, H.J.; Kaur, T.; Amin, A.; Johnson, F.; Slayden, R.A.; Kisker, C. & Tonge, P.J. (2006). High affinity InhA inhibitors with activity against drug-resistant strains of Mycobacterium tuberculosis. *ACS Chemical Biology*, Vol.17, No.1, (February 2006), pp. 43-53

Timmins, G.S. & Deretic, V. (2006). Mechanisms of action of isoniazid. *Molecular Microbiology*, Vol.62, No., (December 2006), pp. 1220-1227

Tong, W.; Lowis, D.R.; Perkins, R.; Chen ,Y.; Welsh, W.J.; Goddette, D.W.; Heritage, T.W. & Sheehan, D.M. (1998). Evaluation of quantitative structure–activity relationship methods for large-scale prediction of chemicals binding to the estrogen receptor. *Journal of Chemical Information and Modeling*, Vol.38, No.4, (July-August 1998), pp. 669-677

Vilcheze, C.; Wang, F.; Arai, M.; Hazbon, M.H.; Colangeli, R.; Kremer, L.; Weisbrod, T.R.; Alland, D.; Sacchettini, J.C. & Jacobs, W.R., Jr. (2006). Transfer of a point mutation in Mycobacterium tuberculosis inhA resolves the target of isoniazid. *Nature Medicine*, Vol.12, No.9, (September 2006), pp. 1027-1029

World Health Organization (WHO). (2010). Global tuberculosis control 2010, WHO report 2010, pp. 5, ISBN 9789241564069, Geneva, Switzerland

WHO. (2010). Multidrug and extensively drug-resistant TB (M/XDR-TB), 2010 Global report on surveillance and response, ISBN 9789241599191, Geneva, Switzerland

Wen, L.; Chmielowski, J.N.; Bohn, K.C.; Huang, J.K.; Timsina, Y.N.; Kodali, P. & Pathak, A.K. (2009). Functional expression of Francisella tularensis FabH and FabI, potential antibacterial targets. *Protein Expression and Purification*, Vol.65, No.1, (May 2009), pp.83-91

White, S.W.; Zheng, J.; Zhang, Y.M. & Rock, C.O. (2005). The structural biology of type II fatty acid biosynthesis. *Annual Review of Biochemistry*, Vol.74, (2005), pp.791-831

Wright, H.T. & Reynolds, K.A. (2007). Antibacterial targets in fatty acid biosynthesis. *Current Opinion in Microbiology*, Vol.10, No.5, (October 2007), pp.447-453

Zhang, Y.M.; Lu, Y.J. & Rock, C.O. (2004). The reductase steps of the type II fatty acid synthase as antimicrobial targets. *Lipids*, Vol.39, No.11, (November 2004), pp.1055-1060

Zhao, X.; Yu, H.; Yu, S.; Wang, F.; Sacchettini, J.C. & Magliozzo, R.S. (2006). Hydrogen peroxide-mediated isoniazid activation catalyzed by Mycobacterium tuberculosis catalase-peroxidase (KatG) and its S315T mutant. *Biochemistry*, Vol.45, No.13, (April 2006), pp. 4131-4140

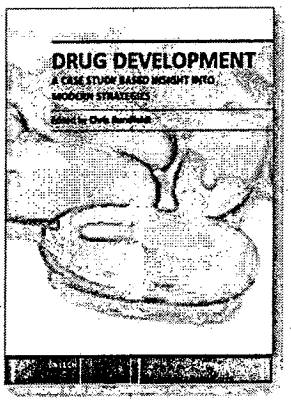

Drug Development - A Case Study Based Insight into Modern Strategies

Edited by Dr. Chris Rundfeldt

ISBN 978-953-307-257-9
Hard cover, 654 pages
Publisher InTech
Published online 07, December, 2011
Published in print edition December, 2011

This book represents a case study based overview of many different aspects of drug development, ranging from target identification and characterization to chemical optimization for efficacy and safety, as well as bioproduction of natural products utilizing for example lichen. In the last section, special aspects of the formal drug development process are discussed. Since drug development is a highly complex multidisciplinary process, case studies are an excellent tool to obtain insight in this field. While each chapter gives specific insight and may be read as an independent source of information, the whole book represents a unique collection of different facets giving insight in the complexity of drug development.

InTech Europe
University Campus STeP Ri
Slavka Krautzeka 83/A
51000 Rijeka, Croatia
Phone: +385 (51) 770 447
Fax: +385 (51) 686 166
www.intechopen.com

InTech China
Unit 405, Office Block, Hotel Equatorial Shanghai
No.65, Yan An Road (West), Shanghai, 200040, China
中国上海市延安西路65号上海国际贵都大饭店办公楼405单元
Phone: +86-21-62489820
Fax: +86-21-62489821

Elucidating the action mode of the bi-substrate InhA inhibitors as anti-tuberculosis agents through molecular dynamics simulations

Auradee Punkvang[1], Pharit Kamsri[2], Dararat Kasamsri[2], Apinya Srisupan[2], Patchreenart Saparpakorn[3], Supa Hannongbua[3], Peter Wolschann[4,5], Supakit Prueksaaroon[6], Pornpan Pungpo[2]*

[1]*Faculty of Liberal Arts and Sciences, Nakhon Phanom University Nakhon Phanom, 48000, Thailand*
[2]*Department of Chemistry, Ubon Ratchathani University, 85 Sthollmark Rd., Warinchamrap, Ubonratchathani, 34190, Thailand*
[3]*Department of Chemistry, Kasetsart University, Chatuchak, Bangkok, 10900, Thailand*
[4]*Institute for Theoretical Chemistry, University of Vienna, Waehringerstrasse 17, A-1090 Vienna, Austria*
[5]*Department of Pharmaceutical Technology and Biopharmaceutics, Faculty of Life Sciences, University of Vienna, Althanstrasse 14, A-1090 Vienna, Austria*
[6]*Large-Scale Simulation Research Laboratory, National Electronic and Computer Technology Center (NECTEC), Phatumtani, 12120, Thailand*

Correspondence to: Pornpan Pungpo (E-mail: pornpan_ubu@yahoo.com)

ABSTRACT

The potential bi-substrate inhibitors of an enoyl-ACP reductase (InhA) of *Mycobacterium* tuberculosis have been synthesized with the aim for fighting drug resistance of isoniazid (INH) related to KatG or InhA mutation. These compounds were designed based on a covalent association between molecules mimicking the InhA substrate and the NADH cofactor. Remarkably, the bi-substrate inhibitors have been speculated that these compounds would be recognized by the substrate binding site and the cofactor pocket of InhA leading to act as dual inhibitors of InhA. Furthermore, based on InhA enzyme and antimycobacterial assays, some of the bi-substrate inhibitors display very significant inhibitory activities against InhA enzyme and mycobacterial growth. However, the action mode of the bi-substrate inhibitors could not yet be clearly demonstrated. Accordingly, to model the potential binding modes of these inhibitors in InhA binding pocket, molecular dynamics (MD) simulations were employed in this chapter. Based on the obtained results, the potential binding modes of the bi-substrate inhibitors in InhA binding pocket are successfully proposed. Moreover, to explore the key residues for binding of the bi-substrate inhibitors in InhA, interaction energies of inhibitors with individual residue were investigated. Therefore, the obtained results should guide the inhibition mechanism and the important interactions for binding of bi-substrate inhibitors in InhA pocket. Consequently, the guidelines for further design of the novel inhibitors with the prominent mechanism to inhibit InhA leading to overcome the resistance of isoniazid are available in this chapter.

INTRODUCTION

Tuberculosis (TB) caused by *Mycobacterium tuberculosis* (*M. tuberculosis*) is one of the leading reason of mortality and is still spread worldwide. In 2010, there were 8.8 million incident cases of TB, 1.1 million deaths from TB among HIV-negative people and an additional 0.35 million deaths from HIV-associated TB [1]. Because the extensively drug-resistant tuberculosis (XDR-TB) is resistant to existing drugs including first- and second-line drugs, current standard treatment regimens of TB are seriously limited. Moreover, in last thirty years, no new promising antituberculosis agents have been introduced into the pharmaceutical market. Accordingly, the development of novel and more potent drug candidates for fighting *M. tuberculosis* strains resistant to existing drugs is an urgent need. The enoyl acyl carrier protein reductase (InhA) of *M. tuberculosis* catalyzing the NADH-specific reduction of 2-trans-enoyl-ACP [2] is an attractive target for designing novel antibacterial agents [3-8]. InhA has been identified as the primary target of isoniazid (INH), one of the most effective first-line anti-TB drugs [9-14]. INH is a pro-drug that must be activated by catalase-peroxidase (KatG) [15-21]. The activated form of INH is covalented with NAD+ cofactor to form the adduct INH-NAD which blocks the InhA enzyme of *M. tuberculosis* [22-23]. The mutations in KatG have been linked to the major mechanism of INH resistance [24-25]. To overcome the INH resistance associated with mutations in KatG, compounds that directly inhibit the InhA enzyme without the activation of KatG have been developed as new promising agents against tuberculosis [26-32]. With this consideration, new inhibitors based on a covalent association between molecules mimicking the InhA substrate and the NADH cofactor were designed, synthesized and evaluated as the direct InhA inhibitors [33]. These inhibitors were planed as bi-substrate inhibitors of InhA. The lipophilic chain of bi-substrate inhibitors mimicking the substrate would be recognized by the substrate binding site of InhA and that mimicking the NADH cofactor would interact with the cofactor pocket. Therefore, these inhibitors would act as bi-substrate inhibitors of InhA [33]. Based on the experimental data, several synthesized compounds are able to inhibit the InhA activity and show promising antimycobacterial agents [33]. However, the bi-substrate mode of action of these compounds did not yet be investigated. Therefore, molecular dynamics (MD) simulations were employed in this chapter to model the potential binding mode of bi-substrate inhibitor in InhA binding pocket.

MATERIAL AND METHOD

Molecular dynamics simulations

The bi-substrate inhibitor, the best active compound 12 which was able to inhibit 91% of InhA activity at 100 μM [33], was selected to study. The initial coordinates for MD simulations of compound 12/NAD+/InhA complex was taken from molecular docking calculations. The MD simulations for this complex were carried out using GROMACS 4.5.4 [34-38] with AMBER03 force field [39]. In addition, AnteChamber PYthon Parser interfacE (ACPYPE) tool [40] was employed to generate parameters for the MD force field of compound 12 and NAD+. The

starting complex was solvated by TIP3P water molecules [41] in a cubic periodic box extending up to 12 Å from the solute species. 4 Na^+ ions were added to neutralize the charge of system. To remove bad contacts before MD simulations, an energy minimization with all bonds constrained using the steepest descent algorithm (2000 steps) was performed. Afterwards, a 200 ps simulation was performed in the NVT ensemble at 300 K with a time step of 0.002 ps under the conditions of position restraints and LINCS constraints [42]. Finally, 10 ns MD simulations without the position restraints were performed under the same conditions. Long-range electrostatic interactions were evaluated by the particle-mesh Ewald method [43]. Coulomb and van der Waals interactions were cut off at 10 Å. The equilibrium state over simulations was selected for detailed analysis.

Molecular docking calculations

The X-ray structure of *trans*-2-hexadecenoyl-(N-acetylcysteamine)-thioester substrate/NAD+/InhA complex taken from the Protein Data Bank (PDB code 1BVR) [44] was used for molecular docking calculations. Compound 12 was constructed using the standard tools available in GaussView 3.07 program [45] and was then fully optimized using the HF/3-21G method implemented in the Gaussian 03 program [46]. Compound 12 was docked into the substrate binding site of InhA by molecular docking calculations using the Autodock 3.05 program with Lamarckian Genetic Algorithm (LGA) [47]. Docking parameters were used as default values, except for the number of docking runs which was set to 50. The docking calculation was validated by reproducing the X-ray conformation of the substrate as well as the orientation in its pocket. A RMSD value between the original and docked coordinates lower than 1Å is acceptable. The ligand pose with the lowest final docked energy was selected as the best binding mode of inhibitors.

Cluster Analysis

The cluster analysis using GROMOS method [48] was performed to cluster the binding mode of compound 12 in the substrate binding site of InhA during the simulation. 4000 snapshots of compound 12 extracted from the last 8 ns simulation time were selected for this cluster analysis. The number of neighbors of each structure (snapshot) within the RMSD cut-off of 1 Å was counted. The structure with largest number of neighbors and all its neighbors as cluster were taken and eliminated from the pool of clusters. Then, this algorithm was repeated for the remaining structures in pool. When the clustering algorithm assigns each structure to exactly one cluster, the structure with the smallest average distance to the others for each cluster will be written as the representative of each cluster.

RESULT AND DISCUSSION

Structural stability

To reveal the stability of the system, the root mean square deviations (RMSD) as a function of the simulation time with respect to the initial coordinates of each species in compound 12/NAD+/InhA complex were analyzed (Figure 1). Compound 12, NAD+ and InhA reaches an equilibrium state beyond 1.5 ns of the simulation time. These results indicate that 10 ns unrestrained simulation is enough for stabilizing the fully relaxed system.

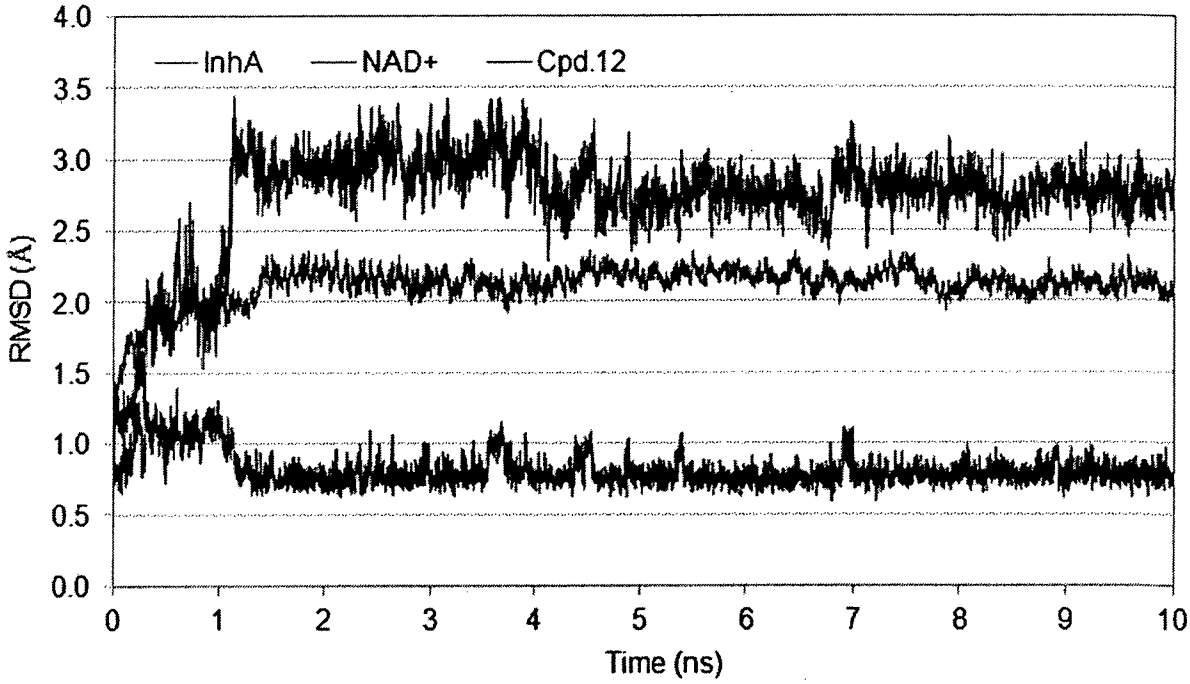

Figure 1 RMSDs of all atoms of each species in compound 12/NAD+/InhA complex

Cluster Analysis and Conformational Changes

Table 1 shows the number of clusters and members of each cluster obtained from cluster analysis of compound 12. The binding conformations of compound 12 bound to NAD+/InhA are divided into 11 clusters. Figure 2 presents the superimposition of the binding conformations of compound 12 selected from each cluster. The conformations and orientations of the C12 alkyl and the CH_2COOEt substituents of compound 12 selected from 11 clusters are significantly changed. With the highest member in cluster, the conformation of compound 12 found in cluster 1 is the major binding conformation of this compound. Therefore, the representative conformation of cluster 1 was selected as the binding mode of compound 12 in the substrate binding site of InhA.

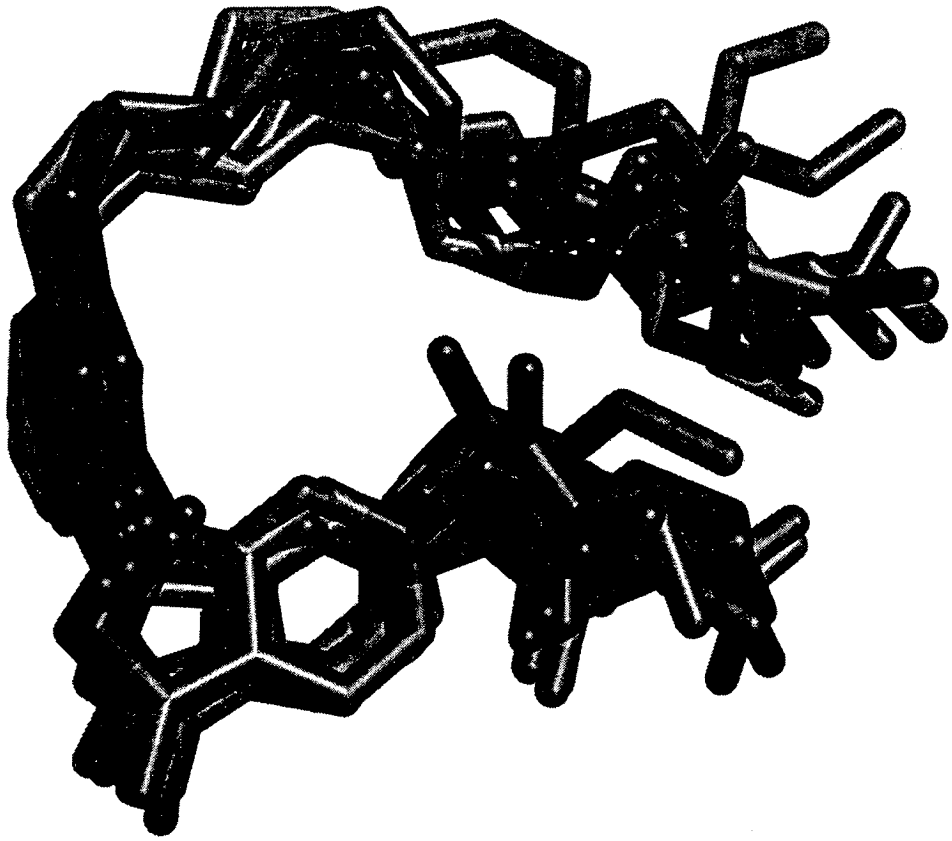

Figure 2 The binding conformations of compound 12 without hydrogen atoms selected from each cluster

Table 1 Cluster analysis of compound 12 bound to NAD+/InhA

Cluster	Member in cluster
1	3628
2	160
3	130
4	43
5	18
6	9
7	4
8	4
9	2
10	1
11	1

The binding mode of compound 12 in the substrate binding site of InhA

To compare the binding mode of compound 12 with that of substrate of InhA (*trans*-2-hexadecenoyl-(N-acetylcysteamine)-thioester; Figure 3), the compound 12/NAD+/InhA structure obtained from MD simulations was overlayed with the X-ray crystal structure of substrate/NAD+/InhA (PDB code 1BVR). Moreover, to compare the binding mode of compound 12 with that of diphenyl ether (5-octyl-2-phenoxyphenol; Figure 3) as the direct InhA inhibitor bound in the substrate binding site of InhA [29], the X-ray crystal structure of diphenyl ether/NAD+/InhA (PDB code 2B37) was used for the superimposition. Figure 4 shows the superimpositions of three structures. The superposition of these structures reveals that the C12 alkyl substituent of compound 12 mimicking the substrate is superimposed with the C15 alkyl chain of substrate which forms a U-shape within the InhA pocket. The phenyl ring of compound 12 is overlayed with the phenyl ring A of diphenyl ether inhibitor, whereas the pyrrolo pyridinium is superimposed with the phenyl ring B of diphenyl ether inhibitor. These results show that the binding mode of compound 12 in the InhA pocket is similar to those of substrate and diphenyl ether inhibitor. Compound 12 has been planed as the bi-substrate inhibitors [33] that could bind in both of the substrate binding site and cofactor binding site of InhA, to block the enzymatic activity of InhA. However, based on the finding in this chapter, compound 12 has high possibility to bind only in the substrate binding site of InhA, like diphenyl ether inhibitor.

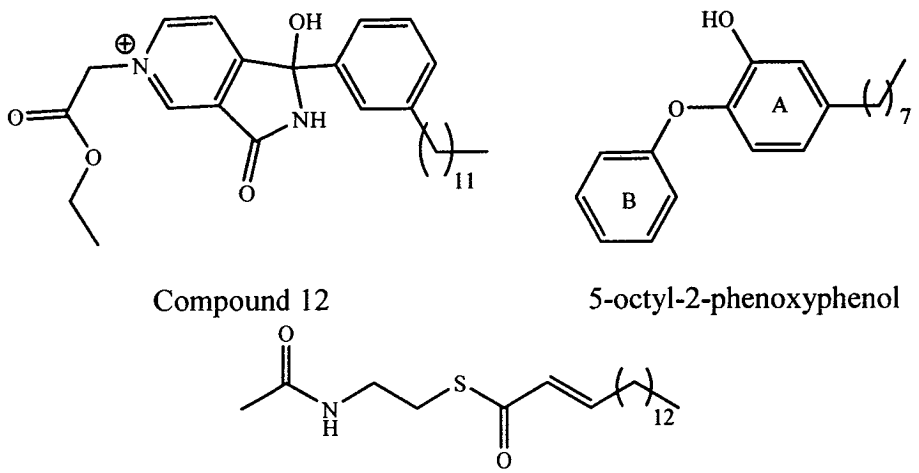

Figure 3 Chemical structures of compound 12, *trans*-2-hexadecenoyl-(N-acetylcysteamine)-thioester and 5-octyl-2-phenoxyphenol

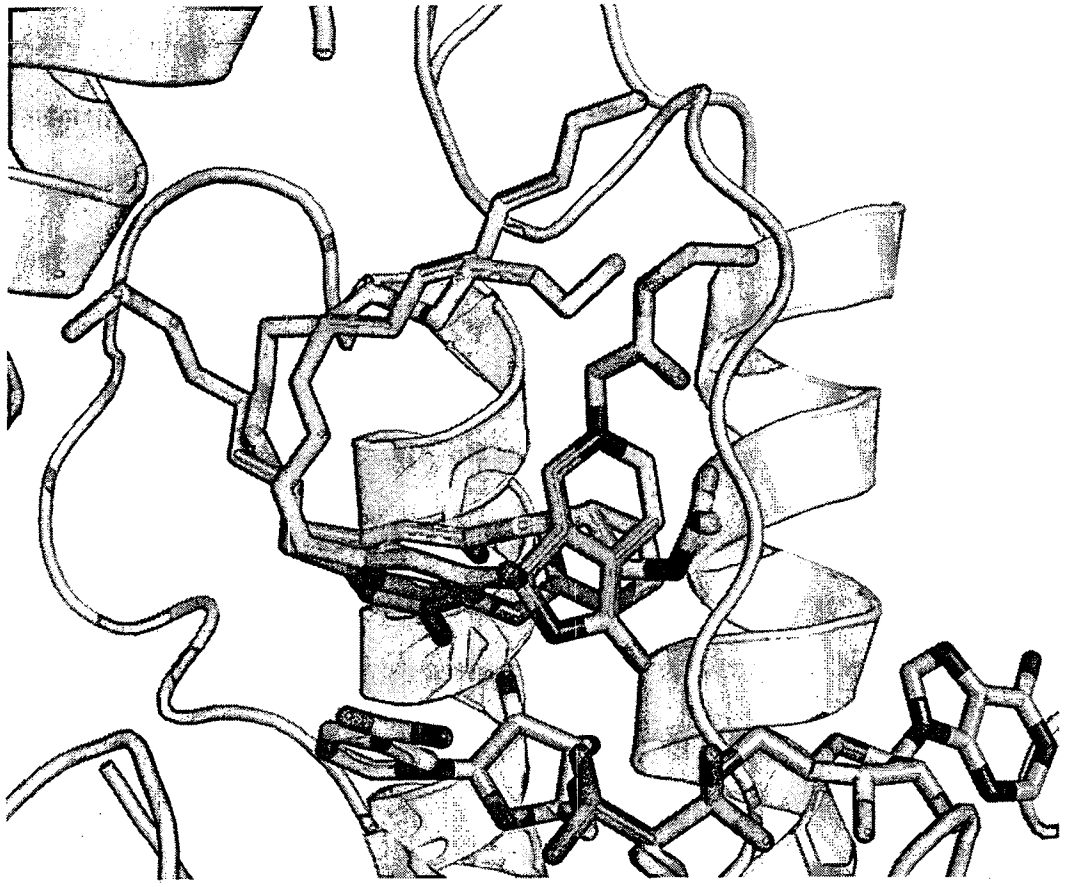

Figure 4 The binding modes of compound 12 (carbon atoms colored by cyan), substrate (carbon atoms colored by yellow) and diphenyl ether inhibitor (carbon atoms colored by pink) in the substrate binding site of InhA

Interaction of compound 12 with InhA

To explore the quantitative contribution of each residue to the binding of compound 12 in the substrate binding site of InhA, the interaction energies of compound 12 with individual amino acids derived from MD simulations are listed (Table 2). The phenyl ring of compound 12 is stacked with the nicotinamide ring of NAD+ (Figure 5). Moreover, the NH of the pyrrolo ring of this compound forms the hydrogen bond with the pyrophosphate oxygen of NAD+. These interactions of compound 12 with NAD+ produce an attractive energy of -14.9 kcal/mol (Table 2). Among all interaction energies, the interactions of compound 12 with NAD+ shows the highest attractive energy which indicates that NAD+ displays the largest contribution to the binding of this compound in the substrate binding site of InhA. The C12 alkyl substituent of compound 12 is occupied in the hydrophobic pocket of Met155, Pro156, Ala157, Tyr158, Met199, Ile202, Leu207 and Ile215. These residues form the attractive interactions with compound 12 with the attractive energies in range of -1.5 to -6.6 kcal/mol. The C12 alkyl substituent of compound 12 would help to increase the affinity and selectivity of this compound to bind in the substrate binding site of InhA. In case of the CH_2COOEt substituent of pyridinium ring of compound 12, this substituent interacts with the C12

alkyl substituent. The interaction between the CH_2COOEt substituent and the C12 alkyl substituent of compound 12 holds the pyrrolo pyridinium in where the NH could form the hydrogen bond with the pyrophosphate oxygen of NAD+.

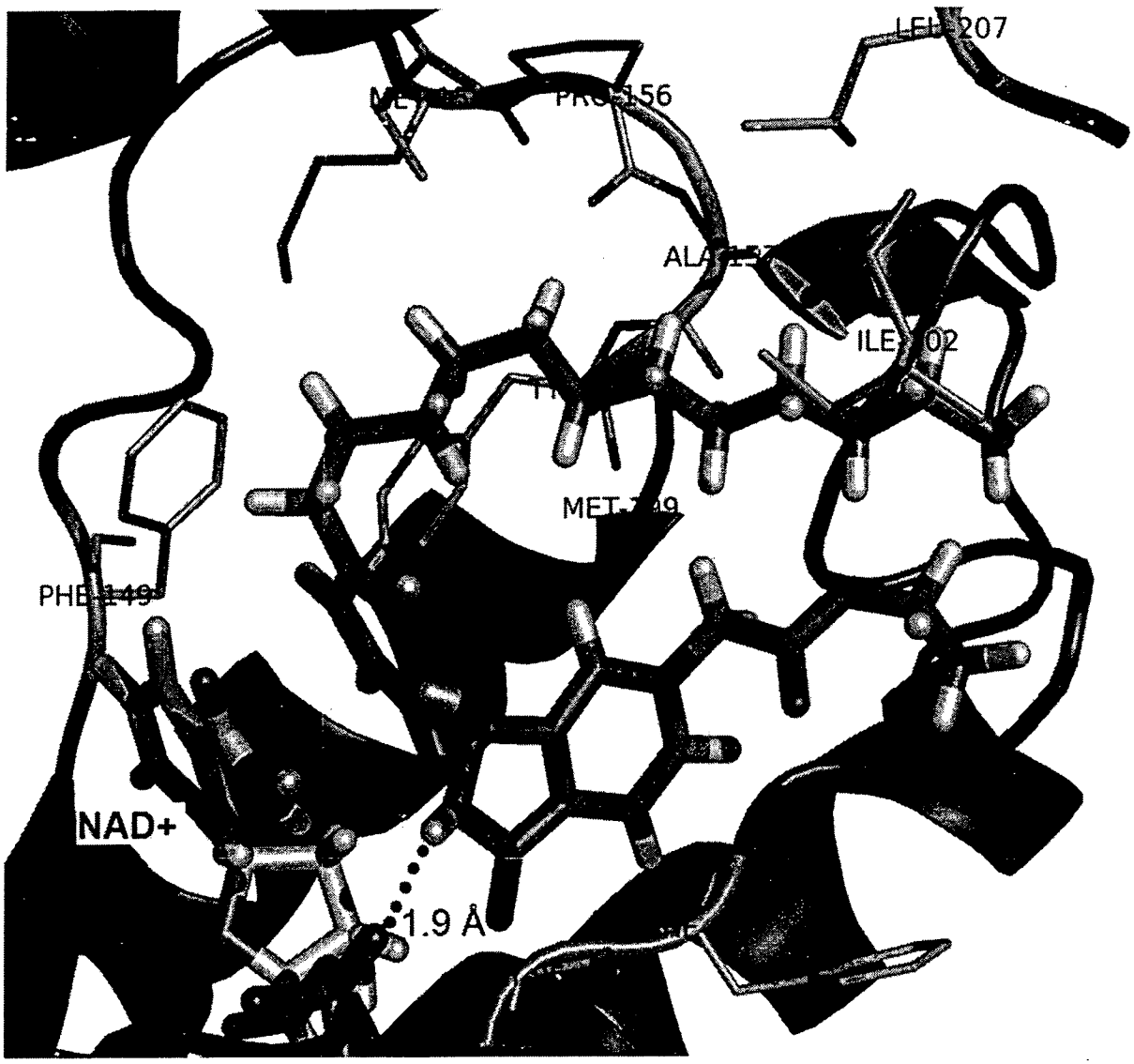

Figure 5 The binding mode of compound 12 (carbon atoms colored by cyan) in the substrate binding site of InhA obtained from MD simulations. The red dot line indicates the hydrogen bond.

Table 2 Interaction energies of compound 12 with individual residues in the substrate binding site of InhA

Residue	Interaction energy (kcal/mol)
NAD+	-14.9
Gly96	-0.8
Met103	-5.2
Gly104	-1.3
Phe149	-2.9
Thr196	-0.9
Ala198	-1.5
Met155	-1.5
Pro156	-1.6
Ala157	-2.2
Tyr158	-4.8
Met199	-6.6
Ile202	-6.3
Leu207	-3.8
Ile215	-2.0

CONCLUSION

MD simulations using the GROMACS program are successful to simulate the reasonable binding mode of compound 12 in the substrate binding site of InhA. Compound 12 planed as the bi-substrate inhibitor has high possibility to bind only in the substrate binding site of InhA, not in the cofactor binding site. NAD+ displays the largest contribution to the binding of compound 12 in the substrate binding site of InhA, whereas the C12 alkyl substituent helps to increase the affinity and selectivity of this compound to bind in this binding site of InhA. Concluding, the obtained results from this chapter provide a better understanding on the binding mechanism and dynamical behaviors of novel InhA inhibitor in the substrate binding site of InhA.

ACKNOWLEDGEMENTS

This research was supported by the Thailand Research Fund (DBG5380006, RTA5380010, DBG5380042). Faculty of science, Ubon Ratchathani University, National Electronic and Computer Technology Center (NECTEC), Thailand, University of Vienna and ASEA-Uninet are gratefully acknowledged for supporting this research.

REFERENCES

1. World Health Organization (WHO). Global tuberculosis control: WHO report 2011
2. Quemard, A; Sacchettini, JC; Dessen, A; Vilcheze, C; Bittman, R; Jacobs, WR, Jr; Blanchard, JS. (1995). Enzymatic characterization of the target for isoniazid in *Mycobacterium tuberculosis*. *Biochemistry*, Vol.34, No.26, 8235-8241.
3. Campbell, JW; Cronan, JE, Jr (2001). Bacterial fatty acid biosynthesis: Targets for antibacterial drug discovery. *Annual Review of Microbiology*, Vol.55, 305-332.
4. Heath, RJ; Rock, CO (2004). Fatty acid biosynthesis as a target for novel antibacterials. *Current Opinion in Investigational Drugs*, Vol.5, No.2, 146-153.
5. White, SW; Zheng, J; Zhang, YM; Rock, CO (2005). The structural biology of type II fatty acid biosynthesis. *Annual Review of Biochemistry*, Vol.74, 791-831.
6. Zhang, YM; Lu, YJ; Rock, CO (2004). The reductase steps of the type II fatty acid synthase as antimicrobial targets. *Lipids*, Vol.39, No.11, 1055-1060.
7. Wen, L; Chmielowski, JN; Bohn, KC; Huang, JK; Timsina, YN; Kodali, P; Pathak, AK (2009). Functional expression of Francisella tularensis FabH and FabI, potential antibacterial targets. *Protein Expression and Purification*, Vol.65, No.1, 83-91.
8. Wright, HT; Reynolds, KA (2007). Antibacterial targets in fatty acid biosynthesis. *Current Opinion in Microbiology*, Vol.10, No.5, 447-453.
9. Rozwarski, DA; Grant, GA; Barton, DH; Jacobs, WR, Jr; Sacchettini, JC (1998). Modification of the NADH of the isoniazid target (InhA) from *Mycobacterium tuberculosis*. *Science*, Vol.279, No.5347, 98-102.
10. Vilcheze, C; Wang, F; Arai, M; Hazbon, MH; Colangeli, R; Kremer, L. Weisbrod, TR; Alland, D; Sacchettini, JC; Jacobs, WR, Jr (2006). Transfer of a point mutation in *Mycobacterium tuberculosis* inhA resolves the target of isoniazid. *Nature Medicine*, Vol.12, No.9, 1027-1029.
11. Dessen, A; Quemard, A; Blanchard, JS; Jacobs, WR, Jr; Sacchettini, JC (1995). Crystal structure and function of the isoniazid target of *Mycobacterium tuberculosis*. *Science*, Vol.267, No.5204, 1638-1641.
12. Lei, B; Wei, CJ; Tu, SC (2000). Action mechanism of antitubercular isoniazid. Activation by *Mycobacterium tuberculosis* KatG, isolation, and characterization of inha inhibitor. *Journal of Biological Chemistry*, Vol.275, No.4, 2520–2526.
13. Johnsson, K; King, DS; Schultz, PG (1995). Studies on the mechanism of action of isoniazid and ethionamide in the chemotherapy of tuberculosis. *Journal of the American Chemical Society*, Vol.117, No.17, 5009–5010.
14. Quemard, A; Dessen, A; Sugantino, M; Jacobs, WR, Jr; Sacchetini, JC (1996). Blanchard JS. Binding of catalase-peroxidase-activated isoniazid to wild-type and mutant *Mycobacterium tuberculosis* enoyl-ACP reductases. *Journal of the American Chemical Society*, Vol.118, No.6, 1561-1562.

15. Saint-Joanis, B; Souchon, H; Wilming, M; Johnsson, K; Alzari, PM; Cole, ST (1999). Use of site-directed mutagenesis to probe the structure, function and isoniazid activation of the catalase/peroxidase, KatG, from *Mycobacterium tuberculosis*. *Biochemical Journal*, Vol.338, No.Pt.3, 753-760.
16. Zhao, X; Yu, H; Yu, S; Wang, F; Sacchettini, JC; Magliozzo, RS (2006). Hydrogen peroxide-mediated isoniazid activation catalyzed by *Mycobacterium tuberculosis* catalase-peroxidase (KatG) and its S315T mutant. *Biochemistry*, Vol.45, No.13, 4131-4140.
17. Metcalfe, C; Macdonald, IK; Murphy, EJ; Brown, KA; Raven, EL; Moody, PC (2008). The tuberculosis prodrug isoniazid bound to activating peroxidises. *Journal of Biological Chemistry*, Vol.283, No.10, 6193-6200.
18. Sinha, BK (1983). Enzymatic activation of hydrazine derivatives. Journal of Biological Chemistry, Vol.258, No.2, 796-801.
19. Nguyen, M; Claparols, C; Bernadou, J; Meunier, B 2001. A fast and efficient metal-mediated oxidation of isoniazid and identification of isoniazid-NAD(H) adducts. *ChembioChem*, Vol.2, No.12, 877-883.
20. Heym, B; Zhang, Y; Poulet, S; Young, D; Cole, ST (1993). Characterization of the katG gene encoding a catalase-peroxidase required for the isoniazid susceptibility of *Mycobacterium tuberculosis*. *Journal of Bacteriology*, Vol.175, No.13, 4255-4259.
21. Johnsson, K; Schultz, PG (1994). Mechanistic studies of the oxidation of isoniazid by the catalase peroxidase from *Mycobacterium tuberculosis*. *Journal of the American Chemical Society*, Vol.116, No.16, 7425–7426.
22. Timmins, GS; Deretic, V (2006). Mechanisms of action of isoniazid. *Molecular Microbiology*, Vol.62, No., 1220-1227.
23. Johnsson, K; Froland, WA; Schultz, PG (1997). Overexpression, purification, and characterization of the catalase-peroxidase KatG from *Mycobacterium tuberculosis*. *Journal of Biological Chemistry*, Vol.272, No.5, 2834-2840.
24. De La Iglesia, AI; Morbidoni, HR (2006). Mechanisms of action of and resistance to rifampicin and isoniazid in *Mycobacterium tuberculosis*: new information on old friends. *Revista Argentina de microbiología*, Vol.38, No.2, 97-109.
25. Banerjee, A; Dubnau, E; Quemard, A; Balasubramanian, V; Um, KS; Wilson, T; Collins, D; de Lisle, G; Jacobs, WR, Jr (1994). inhA, a gene encoding a target for isoniazid and ethionamide in Mycobacterium tuberculosis. *Science*, Vol.263, No.5144, 227–230.
26. Freundlich, JS; Wang, F; Vilcheze, C; Gulten, G; Langley, R; Schiehser, GA; Jacobus, DP; Jacobs, WR, Jr; Sacchettini, JC (2009). Triclosan derivatives: Towards potent inhibitors of drug-sensitive and drug-resistant *Mycobacterium tuberculosis*. *ChemMedChem*, Vol.4, No.2, 241-248.
27. am Ende, CW; Knudson, SE; Liu, N; Childs, J; Sullivan, TJ; Boyne, M; Xu, H; Gegina, Y; Knudson, DL; Johnson, F; Peloquin, CA; Slayden, RA; Tonge, PJ (2008). Synthesis